DYNAMICAL PROCESSES OF RARE EARTH IONS DOPED IN NANO-CRYSTALS EMBEDDED IN AMORPHOUS MATRICES

by

HAIRONG ZHENG

(Under the Direction of RICHARD S. MELTZER)

ABSTRACT

The optical dephasing processes of rare earth ions doped in nanocrystals embedded in glass are studied at low temperatures with both time and frequency domain coherent spectroscopic techniques – the two-pulse photon echo and spectral hole burning. The temperature and nanocrystal size dependence of the homogeneous linewidth and the optical dephasing time are investigated, and the spectral diffusion effects occurring in the time scale of the hole burning measurement is discussed.

The quasi-linear temperature dependence of the homogeneous linewidth obtained with spectral hole burning at low temperatures for Eu^{3+} ions doped in nanocrystals embedded in amorphous matrices is similar in character to what is observed from the ions directly doped in glass. This suggests that the interaction of the Eu^{3+} ions doped in nanocrystals with the two-level system of the glass matrix dominate the optical dephasing of Eu^{3+} ions. For the Pr^{3+}:LaF_3 nanocrystals embedded in oxyfluoride glass, the results of the two-pulse photon echo and spectral hole burning further support this assertion that the interaction of the Pr^{3+} ions in nanocrystals with the two-level system of the glass dominates the optical dephasing at low temperatures. However, a higher power term appeared in the temperature dependence of the line width, which is observed only in the hole burning measurement at temperatures greater than 4 K, suggesting that another new mechanism begins to dominate the dephasing process instead of the interaction with the two-level system. Attempts to identify spectral diffusion are made by comparing the homogeneous broadening measured with the two-pulse photon echo and spectral hole burning.

In addition to the homogeneous broadening, other effects on the excited state dynamics resulting from the confinement effect of the nanocrystals and from the interaction with the surrounding glass matrix are studied. These include the effects of the size and the surrounding medium on the fluorescence lifetime and the effect of confinement on the relaxation rate between two closely spaced electronic levels due to single phonon processes.

INDEX WORDS: Optical Dephasing, Homogeneous Broadening, Two-Level System, Rare Earth Ions, Nanocrystal, Glass, Photon Echo, Hole Burning.

DYNAMICAL PROCESS OF RARE EARTH IONS DOPED IN NANOCRYSTALS EMBEDDED IN AMORPHOUS MATRICES

By

HAIRONG ZHENG

B.S., ShaanXi Normal University, China, 1984

M.S., ShaanXi Normal University, China, 1990

M.S., The University of Puerto Rcio, Puerto Rico, 1999

A Dissertation Submitted to the Graduate Faculty of The University of Georgia in partial Fulfillment of the Requirements for the Degree

DOCTOR OF PHILOSOPHY

ATHENS, GEORGIA

2003

DYNAMICAL PROCESS OF RARE EARTH IONS DOPED IN NANOCRYSTALS EMBEDDED IN AMORPHOUS MATRICES

By

HAIRONG ZHENG

Major Professor: Dr. Richard S. Meltzer

Committee: Dr. Todd Baker
Dr. David. P. Landau
Dr. Bill Dennis
Dr. Mike Geller

Electronic Version Approved:

Maureen Grasso
Dean of the Graduate School
The University of Georgia
May 2003

ACKNOWLEDGEMENTS

I would like to express my deepest appreciation and sincere thanks to Dr. Richard S. Meltzer for his generous devotion of time, talent, support and help throughout the course of my Ph.D program. I am very grateful to his presence, valuable guidance during the experimentation, study and research. I thank him for all of his efforts in teaching me the art of the experimental physics and scientific research.

The collaboration with Dr. Sergey P. Feofilov from Ioffe Physico-Technical Institute, St. Petersburg, Russia, has been essential for starting and fulfilling the goals of this work. I thank him for his valuable help and discussions. Special thanks to Dr. Bill Dennis for his kindly help and support on the experiment. The use of some important pieces of equipment from his lab and helpful suggestions and discussions made my work keep moving on a steady and smooth stage. I thank Dr. William Yen for the use of the laser and help on the samples. Without his help, the photon echo experiment would not be done timely. I wish to thank Dr. Matthew J. Dejneka at Corning Inc. Corning, for his great support on the preparation and characterization of the samples, and very kind advice on the heat treatment of the samples. Help on the experiment from Dr. Xiaojun Wang at Georgia Southern University are highly appreciated. I acknowledge the help from Ms Lizhu “Luli” Lu during my stay at Athens and her assistance on the post treatment of the samples. I thank Dr. Yangsoo Kim and many of my fellow graduate students, especially Carl Liebig, Hong Long Pham for their friendship and help.

I thank my committee members, Dr. Todd Baker, Dr. David. P. Landau, Dr. Mike Geller, and Dr. Bill Dennis for their time and advice on my programs and the dissertation.

I would like to express my grateful attitude to my parents in China. It is their love and concern that made me keep going all the way on my scientific career, and that encouraged me to face and overcome any difficulties.

Finally, I thank my husband, Shixian Qu, and our lovely son, Yingqi Qu, for their understanding and devotion. Without their love and constant support, I would never have been able to get the program done.

TABLE OF CONTENTS

LIST OF TABLES

Page

LIST OF FIGURES

Page

CHAPTER 1

INTRODUCTION

1.1 Background on optical dephasing of ions in crystals and glasses

The individual spectral lines of optical transitions are usually broadened homogeneously and/or inhomogeneously. The homogeneous broadening results from dynamical perturbations on the optical transition frequency and is experienced equally by all ions in the solid. The homogeneous linewidth is controlled by dynamical process in solids, such as phonon dynamics, nuclear or electronic spin flip-flop process, and other interactions of the ions with their surrounding environment. On the other hand, static effects such as lattice strains and crystal imperfections also influence the transition frequency statistically, causing a time independent but position dependent frequency shift which produces inhomogeneous broadening of the spectral transition. In practice, the inhomogeneous broadening often dominates the spectral linewidth even in good quality crystals due to the fact that no crystal is perfect. Thus the information contained in the homogeneous linewidth is usually lost behind the inhomogeneous profile. High resolution non-linear techniques such as the photon echo and spectral hole burning are effective ways to eliminate the screen of the inhomogeneous broadening so that the wealth of information contained in the homogeneous line can be revealed. The photon echo method measures the optical dephasing/homogeneous broadening in the time

domain, while the spectral hole burning (SHB) works in the frequency domain. In the later case (SHB), the measurement process requires a longer time so that the effective linewidth includes effects of spectral diffusion. The combination of the two methods is a powerful way to study the spectral diffusion that occurs in the time scale of the spectral hole burning.

Optical dephasing of rare earth (RE) ions doped in single crystals and glasses have been extensively studied in the past years [1]. At low temperatures, a T^7 temperature dependence of the homogeneous linewidth in single crystals is well understood by the two-phonon Raman process [2], and a quasi-linear temperature dependence for the glass was explained by the interaction of the ions with the two-level systems of the glass [2]. For the ions doped in nanocrystalline materials whose optical properties may have potential applications, the optical dephasing could be very different from what is observed in either single crystals or glasses. For example, the investigation of RE ions doped in free-standing nanocrystals showed a strong confinement effect on the phonon density distribution, resulting in a T^{α} ($3<\alpha<3.5$), rather than a T^7, temperature dependence of the homogeneous linewidth for Eu^{3+} ions, which was successfully explained by the two-phonon Raman process with enhanced coupling and a modified phonon density of states [3]. When the RE ion doped nanocrystals are embedded in glass, the interactions of the RE ions with the surrounding matrix also plays an important role in the homogeneous broadening in addition to the effects of confinement on the phonon modes. A quasi-linear temperature dependence of the homogeneous linewidth, with some high power terms appearing at higher temperatures (from 5 to 10 ^{o}K) was reported in Ref. [4] for Tm^{3+} ions doped glass ceramics.

1.2 Objectives

The purpose of this dissertation is to study the dynamical properties of rare earth ions doped in nanocrystals when these nanocrystals are placed in an amorphous matrix. The properties examined include optical dephasing, fluorescence lifetime and phonon-induced relaxation processes. All of these can be affected by confinement effects and the interaction with the surrounding matrix. Both time domain and frequency domain non-linear spectroscopic techniques, namely the two-pulse photon echo and spectral hole burning, respectively, are employed to investigate the optical dynamical processes of RE ions doped in nanocrystals embedded in glass. The purpose of our study is to: measure the dephasing rate (homogeneous linewidth) for ions doped in nanocrystals embedded in glass and its dependence on the nanocrystal size; identify the interactions that dominate the homogeneous broadening and optical relaxations; and explore the spectral diffusion processes that occurs during the measurements. In addition, their optical properties including their spectroscopy, fluorescence lifetime and single phonon relaxation rates are also examined to obtain a more complete picture for the dynamical properties of ions in nanocrystals embedded in glass.

1.3 The organization of the dissertation

The material in this dissertation is arranged in the following manner:

Chapter 2 is a review of the theoretical development of the optical coherent transients relevant to this work. The density matrix, the basic Bloch vector model and the master equations are used to present a quantum mechanical and semiclassical recipe for deriving the photon echo signals, in order to show how the optical dephasing can be

obtained from these signals. In this chapter, some terminology related to this work is also introduced. The optical absorption with the concept of the oscillator strength is included in the chapter for estimating the intensity of the light required for creating expected photon echo signals.

In Chapter 3, the experimental techniques employed in the study are discussed for both the frequency domain and time domain experiments. The experimental setups and the basic procedures for the spectral hole burning and the two-pulse photon echo are described.

In chapter 4, we present the results of the investigation of the basic optical properties and population relaxation including the fluorescence lifetime, and the one-phonon relaxation between closely spaced levels of rare earth ions doped in nanocrystal systems, especially as they are affected by confinement and the surrounding matrix. Some basic characteristics of the sample and its optical transitions are also discussed.

Chapters 5 to 7 deal with the study of the homogeneous broadening of the rare earth ions doped in nanocrystals embedded in glass matrix at low temperatures. In chapter 5, the theories of the homogeneous broadening in crystal and glass, the two-level system model of the glass, and the concept of the spectral diffusion are reviewed. The results of our experimental investigations are presented in chapters 6 and 7. In chapter 6, the spectral hole burning method is used to study the homogeneous broadening of Eu^{3+} and Pr^{3+} ions doped in nanocrystals embedded in amorphous glass matrices. A quasi-linear temperature dependence of the homogeneous linewidth is obtained experimentally. The interactions of the ions in nanocrystals with the two-level system of the glass matrix, which dominate the optical dephasing process of the ions in nanocrystals, are discussed.

The nanocrystal size dependence of the homogeneous linewidth is also reported in this chapter. In chapter 7, we study the optical dephasing of Pr^{3+} ions doped in LaF_3 nanocrystals embedded in oxyfluoride glass with the two-pulse photon echo technique. The optical dephasing time, T_2, for different nanocrystal sizes and their temperature dependence is presented. The possible mechanisms which dominated the dephasing process and the spectral diffusion effects are discussed.

Finally, we summarize the results in chapter 8. Here the significance of the study, the potential applications, and the prospects for further investigation are discussed.

CHAPTER 2.

BASIC THEORY

2.1 Hamiltonian, density matrix and relaxation

The energy levels of an element, ion or molecule determine all possible optical transitions. The structure of the energy levels is mainly governed by its electronic configuration and the interaction of the electrons with the surrounding environment. The later is very significant for most ions or atoms. For rare earth ions, the energy levels of the 4f electrons are not affected very much by the environment because the 4f electrons are shielded from external electric fields by their outer $5s^2$ and $5p^6$ electrons.

In the study of optical spectroscopy, one usually describe the Hamiltonian, H, in terms of an interaction term, H_I (interactions between the system and the local field) and a relaxation term H_R

$$H = H_0 + H_I + H_R \quad . \tag{2.1}$$

In addition H contains a term H_0 describing the internal working of the isolated static system that specifies the zeroth–order energy eigenstates, which is usually expressed as

$$H_0 = \sum_i H^0(\vec{r}_i) + \sum_{i,j} H'(\vec{r}_i, \vec{r}_j) + \sum_i H_{so}(r_i) + \sum_i H_{CF}(r_i) \tag{2.2}$$

For rare earth ions, H^0 is the central field of the 4f electrons, H' is the interaction among the 4f electrons, H_{so} is the spin orbit interaction of the electrons, and H_{CF} is the interaction with the crystal field determined by the surrounding ions. H_I in Eq. (2.1) is the contribution that is responsible for the transitions among zeroth-order energy states. In the simplest and most common case, the matrix describing the interactions of the system with the applied field has zeros along the diagonal and sinusoidal time dependence whose frequency is the same as the sinusoidal applied field. In H_R the most important relaxation processes is spontaneous emission, collisions (in gas), phonons in solids, and in molecules coupling between rotational, vibrational, and electronic excitations. Because of the complexity of these phenomena, they are usually dealt with in a quasi-phenomenological manner. The form of the Hamiltonian defines the state/wave function of the element/or system through the Schrodinger equation.

The state of an ensemble is usually described by its density matrix. In the discussion of the density matrix, we follow closely the development by Levinson and Kano [1]. The advantage of the density matrix is that it can correctly describe the observable properties of an ensemble of quantum-mechanical systems. For an ensemble, if the probability of finding the state $|y\rangle$ in the ensemble is P_Y , the density matrix is defined by

$$r = \sum_y P_y |y\rangle\langle y| \tag{2.3}$$

where the summation is over all of the possible quantum states.

For an ensemble such that the probability of finding a system with energy $\boldsymbol{E}$ is proportional to $e^{-E/kT}$ (k = Boltzmann constant), the density matrix is given by

$$r = \frac{\mathrm{e}^{-H/kT}}{\mathrm{Tr}\,\mathrm{e}^{-H/kT}} \tag{2.4}$$

The density matrix is Hermitian. It relates to the Hamiltonian of the system, H, by

$$i\hbar\dot{r} = [H, r]\,. \tag{2.5}$$

Once the density matrix is determined, any measurable quantity, for example quantity Q, can be obtained by calculating the expectation value of the corresponding operator through the formula

$$\langle Q \rangle = \mathrm{Tr}(r\,Q) \tag{2.6}$$

For the simplest two-level quantum-mechanical system consisting of an entity with energy eigenstates $|a\rangle$ and $|b\rangle$ having energies E_a and E_b ($E_b > E_a$), respectively, the most general wave function describing a coherent superposition state is written as

$$|y\rangle = a_y\,\mathrm{e}^{-iE_a t/\hbar}|a\rangle + b_y\,\mathrm{e}^{-iE_b t/\hbar - if_y}|b\rangle \tag{2.7}$$

where a_ψ, b_ψ, and ϕ_ψ are real numbers. Thus, the corresponding density matrix reads

$$r = \begin{pmatrix} a_y\, e^{-iE_a t/\hbar} \\ b_y\, e^{-i(E_b t/\hbar + f_y)} \end{pmatrix} \begin{pmatrix} a_y\, e^{+iE_a t/\hbar} & b_y\, e^{+i(E_b t/\hbar + f_y)} \end{pmatrix}$$
$$= \begin{pmatrix} a_y^2 & a_y b_y\, e^{+if_y}\, e^{-i(E_a - E_b)t/\hbar} \\ a_y b_y\, e^{-if_y}\, e^{+i(E_a - E_b)t/\hbar} & b_y^2 \end{pmatrix} \tag{2.8}$$

The probabilities for finding the system in two basis states is determined by the diagonal elements of the matrix. The decay times of diagonal elements define the lifetime of the corresponding eigenstates, T_a and T_b for the closed two-level system. They are the decay of population out of levels ***a*** and ***b***. The longitudinal relaxation time, named T_1, is defined under the conditions that the system consists of two states $|a\rangle$ and $|b\rangle$ that relax toward equilibrium at the rate $T_a^{-1} = T_b^{-1} = T_1^{-1}$. Off-diagonal elements of the density matrix, which represent the coherence intrinsic to a superposition state, will decay toward an equilibrium in a time that is named the transverse relaxation time, T_2. T_2 is also called dephasing time. It is the life time of the coherent superposition state.

The relaxation of off-diagonal elements of density matrix is not entirely independent of that of diagonal elements. To get their dependence, we note that the probability to be in level ***a*** must decay as

$$|a_y(t)|^2 = |a_y(0)|^2\, e^{-t/T_a} \tag{2.9}$$

The probability amplitude should vary in time as

$$a_y(t) = a_y(0)\,e^{-i\omega_a t}\,e^{-t/2T_a} \tag{2.10}$$

where $\omega_a = E_a/\hbar$ and $\omega_b = E_b/\hbar$

Likewise, the probability amplitude of being in level ***b*** must vary as

$$b_y(t) = b_y(0)\,e^{-i\omega_b t}\,e^{-t/2T_b} \tag{2.11}$$

Thus, the coherence between the two levels must vary as

$$a_y^*(t)b_y(t) = a_y^*(0)b_y(0)\,e^{-i\omega_{ab} t}\,e^{-t(1/2T_a + 1/2T_b)} \tag{2.12}$$

The ensemble average of $a_y^*(t)b_y(t)$ is just the off-diagonal element ρ_{ab} of the density matrix ρ. Its relaxation rate is denoted as $1/T_2$. Therefore,

$$T_2^{-1} = \tfrac{1}{2}(T_a^{-1} + T_b^{-1}) \tag{2.13}$$

This is true in the absence of pure dephasing. Under more general conditions, they are related by[1]

$$T_2^{-1} = \tfrac{1}{2}(T_a^{-1} + T_b^{-1}) + \gamma_f \tag{2.14}$$

where γ_ϕ is the pure dephasing rate, which is the relaxation rate due to events that perturb only the phase of the wave functions without inducing decay of eigenstates. In other words, it results from processes (such as magnetic dipole or multipole interactions, electric dipole interactions in solids, or elastic collisions of ions/or atoms in gas.) that are not associated with the transfer of population. If the lifetime of the lower level T_a is infinite, then

$$T_2^{-1} = \tfrac{1}{2} T_b^{-1} + g_f \qquad (2.15)$$

2.2 Master equation, Bloch vector, and dephasing process

The master equations are equations of motion for the elements of the density matrix. They can be written down directly using Eq.(2.5) with the matrix representation of H and r. Considering the interaction of a closed two-level system with an applied field $E(t)=E_\omega \cos(\omega t)$ (where ω is the frequency of the field) whose Hamiltonian is

$$H_I(t) = -m \cdot E(t) = \begin{bmatrix} 0 & H_w^*(t) \\ H_w(t) & 0 \end{bmatrix} \cos wt, \qquad (2.16)$$

one defines the Rabi frequency $c(t)$ as

$$c_0(t) = \frac{m \cdot E_w}{\hbar} \qquad (2.17)$$

While m represents the electric dipole moment of the system. Combining equations (2.2), (2.5), (2.8), and (2.17), we obtain the master equations of the closed two-level system in the form of [1]

$$\dot{r}_{aa} = -\frac{i}{2}\left[(r_{ba}c_w^*(t) - r_{ab}c_w(t))(e^{iwt} + e^{-iwt})\right] + [H_R, r\ ]_{aa}/i\hbar \tag{2.18a}$$

$$\dot{r}_{bb} = \frac{i}{2}\left[(r_{ba}c_w^*(t) - r_{ab}c_w(t))(e^{iwt} + e^{-iwt})\right] + [H_R, r\ ]_{bb}/i\hbar \tag{2.18b}$$

$$\dot{r}_{ab} = -\frac{i}{2}(r_{bb} - r_{aa})(c_w^*(t)(e^{iwt} + e^{-iwt}))\ + i\Omega\ r_{ab} + [H_R, r\ ]_{ab}/i\hbar \tag{2.18c}$$

$$\dot{r}_{ba} = +\frac{i}{2}(r_{bb} - r_{aa})(c_w(t)(e^{iwt} + e^{-iwt}))\ - i\Omega\ r_{ba} + [H_R, r\ ]_{ba}/i\hbar\ = \dot{r}_{ab}^* \tag{2.18d}$$

where $\Omega\ = (E_a - E_b)/\hbar\ = w_a - w_b = w_{ab}$ is the transition frequency between states $|a\rangle$ and $|b\rangle$. All elements of the 2x2 density matrix thus can be obtained by solving the Eqs. (2.18).

Mapping the density matrix into a vector in an abstract three-dimensional vector space, whose unit vectors are $1'$, $2'$, and $3'$, makes it possible to illustrate a geometrical picture of the interaction. For this purpose, we need to introduce the Bloch-Feynman vector $\vec{R}$ and pseudofield vector $\vec{b}$, which are defined as

$$\vec{R}'\ = u'\ \hat{1}' + v'\ \hat{2}' + w'\ \hat{3}' \tag{2.19}$$

and

$$\vec{b}' = \mathrm{Re}\ c^*(t)\hat{1}' + \mathrm{Im}\, c^*(t)\hat{2}' + \Omega\ \hat{3}', \tag{2.20}$$

respectively. Here the components of the $\vec{R}$ vector relates to the elements of the density matrix by

$$u' = r_{ab} + r_{ba} \tag{2.21a}$$

$$v' = i(r_{ba} - r_{ab}) \tag{2.21b}$$

$$w' = r_{bb} - r_{aa}. \tag{2.21c}$$

The components in the definition of Eq.(2.20) are expressed as $c^*(t) = c_0^*(t)\mathrm{e}^{iwt}$. At thermal equilibrium, most of the two-level systems are in the lower energy eigenstate and coherence is absent so that the Bloch vector points downward along the $\hat{3}'$ axis.

In order to accomplish the illustration of the geometrical picture of the interaction of the closed two level system with the applied field, we need to know the time dependence of the vectors $\vec{R}$ and $\vec{b}$. Hence the equation

$$d\vec{R}'/dt = \vec{b}' \times \vec{R}' + [\text{relaxation terms}], \tag{2.22}$$

which is the equation of the motion for the density matrix expressed in terms of $\vec{R}'$ and $\vec{b}'$, needs to be solved. The first term on the right side of the Eq. (2.22) suggests that without the relaxation, the vector $\vec{R}'$ rotates around the moving pseudofield $\vec{b}'$ in a

plane, where the change of the Bloch vector $\vec{R}'$ is always perpendicular to the plane defined by $\vec{R}'$ and $\vec{b}'$. It is useful to set up a reference frame that rotates around the $\hat{3}'$ axis at the frequency of the applied field. In practice, the optical field is not monochromatic so some components of the field oscillate at frequencies slightly greater or less than the rotating frame. The movement of the Bloch vectors thus can be described in a simple way in the rotating frame. If we name the unit vectors of the rotated reference frame as $\hat{1}$, $\hat{2}$, and $\hat{3}$, then the pseudofield vector can be represented as

$$\vec{b} = \left| c_w^*(t) \right| \hat{1} + \Delta \hat{3}, \tag{2.23}$$

which will be always in the plane $\hat{1}$-$\hat{3}$. Here $\Delta = \Omega - w$ is the detuning from resonance. The components of the vector R in the rotating frame thus become

$$u = u' \cos wt + v' \sin wt = 2\,\mathrm{Re}(r_{ba} e^{+iwt}) \tag{2.24a}$$

$$v = -u' \sin wt + v' \cos wt = -2\,\mathrm{Im}(r_{ba} e^{+iwt}) \tag{2.24b}$$

$$w = w' = r_{bb} - r_{aa} \tag{2.24c}$$

The equation of motion, $d\vec{R}/dt = \vec{b} \times \vec{R} + [\text{relaxation terms}]$ continues to describe the motion of the system in the rotating reference frame. The vector $\vec{R}$ now processes around a pseudofield vector $\vec{b}$ in the rotating frame.

From Eqs. (2.23) and (2.24), it is seen that the $\vec{R}$ vector is parallel to the negative $\hat{3}$ axis in the absence of an applied field**.** If an optical field, whose frequency is in

resonance with the system (Δ=0), is applied at time t=0, it will cause $\vec{b}$ vector to point along the $\hat{1}$ axis ($\vec{b} = \chi_0 \hat{1}$). The $\vec{R}$ vector will rotate in the $\hat{2} - \hat{3}$ plane around $\vec{b}$ until it points along the $\hat{2}$ axis at time $\pi/2\chi_0$. If the field were turned off at this point, the optical field that had been applied from t=0 to t= $\pi/2\chi_0$ would be a $\pi/2$ pulse. Here we introduce the concept of the pulse area that describes the angle through which the $\vec{R}$ vector rotates when the frequency of the incident field is in resonant with the transition. It is defined as $\Theta = \int_0^t c_w(t')dt'$. A $\pi/2$ pulse infers a pulse that can make $\vec{R}$ vector to rotate through an angle $\pi/2$ about the $\vec{b}$ axis. At the time t= $\pi/2\chi_0$, the states $|a\rangle$ and $|b\rangle$ are evenly populated. If the optical field is not been terminated at t= $\pi/2\chi_0$, the $\vec{R}$ vector will continue to rotate until it points upward along the positive $\hat{3}$ axis at the time t = π/χ_0. After this π pulse, the population of the two-level system is inverted. After an additional time period (π/χ_0), the $\vec{R}$ vector will return to its initial state at time t = $2\pi/\chi_0$. The pulse area of the field at this point is 2π (2π pulse). In this case, no energy has been transferred from the applied fields to the ensemble in the whole process.

Under the assumption that the initial value of the Bloch vector $\vec{R}$ is $\vec{R}_0$ and the generalized Rabi frequency is constant, the equations of motion in terms of the components become

$$\dot{u} = -\Delta v - \frac{u}{T_2} \tag{2.25a}$$

$$\dot{v} = \Delta u - w\, c_w(t) - \frac{v}{T_2} \tag{2.25b}$$

$$\dot{w} = c_w(t)v - \frac{1+w}{T_b} \tag{2.25c}$$

in the case the two-level atom approximation. The magnitude of the Bloch vector $\vec{R}$ will decrease in the process of relaxation. After the excitation pulse terminates, the projection of $\vec{R}$ along the $\hat{3}$ axis relaxes toward its equilibrium value at the longitudinal relaxation rate ($1/T_b$), which corresponds to the population decay. The contributions from each ion to the components of $\vec{R}$ in the $\hat{1}-\hat{2}$ plane will rotate with respect to the rotating frame, with the result that $\vec{R}$ (ensemble average) will relax towards zero at the transverse relaxation rate ($1/T_2$)[1]. This describes the dephasing of the coherence ("pure" dephasing). In practice, both the longitudinal and transverse relaxations occur simultaneously during the relaxation; the dephasing time measured experimentally is the result of both effects.

2.3 Optical transition and oscillator strength

If we define the transition probability W_{ab} as the probability of a transition |a> to |b> per unit time, Fermi's Golden rule says[3]

$$w_{ab} = \frac{2p}{\hbar^2}\left|(H_w)_{ab}\right|^2 r(w) \tag{2.26}$$

where $\hbar w = \pm(E_b - E_a)$, and the positive sign implies an absorption transition and the negative sign an emission transition. $(H_w)_{ab}$ represents the matrix element of the

interaction Hamiltonian H_I (the interaction of the ensemble and the applied field), and $r(w)$ is the field density of states. If the degeneracy of state $|a\rangle$ is g_a and $|b\rangle$ is g_b, then the emission and absorption probability are related by $g_a w_{ab} = g_b w_{ba}$. The selection rules governing the transition can be obtained by analyzing the matrix elements of H_I.

According to the Debye approximation [4], the density of photons for the light in a crystal with volume V is

$$r(w) = \frac{2Vw^2}{2pn^3} \tag{2.27}$$

where v is the velocity of the light in the crystal.

To measure or represent the strength of a transition, another dimensionless quantity, the oscillator strength or f number is introduced in optical spectroscopy. If |M| represents the matrix element of the electric dipole or magnetic dipole operator, the oscillator strength f is defined as

$$f = \frac{2mw}{3\hbar e^2}|M|^2 \tag{2.28}$$

The spontaneous transition rate in an electronic dipole (ED) process can be expressed with the f number in the form of [3, 5]

$$A(\mathrm{ED}) = \frac{1}{t_R} = \frac{1}{4pe_0}\frac{2w^2e^2}{mc^3}[(\frac{E_{loc}}{E})^2 n] f(\mathrm{ED}) \tag{2.29}$$

where E_{loc}/E is the local field correction in solids, which is $\frac{1}{3}(n^2+2)$ in high local symmetry crystals (n is the refractive index of the material). By inserting numerical values for the physical constants and the local field correction in terms of the refractive index, we deduce (in SI units)

$$f(\mathrm{ED})t_R = 1.5\times10^4 \frac{l_0^2}{[\frac{1}{3}(n^2+2)]^2 n} \quad . \tag{2.30}$$

l_0 is the wavelength of the radiation in the vacuum. The analog relationship for a magnetic dipole process is

$$f(\mathrm{MD})t_R = 1.5\times10^4 \frac{l_0^2}{n^3} \tag{2.31}$$

For l = 0.5 μm and n = 1, $f(\mathrm{ED})t_R \approx 4 \times 10^{-9}$. Thus an allowed electric dipole transition (f = 1) in the visible on a free atom has a radiative decay time of 4×10^{-9} s whereas for an electronic center in a solid for which n ≈ 1.5, $t_R \approx 4 \times 10^{-8}$ s. The measured radiative decay times for dopant ions in solids are generally longer than this, indicating that the oscillator strengths are significantly less than unity. These transitions are either weakly allowed electric dipole processes or magnetic dipole processes.

2.4 Optical absorption

For a solid containing N non-interacting absorbing centers per unit volume which absorb radiation at frequency ν, the attenuation of a beam of intensity $a(n)$ by a solid of thickness of *l* is given by Lambert's law

$$I^n = I_0^n \, e^{-a(n)l} \tag{2.32}$$

Where α(ν) is the absorption coefficient at the frequency ν. The variation of the absorption coefficient with frequency is difficult to predict. In general, the absorption transition has a finite width. The absorption strength, $\int a(n)dn$, is related to the density of absorbing centers and to the transition probability. The value of the absorption coefficient for a particular polarization dependents upon the value of matrix elements of H_I, i.e., $m_e \cdot E$ or $m_M \cdot B$. In the case of centers in sites of high symmetry, where the material acts isotropically, the absorption coefficient is independent of polarization and has the form

$$a(n) = \left(N_a \frac{g_b}{g_a} - N_b \right) A_{ba} \frac{c^2}{8\pi n^2} \frac{1}{n^2} g(n) \quad . \tag{2.33}$$

N_a and N_b are the population densities in the ground and excited states, respectively. Here g_a and g_b are the statistical weights of the states, g(ν) is the line shape function($\int g(n)dn = 1$), and n is the refractive index. Here N_a and N_b have been assumed

to be invariant with time and unaffected by the absorption process. However, if N_a and N_b do change with time then $a(n)$ will vary with time.

Under weak excitation, N_b can be neglected, $N_a = N$ = density of centers. If we define $s(n) = a(n)/N$ as the absorption cross section, then we have for the integrated cross section [5,6]

$$\int s(n)dn = \frac{l^2}{8p}\frac{g_b}{g_a}\frac{1}{t_0} \tag{2.34}$$

where τ_0 is radiative lifetime of the excited state and λ is wavelength of the transition in medium. In terms of oscillator strength f, the above relation can be written in the following form for electric dipole (ED) and magnetic dipole (MD) transition.

$$\int s(n)dn = f(\mathrm{ED})\frac{e^2}{4e_0 mc}\left[\left(\frac{E_{loc}}{E}\right)^2\frac{1}{n}\right] \tag{2.35}$$

and

$$\int s(n)dn = f(\mathrm{MD})\frac{e^2}{4e_0 mc}n \tag{2.36}$$

where n is the refractive index of the medium.

When the absorption line has a Lorentzian shape, the cross section is given by[5]

$$s(n) = \tfrac{1}{2}(\Delta n)s_0 g(n); \qquad s(n_0) = s_0 \tag{2.37}$$

where

$$g(n) = \frac{\Delta n}{2p}\left[(n - n_0)^2 + \left(\frac{\Delta n}{2}\right)^2\right]^{-1}; \qquad \int g(n)dn = 1 \tag{2.38}$$

and $\Delta\nu$ is the line width at half intensity. When the absorption line has a Gaussian shape, the cross section is

$$s(n) = s_0 \exp\left\{-\left[\frac{(n - n_0)}{\Delta n}\sqrt{\ln 2}\right]^2\right\}; \qquad s(n_0) = s_0 \tag{2.39}$$

CHAPTER 3

EXPERIMENTAL TECHNIQUES OF HIGH RESOLUTION SPECTROSCOPY

Optical transitions in crystals are broadened homogeneously and inhomogeneously. The homogeneous broadening is experienced by all ions in a crystal. It results from dynamical perturbations on the optical transition frequency, which most commonly are caused by lattice phonons or fluctuating nuclear or electron spins. The homogeneous broadening provides information on the dynamical process taking place in solids. This includes phonon dynamics, dephasing processes, spectral diffusion, hyperfine and super-hyperfine interactions, and Stark and Zeeman splittings of nuclear or electron spins.

In addition to homogeneous broadening, there is an inhomogeneous contribution to the linewidth due to static lattice strains inherent in all crystals or the strains that are produced by chemical impurities or other point defects. In practice, inhomogeneous broadening often dominates the spectral line width of interest even in good quality crystals. Therefore, eliminating the resolution limit imposed by inhomogeneous broadening has become a major goal in the field of spectroscopy of solids. Optical spectral holeburning (SHB), fluorescence line narrowing(FLN), and optical coherent transient methods including photon echoes, optical free induction decay (FID) etc., are techniques developed for that purpose.

3.1 Spectral hole burning and fluorescence line narrowing

3.1.1 Theory

SHB and FLN are two major methods for measuring homogeneous broadening in the frequency domain. FLN consists of selectively exciting a narrow portion of an inhomogeneously broadened absorption line with a narrow-band light source, and spectrally dispersing the fluorescence with a monochromator or a Fabry-Perot interferometer. In resonance FLN, fluorescence arises from the same electronic transition as that involved in the excitation process. Hence, its linewidth is determined by the homogeneous linewidth of the transition. Inhomogeneous contributions will arise from the lack of correlation between the inhomogeneous broadening of two different transitions in the nonresonant case. In resonant FLN it is necessary to discriminate against the exciting light, usually by temporal gating, which is difficult for short-lived levels but easy for metastable ones. FLN has been used to measure ground and excited hyperfine splitting, energy levels, homogeneous linewidths, and energy transfer in rare earth doped solids[1]. The resolution of FLN measurements is limited both by the linewidth and stability of the laser and the instrumental resolution of the analyzer.

In SHB, the bleaching of the absorption due to the removal of ions from the ground state is observed rather than resolving the fluorescence from those excited ions. This is done by monitoring the absorption of the bleaching laser, or possibly a second laser, while scanning it through the frequency originally excited. Holes can be detected in any convenient way that measures absorption of the laser. However, the holes can also be detected by laser-induced fluorescence excitation, which allows holeburning to be used even when absorption cannot be detected directly.

There are different kinds of population reservoirs that can be used in holeburning experiments. The simplest, two-level saturation holeburning, uses the excited state itself as the reservoir[2]. The time that the hole can persist is determined by the lifetime of the corresponding excited state. For rare earth ions, the most important population reservoirs are provided by hyperfine splitting of the ground electronic state for rare earth ions. These reservoirs make holes in the inhomogeneous line persist for seconds to minutes, which is mostly determined by spin relaxation among the hyperfine levels[3]. If the hiperfine splittings are larger than the homogenous linewidth of the transition, which happens to the transitions of the Pr^{3+} ions doped in LaF_3 crystal or oxyfluoride glass ceramics, the population reservoir can not be provided by the hyperfine splittings of the ground electronic state. In this case, the population reservoir can be provided by photophysical process that involves the rearrangement of the surroundings. The frequency stability of the laser affects the ultimate resolution of holeburning because laser jitter directly adds to the linewidth by bleaching a hole broader than homogeneous packet.

Both SHB and FLN can be well understood by considering Fig.3.1[4]. An inhomogeneously broadened line of width Γ_{inh} is produced by many narrow components of homogeneous width ($\Gamma_{hom} << \Gamma_{inh}$), each component being centered at a different frequency within the inhomogeneous line profile. If a narrow laser line ν_L and bandwidth $\Gamma_L < \Gamma_{hom}$ is incident upon an ensemble having an inhomogeneously broadened linewidth Γ_{inh}, the resulting absorption of laser radiation depletes only that sub-assembly of excited centers whose energies are within Γ_{hom} of the laser line frequency $\nu_{L.}$ In other words, the absorption signal is determined selectively by some atoms with absorption transitions

within the overall line profile but not by others. Consequently there is a distortion of the line shape in the neighborhood of $\nu_{L;}$ a "hole" is burned in the inhomogeneously broadened line. Resolution of the homogeneous width requires that $\Gamma_L < \Gamma_{hom} << \Gamma_{inh}$. In the FLN technique, a narrow laser line is used to pump within the inhomogeneous linewidth, Γ_{inh}. The laser interacts only with the subset of levels spanning the bandwidth

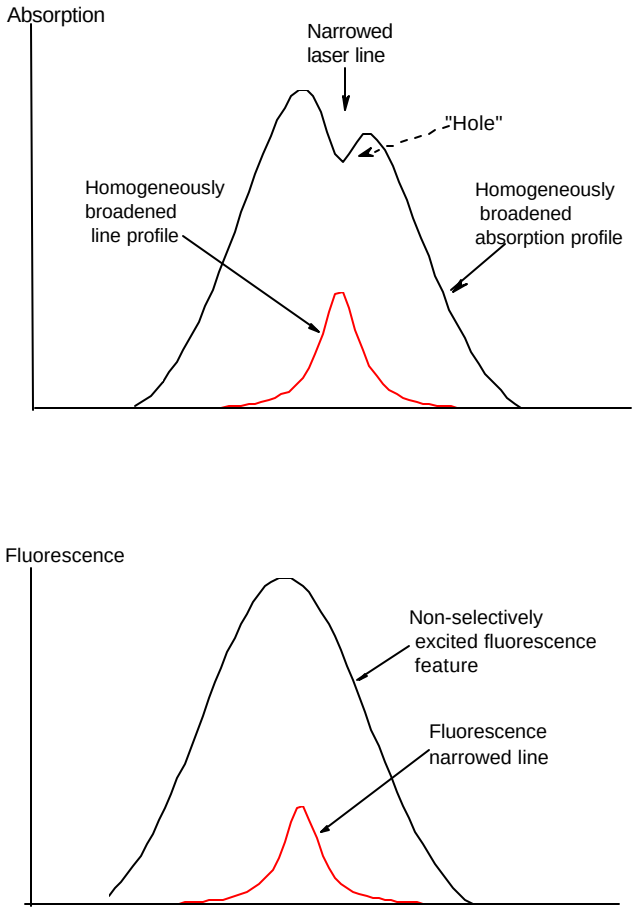

Fig.3.1 Optical spectral holeburning (top) and fluorescence line narrowing (bottom) of an inhomogeneously broadened spectroscopic line.

of the laser, Γ_L. These centers re-radiate to some lower-lying level, which may or may not be the ground state. The fluorescence line width is then much narrower than the inhomogeneous width, and the fluorescence linewidth approaches the homogeneous width. In fact, for centers involved in a resonant transition the total FLN lineshape is a convolution of the laser lineshape and twice the homogeneous lineshape (once for the pump bandwidth and once for the fluorescence). The FLN linewidth, Γ, is then usually written as $\Gamma = \Gamma_L + 2\Gamma_{hom}$. The situation is more complex for non-resonance fluorescence.

Information on the dephasing of a transition can be obtained by measuring the holewidth because it is determined by the homogeneous linewidth of the optical transition. Since it usually requires milliseconds to seconds to burn and scan the hole, an intrinsic time scale on that order is imposed on the experiment. Therefore, the interactions that occur in the system on a time scale much longer than the dephasing time T_2 may also contribute to the observed holewidth. Thus, in a SHB study, spectral diffusion that happens on a time scale much longer than T_2 may broaden the hole. This effect can be studied by combining SHB with time domain coherence technique such as the photon echo.

3.1.2 Homogeneous linewidth and optical dephasing

The homogeneous linewidth, Γ_{hom}, which yields information on the relaxation processes of excited ions, is related to the effective optical dephasing time T_2

$$\Gamma_{hom} = 1/\pi T_2 = 1/2\pi T_1 + 1/\pi T_2^* \qquad (3.1)$$

where T_1 is the population decay time or excited state lifetime (also called longitudinal relaxation time in magnetic resonance), and T_2^* is pure dephasing time determined by dynamical fluctuations at the optical transition frequency (see Eq.2.15)[5]. In crystals, pure dephasing usually stems from coupling of the electronic transition to phonons, interactions with surrounding magnetic or electric dipoles, etc. "Pure" is used to distinguish it from the lifetime broadening(which is defined as the width of the Lorentzian line shape that results from the excited state lifetime). Since the population decay time is usually temperature independent (though the energy transfer and small crystal field splitting can lead to temperature dependence too), the temperature dependence of the decay time is mainly contained in the dephasing term alone for low concentrations of optical active ions and at low temperatures.

The holewidth Γ_{hole}, is equal to twice of the homogeneous linewidth. This is because the laser interacts with a spectral range equal to one homogeneous linewidth during initial excitation and the probe beam interacts with sites having a spread of Γ_{hom}, which creates a bleaching in the original absorption band at ν_{laser}. The laser does not select impurity ions in a specific environment but a set of impurity ions absorbing at the same frequency ν_{laser}.

3.1.3 Experimental setup

Based on the basic theory of hole burning, the experimental setup for the hole burning should consist of the following parts: (1) light sources (dye laser pumped by a cw Ar^+ laser in our experiment); (2) function wave generator that synthesizes the desired frequency and wave form to control the burning and scanning time of the laser on the

hole; (3) the sample which is mounted in helium cryostat; (4) the components for detecting and collecting the data, which include a photomultiplier tube (PMT) and digital oscilloscope in our measurement. Fig.3.2 shows the block diagram of the experimental setup used in our hole burning experiment. The samples were mounted in a liquid helium cryostat during the measurement. A few mW of cw laser from a dye laser, Coherent CR599 (frequency jitter ~ 4MHz), was tuned to the expected transitions (for example transitions of $^7F_0$ - $^5D_0$ transition for Eu^{3+} or the $^3H_4$ –$^1D_2$ for Pr^{3+}) and loosely (d ~ 0.5mm) focused into the sample. The transient hole spectrum (lifetime seconds (Pr) to minutes (Eu)) was obtained with a repetitive burn/scan sequence (scan time ~0.5 s) using fluorescence detection with a PMT through appropriate interference filters or a spectrometer. The data were averaged and stored on a digital oscilloscope. The hole widths obtained on single-crystals, for which the homogeneous linewidth is much less than the spectral resolution for the HB technique, were used to estimate the instrumental contribution to the line width that was subtracted from all data. A wavemeter is introduced here to monitor the wavelength of the laser. The spectrum analyzer was used to trace the spectral output characteristics of the dye laser.

Setup for Hole Burning

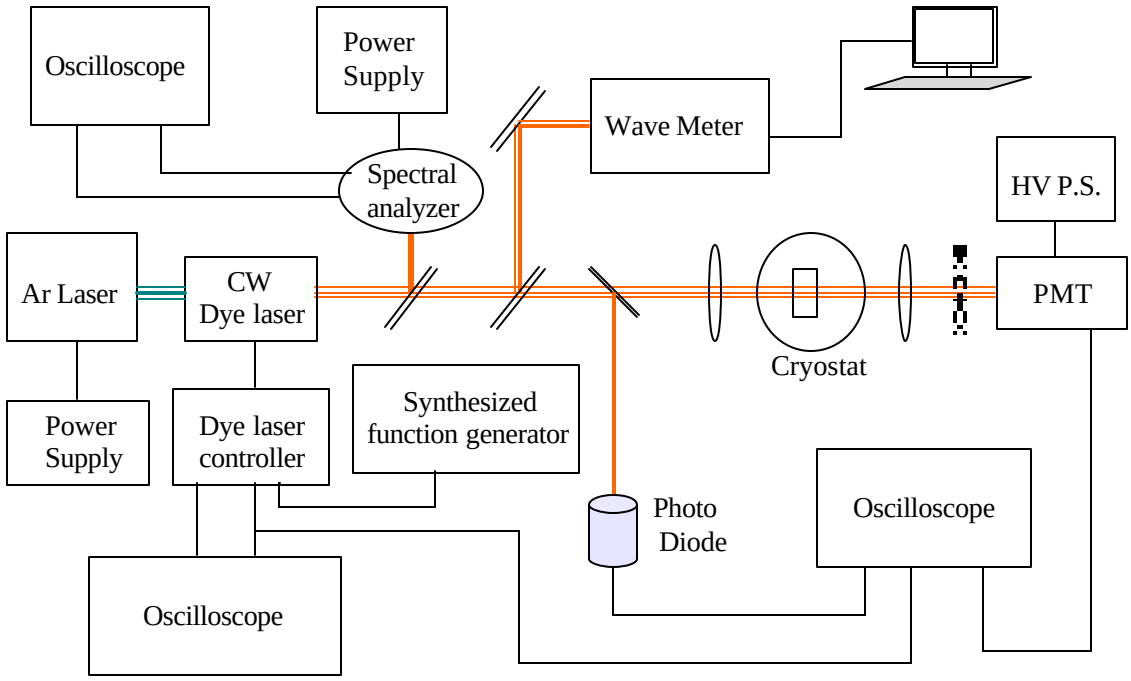

Fig.3.2 Schematic setup for holeburning experiment.

3.2 Photon echoes and OFID

The photon echo and optical free induction decay (OFID) are techniques that the coherent information is recorded as a signal in the time domain. This technique also includes phase switched coherent transients and quantum beat interference experiments. The central ingredient of these techniques is the ability to prepare ensembles of quantum systems coherently and exam them in a time comparable to the optical dephasing time T_2.

3.2.1 OFID

In the OFID technique, the laser coherently prepares and partially saturates a narrow frequency "packet" within the inhomogeneous line. When the frequency of the incident laser beam is suddenly switched to a frequency that is away from resonance with the coherently prepared frequency packet, the coherence evolves freely. This coherence will decay at a rate that is determined by the width of the narrow saturation hole burned in the line during the preparation of the coherence. In the OFID signal, a heterodyne beat will be formed between the frequency switched laser beam and the radiation emitted by the optical polarization associated with this freely evolving coherence. The frequency of the beat is the frequency shift of the incident laser during the above process. Techniques for observing the OFID include frequency switching with either an intracavity phase modulator or an external electro-optic or acousto-optic modulator.

The magnitude of the OFID depends linearly on the Rabi frequency of the incident laser beam if the absorption is not saturated. In this case, the OFID is called the "linear" or "first order" OFID. Practically, it is more complicated for an inhomogeneously broadened system. If the laser beam intensity is sufficient to saturate the transition, the line-shape of the absorption will be affected by the intensity of the laser beam and a new component will appear in the OFID signal. This new component is the "third order" OFID. Its amplitude is proportional to the product of the depth of the hole (which varies as χ^2) and the Rabi frequency, χ [6]. The third order OFID decays in a time proportional to T_2, while the first order OFID relaxes in a time T_2^* that is about the inverse of the inhomogeneous linewidth. In most cases, $T_2 >> T_2^*$. This difference gives the possibility to distinguish the first and third order OFID both experimentally and

theoretically. This also explains why the observed OFID in practice is the third order FID signal.

The decay time of OFID signal can be obtained by considering the relaxation of dielectric polarization density in terms of components of the Bloch vector. Assuming that N is number density in the ensemble, and a single frequency(ω) field is applied to the ensemble at resonance, one can write the dielectric polarization density for the two-level system as

$$P(t) = N\mathrm{Tr}(mr) = N(m_{ab}r_{ab} + m_{ba}r_{ba}) = N\,\mathrm{Re}\{m_{ab}(u - iv)\mathrm{e}^{-iwt}\} \qquad (3.2)$$

where u and v are transverse components of the Bloch-Feynman vector in the reference frame rotating at frequency ω. If the absorption line is in the shape of g(Δ), where g(Δ) could be a Gaussian or Lorentz distribution, the polarization density should be calculated by integrating Eq. (3.2)

$$P(t) = Nm_{ab}\int d\Delta g(\Delta)\,\mathrm{Re}\{m_{ab}(u - iv)\mathrm{e}^{-iwt}\} \qquad (3.3)$$

Imagine that the external field with Rabi frequency χ_0 began exciting a homogeneously broadened ensemble of two-level system at t = -∞, so that by t = 0 the Bloch vector has reached steady-state values. If the driving field is then suddenly extinguished, the steady-state values of u, v, and w can be inserted into the corresponding equation to find the components of the $\vec{R}$ vector at later times. By doing so, one obtains the decay of third-order density polarization [6]

$$P^{(3)}(t) \propto e^{-(t/T_2)\left[1+\sqrt{c_0^2 T_b T_2 + 1}\right]} \tag{3.4}$$

Therefore, a heterodyne beat signal, the OFID signal, will be produced by the interference of the frequency-shifted incident field and the field radiated by polarization given in Eq.(3.4). The decay rate of the OFID amplitude is $2T_2^{-1}$ in the weakly saturated regime ($c_0^2 T_b << T_2^{-1}$). Half of this decay rate represents the inhomogeneous broadening due to the width of the hole burned during the preparation stage, and half results from the intrinsic transverse decay rate of the ensemble. The jitter of the laser frequency may limit the resolution of the OFID technique by causing a broadening of the frequency packet that is prepared during the excitation step. Comparing to the SHB technique that requires a much longer time for the measurement of the hole width, one measures coherence loss on a time scale of the dephasing itself in the OFID experiment. Measurement of the OFID decay rate as a function of temperature, pressure, etc. is one of the most sensitive means of studying dephasing processes.

The experimental setup for the OFID is rather simple. An internal or external phase modulator is used to create a frequency shift of the laser in an extremely short time. The interference of the FID and the shifted laser source create a optical signal which beats at the frequency difference and this is detected with a photo diode, avalanche photodiode or photomultiplier. We have observed the OFID signal with the 0.5% Pr^{3+}:LaF_3 signal crystal under the excitation of $^3H_4$-$^1D_2$(0), but didn't get any OFID signal for the Pr^{3+}:LaF_3 nanocrystals embedded in glass.

3.2.2 The photon echo

The discovery in 1950 of spin echoes by E. L. Hahn [7] showed that free induction decay is easily reversed. It is not only easily reversed, but also easily reversed long after the free induction signal has disappeared completely. Thus the echo signal, which is the resurrected free induction signal, has the magical quality of something coming from nothing. The principles on which the echoes are based is on the simple possibility that each atom retains its own resonance frequency, out of all possible resonance frequencies within the inhomogeneous line of width Γ_{inhom} , for times long compared to $1/\Gamma_{inhom}$.

In the photon echo, the sequence of the laser pulse itself removes the effect of inhomogeneous broadening though the linewidth of the laser pulses might be really broad. Two laser pulses that are separated by a period of time $\tau = t_2$ are required in the two pulse photon echo experiment. The function of the first pulse is to create a coherent superposition of the ground and excited state wave functions. This coherence is detectable because it leads to a macroscopic oscillating dipole. This oscillating dipole is capable of emitting coherent radiation. This radiation will decay at a rate determined by the width of the broad portion of the inhomogeneous line that was excited. After the first pulse, each excited ion will dephase at its own rate as progresses from 0 to τ. The second pulse, applied at $t = \tau$, inverts the sign of the accumulated phase for each ion. Following an additional time τ, the net phase shift is canceled out for every ion, leading to a rephasing of the coherence and the emission of a burst of coherent radiation (see Fig.3.3 and Fig. 3.4). This burst of the coherent radiation is the photon echo. However, during both legs of the time evolution the ensemble is also dephased irreversibly by the excited

state lifetime and by phonon-induced pure dephasing. Therefore, by measuring the echo intensity as a function of τ, one determines the total irreversible dephasing rate, i.e., the intensity or amplitude of the echo reflects the decay of coherence due to homogeneous relaxation processes occurring during the time 2τ, and a plot of echo amplitude versus 2τ, yields the dephasing time T_2. Ideally, the first pulse should have a pulse area of $\pi/2$ so that a coherent superposition state with equal amplitudes for being in the ground and excited states can be created. The second pulse would have a pulse area of π in order to perfectly exchange magnitudes and phase factors for the ground and excited states. However, in practice, the echo signal can still be observed even when the two pulses are not exactly $\pi/2$ and π pulses, respectively.

The photon echo can also be pictured in terms of a vector model using the construction of Fig.3.3 based on the theory discussed in chapter 2. In the rotating frame, the first $\pi/2$ pulse rotates the $\vec{R}$ vectors for all the members of the ensemble to point along the $\hat{2}$ axis at time t = 0. If we denote these vectors as $\vec{R}_\Delta(0)$, then at t = 0, the $\vec{R}_\Delta$ vectors for all members of the ensemble are parallel and their total summation is nonzero. As time goes on, the $\vec{R}_\Delta(t)$ vectors of the individual members of the ensemble relax around the $\hat{3}$ axis at their own rates. After a time T_2^*, the $\vec{R}_\Delta(t)$ vectors should be uniformly distributed around the $\hat{1}-\hat{2}$ plane. The rotating polarization density is zero at this point (the summation of the $\vec{R}_\Delta(t)$ vectors are zero). In the time interval between

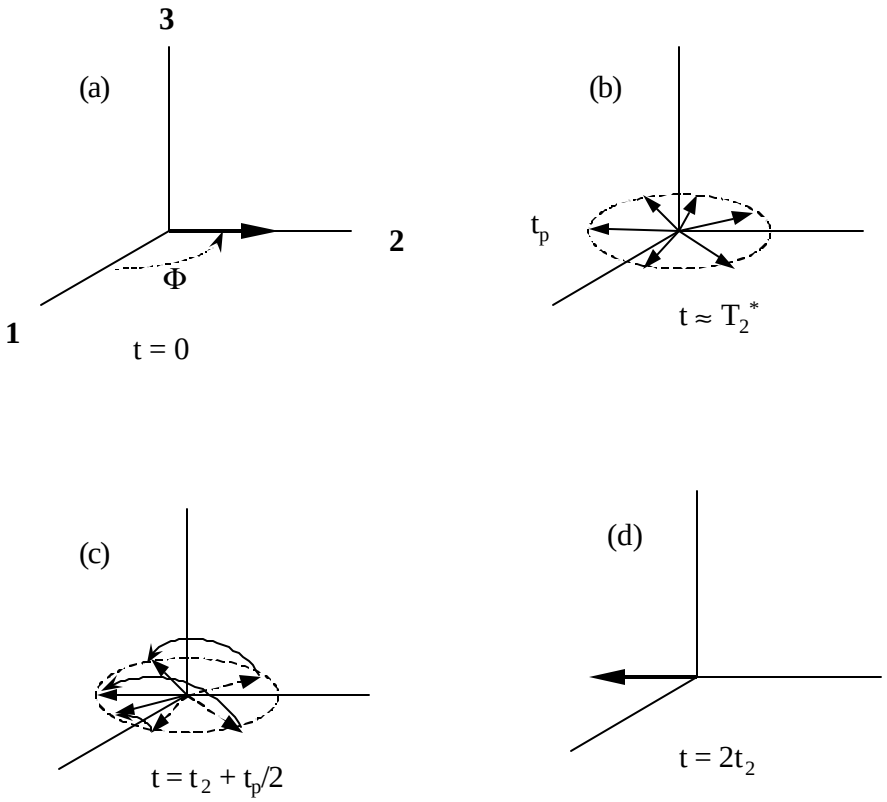

Fig.3.3 The photon echo process pictured by the movement of the Bloch vectors in the rotating reference frame. (a) The first $\pi/2$ pulse rotates the Bloch vectors to point along the $\hat{2}$ axis at t = 0. (b) After the first pulse is turned off, the Bloch vectors begin to dephasing at its own rate. At $t = T_2^*$ they are uniformly distributed around the 1-2 plane. (c) The second pulse with pulse area π rotate each vector by an angle π about the $\hat{1}$ axis, i.e., reverses the phase of each member of the ensemble. After that pulse, the phase increase or decrease at the same rate as before, but. (d) After an additional time t_2, all of the members of the ensemble are again in phase with one another. The summation of the Bloch vectors is nonzero that leads to the burst of the photon echo pulse.

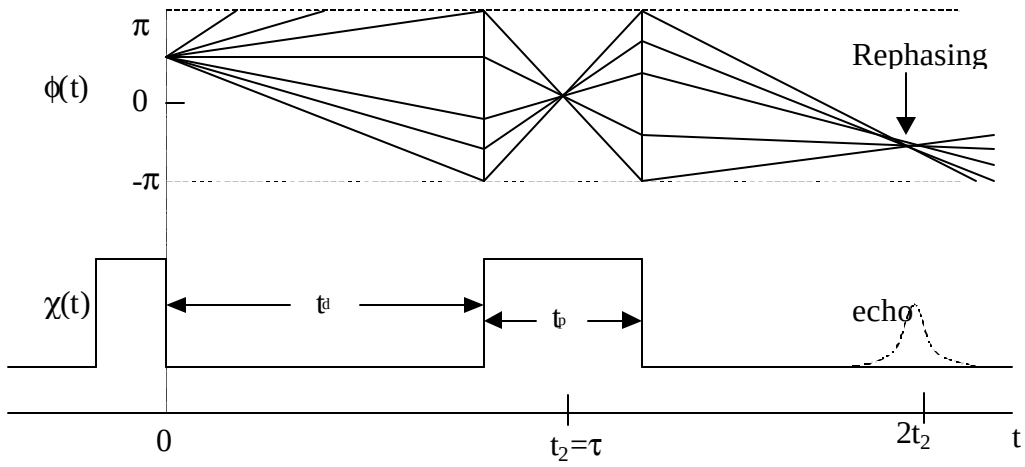

Fig.3.4 The evolution of the phase of typical members of the ensemble corresponding to what illustrated in Fig.3.3.

pulses, the projections of the $\vec{R}_\Delta(t)$ vectors on the $\hat{1}-\hat{2}$ plane rotate and shrink in magnitude. Fig.3.4 is a plot of $\phi_\Delta(t) = \Delta t + \pi/2$; the phase angle measured from $\hat{1}$ axis for typical values of Δ. After time $t_d = t_2 - t_p/2$, a second pulse (π pulse) is applied. This second pulse rotates the $\vec{R}(t)$ vectors through an angle of π around the $\hat{1}$ axis. The phase angles shown in Fig.3.4 are reversed by the π pulse. For $t > t_2 + t_p/2$, the applied field is off and the $\vec{R}_\Delta(t)$ vectors evolve with the phase angle $\phi_\Delta(t)$ increasing or decreasing as in the time interval $0 < t < t_2 + t_p/2$. However, the initial phase at $t = t_2 + t_p/2$ is just the negative of the phase at $t = t_2 - t_p/2$ due to the second pulse that has a pulse area π. After an additional time interval that equals t_2, all the $\vec{R}_\Delta(t)$ vectors are again parallel and $\vec{R}_T$ is again nonzero. Thus, the inhomogeneously broadened ensemble has rephased as a whole at this point, producing a macroscopic polarization density[6]

$$P(t) = -\{-1\} N m_{ab} \int_{-\infty}^{\infty} g(\Delta)\{\cos(\Delta[t - 2t_2'] - \tfrac{1}{2}p) - i\sin(\Delta[t - 2t_2'] - \tfrac{1}{2}p)\} d\Delta e^{-t/T_2} \mathrm{e}^{-i\Omega_{ba}t} \tag{3.5}$$

that peaks at t = $2t_2'$ = 2τ + t_p. A pulse of radiation will be produced by the rephasing ensemble, which is called the photon echo. As t_2 is varied, the amplitude of this polarization appearing at t = $2t_2'$ varies as

$$\left|P(2t_2)\right| \sim \mathrm{e}^{-2t_2'/T_2} \tag{3.6}$$

Because no field is applied to the ensemble except during the two pulses, the photon echo decay rate ($2T_2^{-1}$) is independent of the incident intensity.

Spatially, the echo pulse is highly directional. When the two pulses are collinear, the echo is collinear with lasers. The reason is that any macroscopic emitter with dimension substantially larger than a wave length shows pronounced maxima and minima in its radiation pattern, and the photon echo comes from the coherent radiation of a distribution of dipoles; the maximum radiation therefore occurs along the array in the forward direction for the collinear geometry. Although the polarization amplitude reaches ~ Nμ at its maximum, the echo signal is still weak compared with much stronger scattered light from the π/2 and π pulses. Optical alignment in the collinear geometry makes it easier to focus two beams exactly at the overlapping point, but more careful temporal gating (such as using more Electro-Optic Modulators) is required for eliminating the rather strong scattering from the laser pulses. To avoid too much scattering light from two pulses during the detection of the echo signal, a crossed-beam

geometry, also named the small angle geometry, is introduced [8]. If $\vec{k}_1$, $\vec{k}_2$, and $\vec{k}$ represent wave vectors of $\pi/2$, π and the echo pulse, respectively, the intensity of the echo is found to be at maximum when the wave vectors satisfy

$$\vec{k} - 2\vec{k}_2 + \vec{k}_1 = 0 \tag{3.7}$$

i.e., the echo pulse ($\vec{k}$) is in the plane of $\pi/2$ and π pulses ($\vec{k}_1 - \vec{k}_2$ plane) and inclined by the same angle but to the opposite side of the π pulse ($\vec{k}_2$) [9]. In the small angle geometry, the scattered light from the lasers is easier to block, but the special alignment is more difficult. In addition, the echo signal is generated only from the path length in which the two beams overlap. In a weakly absorbing medium, the collinear geometry maximizes the path length.

3.2.3 Experimental setup for the photon echo

The key point for the two-pulse photon echo experimental setup is the properties of the two synchronized pulsed lasers. The two dye lasers which are pumped by two different pulsed lasers separately should have an output with exactly the same wavelength, and their intensity should be able to generate pulses of $\pi/2$ and π pulse area in the sample, respectively. The delay between the two lasers must be varied continuously from zero to a value that is a few times greater than T_2 of the transition studied. Since the T_2 of Pr ions that we were trying to measure in Pr^{3+}:LaF_3 nanocrystals is less than 100 nanoseconds, the range of the time delay we were working with is from zero to few hundreds of nanoseconds. In a collinear geometry, the excitation lasers come

out the sample with the echo signal in the same direction, and the later is much weaker than the transmitted lasers. Therefore, another crucial point in the collinear geometry is selecting and operating the EOMs carefully in order to obtain a reasonable signal to noise ratio by separating the echo signal from the much stronger transmitted lasers.

Fig. 3.5 shows a brief overview of our experimental setup for the two-pulse photon echo measurement with collinear geometry. Two dye lasers from Quanty Ray, LDL OG505 (pulse 1) and PDL-2 (pulse 2) are pumped by two Nd:YAG pulsed lasers, GCR 100 (for pulse 1) and DCR-1(for pulse 2), respectively. The GCR 100 is used a master trigger for the timing sequence of the two lasers. The details of the timing procedure as well as the alignment procedure of the EOMs are described in the appendix at the end of the dissertation.

In order to make the excitation more efficient, intracavity and external cavity etalons were used for the PDL-2 dye laser and LDL OG505 dye lasers, respectively, which reduced the line width of the dye lasers from 10 GHz to 3 GHz. The energies of the two pulses were about 100 μJ at the sample. A lens of 30 cm focal-length were used to focus the light onto the sample with a spot size of about 100 μm^2. A Burleigh Pulsed Wavemeter was used for monitoring the wavelengths of pulse 1 and pulse 2. There are three electro-optic modulators (EOMs) used in our experiment with four linear polarizers each at 90^o from the next. EOM1 is a high speed electro-optic gating system Pockel's cell (Lasermetrics 5016, driven by Krytron); EOM2 is a Pockel's cell from high speed electro-optic gating system generated by a solid state Pockels' cell driver (model 8251-1, Analog Modules, Inc .); and EOM3 is 301-DM11 pulse picker (Quantum Technology,

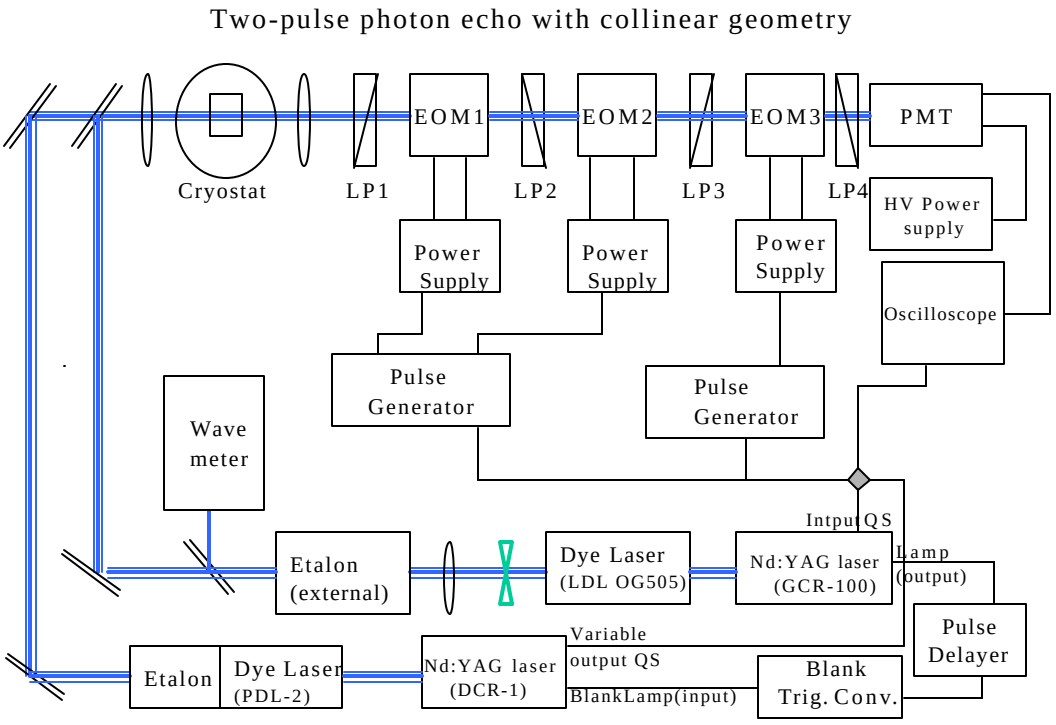

Fig.3.5 Schematic experimental setup for two-pulse photon echo experiment (collinear geometry).

Inc.). The response time of the gate is about 10 ns for all of three EOMs. The EOMs are triggered externally by the Q-switch output of the DCR-1. The echo signal is collected by a photomultiplier tube (PMT) and the data are viewed and saved by TDS 460A Four Channel Digitizing Oscilloscope (Tektronix). The pulse generators/delays in the setup are Four Channel Digital Delay/pulse Generators (Stanford Research System, Inc.). The sample is mounted in the helium cryostat and all of the measurements were conducted at helium temperature.

CHAPTER 4

OPTICAL PROPERTIES OF TRIVALET RARE EARTH IONS DOPED IN NANOCRYSTALS

4.1 Introduction

4.1.1 Characteristics of trivalent Rare earth ions

The 4f electronic levels of the RE ions are characteristic of each ion determined by the number of 4f electrons. Because the 4f electrons are shielded from external electric fields by the outer $5s^2$ and $5p^6$ electrons, their energy level structure is relatively independent of the host. In the case of free RE ions, the outer shell of electrons occupy orbits of the $(4f)^n$ configuration. The inter-electronic Coulomb interaction leads to an initial splitting of states and to the formation of LS terms. The electronic terms are next perturbed by the spin-orbit coupling and under appropriate conditions the LS terms split further into J-multiplets. The spin-orbit interaction can mix J states from different LS terms. Typically for 4f RE ions the states are labeled by $^{2S+1}L_J$, where L, S, and J are quantum numbers of orbital angular momentum, total spin angular momentum, and total angular momentum, respectively. The characteristic energy levels of the trivalent RE ions have been investigated by Dieke and co-works and their results are shown by the well-known Dieke diagram[1]. The diagram was constructed from the energy levels of trivalent RE ions in $LaCl_3$ crystals, but it is applicable to trivalent RE ions in almost any environment because the maximum variation of the energy levels is, at most, of the order of several hundred wave numbers.

4.1.2. Optical transitions of trivalent RE ions

The majority of optical transitions of RE ions in solids that are observed in the visible occur between states which belong to the same $4f^N$ configuration. Absorption and emission originating from electronic transitions between 4f levels is predominantly due to electric dipole or magnetic dipole interactions. Magnetic dipole transitions are very weak and electric dipole f-f transitions in free 4f ions are parity-forbidden. When the crystal field provides an odd component to the perturbation and admixes elements of other configurations into the 4f states, electric dipole transitions become partially allowed. But the radiative transitions remain relatively weak. The effect of mixing is relatively small on the energy of levels, but can have a large influence on their optical transition probabilities.

In appropriate circumstances the weakness of the transitions implies long radiative lifetimes and hence intrinsically very sharp transitions in the absence of other than lifetime broadening mechanisms. The intensity of electric dipole transitions depends strongly on the site symmetry in a host crystal. Magnetic dipole f-f transitions are not affected much by the site symmetry because they are parity-allowed. Typical oscillator strengths are of the order of 10^{-5} to 10^{-8} for the weakly allowed electric dipole transitions, and 10^{-8} for magnetic dipole transitions.

4.1.3 Oxyfluoride glass ceramics

Fluoride glasses and crystals are desirable hosts for optically active ions because of their good transparency, low phonon energy, and high rare earth ion solubility [2]. This makes them attractive for IR amplifiers, up-conversion lasers, and three-dimensional

displays [3,4]. Yet, the quantum efficiency of the glass is low, and they are expensive, toxic, corrosive and unstable, and must be processed in a dry oxygen-free atmosphere. On the other hand, fluoride single crystals can produce narrow fluorescence line widths and enhanced emission cross sections relative to glass, but can not be readily fiberized and are more costly to produce.

Oxyfluoride glass ceramics, i.e., fluoride nanocrystals embedded in oxyfluoride glass, offer the best of both worlds: the low phonon energy of a fluoride and the durability and mechanical properties of an oxide glass. In oxyfluoride glass ceramics, optical active ions partition into low-phonon-energy fluoride crystals that form upon heat treatment [5,6,7]. The crystals are then protected by the oxide glass matrix that will dominate the mechanical and physical properties of the composite (such as adequate thermal and environmental stability), whereas the optical properties of the active ions will be controlled by their fluoride crystal host (a lower phonon energy and high RE ion solubility). Consequently the spectroscopy of optically active ions in nanocrystals should be similar to that of the ions in its counterpart bulk single crystals, though it is expected that the surrounding glass matrix will have some effect on optical spectroscopy and dynamical processes of the ions contained in the nanocrystals [8]. In the following sections, we will discuss the optical transition properties of trivalent RE ions doped in nanocrystals, including their spectroscopy and decay times.

4.2 Experiments

The oxyfluoride glass ceramic samples were prepared by Dr. Matthew Dejneka at Corning, Inc. based on the following procedure: First, an appropriate batch materials

(SiO_2, Al_2O_3, Na_2CO_3, Na_2NO_3, $BaCO_3$, $BaNO_3$, La_2O_6, and/or LaF_3) were melted in an air atmosphere [6,7]. After 3 hours at 1450^{o}C, the melts were poured onto a steel plate and then annealed for 1 hour at 20^{o}C to 30^{o}C below the glass transition temperature which is about 560^{o}C. The obtained glass patties then were heated at 10^{o}C/min to the crystal nucleation temperature, 600^{o}C, and held for 4 hours to nucleate the crystals. Finally, the sample was further heated at a 2^{o}C/min ramp to the ultimate temperatures, usually from 650^{o}C to 825^{o}C and held for 4 hours for the production of 5 to 25 nm crystal particles, respectively. The size of the crystal particles in glass ceramics was measured by electron and atomic force microscopy and by X-ray diffraction. A measurement of the average crystallite size is repeatable to ±1.0 nm and 90% of crystal particles are within 7.5 nm the average. The volume fraction of crystals in the glass ceramics is about 10%. It is found that for the larger RE ions such as Pr^{3+}, the concentration of RE ions in nanoparticles is several times higher than the average concentration of the sample due to the preferential partitioning of the larger RE ions into the crystal. But this partitioning is reversed for the smaller RE ions since the smaller RE ions tend to remain in the glass.

Optical measurements were performed at liquid helium temperatures in order to avoid or reduce possible thermal effects on the transition linewidth and resolve the crystal field splittings of the energy levels. During the optical absorption measurement, a tungsten lamp was used as the light source. The transmitted light was collected by a 0.75 m SPEX 1702 spectrometer and detected with a photomultiplier(PMT) tube. The collected signal was analyzed using a SR 400 Gated photon counter. For fluorescence, excitation, and time domain measurements, a dye laser operating in the red or yellow regions pumped by the second harmonic of a Q-switched Nd:YAG laser(Quanta Ray, 10

ns pulse duration, and 10 Hz repetition), was tuned to excite the RE ions to selected energy levels. A digital oscilloscope(Tektronix TDS 460A Four channel Digitizing Oscilloscope) or a multichannel scalar (EG&G, 5 ns temporal resolution) was used to store the data for the time resolved measurements.

4.3 Results and discussion

4.3.1 Spectroscopy of trivalent RE ions in nanocrystals embedded in glass

The space group of LaF_3 crystals is $D_{3d}^4(p\bar{3}c1)$ and the RE ions occupy sites of C_2 symmetry with identical electrical environments [9]. There are six such sites per unit cell of the crystal, related by six-fold rotation-reflection (S_6) operations about the c axis of the crystal. The C_2 axes for each of the sites are perpendicular to the c axis of the crystal. When the RE ions are doped in a LaF_3 crystal, the free ion states respond to the lowering of symmetry by showing additional splittings. Because the RE ions are shielded by higher quantum shells $5s^2$ and $5p^6$, effects of external perturbations (such as crystal fields) are relatively weak compared to the Coulomb and L-S interactions. The J-multiplets are split into manifolds where the local energy level structure within is each manifold is determined by the local symmetry and the strength of the crystal field which produce admixing of J values and can alter radiative selection rules. In crystal field theory, the effect of the crystal field is treated as a perturbation on the optically active electrons. The consequence of this perturbation is the shifting of energy levels, the lifting of the 2J+1 degeneracy and the alteration of radiative transition probabilities. Due to the low site symmetry(C_2) of RE ions in LaF_3, the degeneracy of energy levels of RE ions is completely lifted by the crystal field for even electron ions, and for odd electron Kramers

ions, only the two-fold spin degeneracy remains. Even at the lowest temperatures and in the best of crystals, transitions of impurity ions have line widths which reflect extrinsic contributions [10] that lead to inhomogeneous broadening. In solids, the sources of inhomogeneous broadening can have a complex origin as might result from clustering occurring during crystal growth, compositional disorder or defects of the lattice if the crystal is not perfect. These perturbations explain the intrinsic linewidth of transitions in a single crystal.

Optical transitions of RE ions in a single crystal occur in groups of sharp lines. The position of the center of gravity of each group is about the same for any compound for the same RE ion. Each group corresponds to transitions between the ground J manifold and an excited J′ manifold level of the free ion. The structure within the group results from the crystal field splitting of each manifold. In LaF_3 glass ceramics, similar optical spectroscopy has been observed. Fig.4.1 shows the absorption spectrum of Pr^{3+} doped LaF_3 nanocrystals embedded in a glass matrix, i.e., Pr^{3+} doped glass ceramics with an average size of 15 nm LaF_3 crystalline particles. Splittings of excited manifolds by the crystal field for the $^3P_1$, $^3P_2$, and $^1D_2$, are clearly exhibited by the sharp and well resolved absorption transitions. The fluorescence spectrum in Fig.4.2 shows the splittings of the $^3H_4$ ground state which corresponds to the transitions of the lowest level of $^1D_2$ to most of the sublevels of $^3H_4$. The excitation spectrum in Fig.4.2 shows the first two sublevels of $^1D_2$; the lowest energy one is lined up with the highest energy fluorescent line indicating that this is the metastable fluorescent level. The transition energies observed in Fig.4.2 are listed in Table 4.1. For the purpose of comparison, the corresponding transitions in the counterpart single crystal are also cited in the table. Shifts in transition energies are no

more than a few wave numbers relative to the transitions in the single crystal. Combining the results of Figs. 4.1 and 4.2, one can say that the energy levels of RE ions in these glass ceramics are essentially the same as that of RE ions in their counterpart single crystals. The similarities between the optical spectra of RE ions doped glass ceramics and single crystals strongly suggests that the LaF_3 nanocrystals are essentially identical to the bulk material, i.e., there are well ordered single crystals.

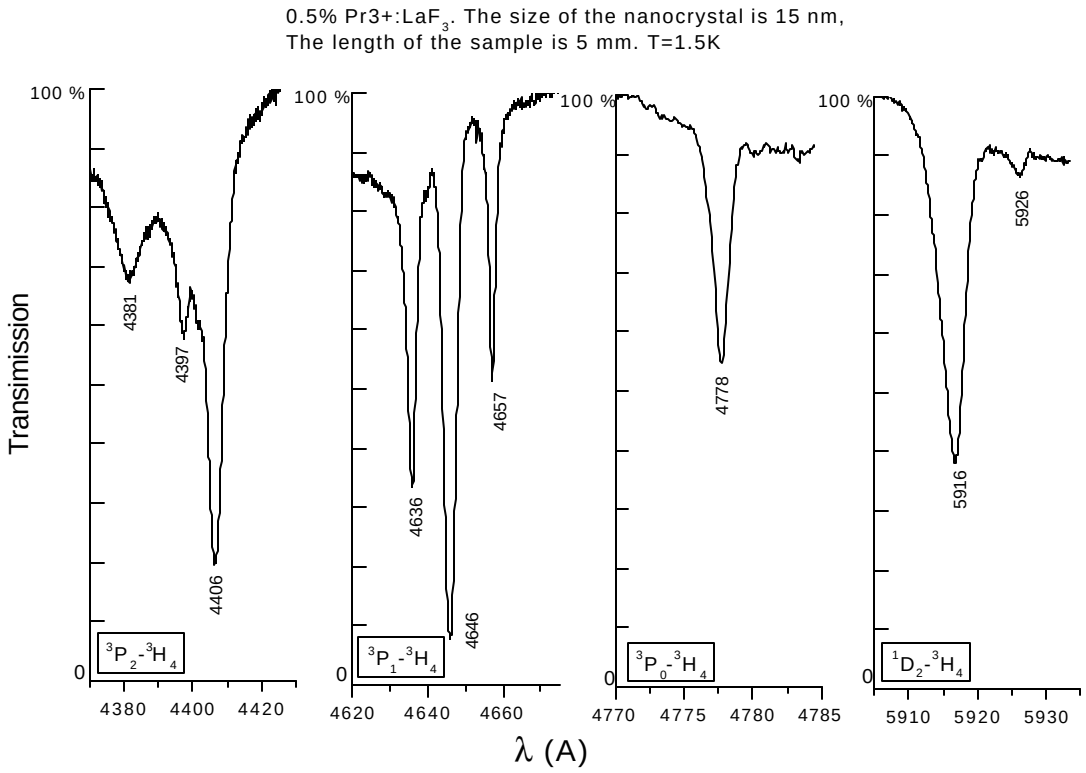

Fig4.1 The absorption spectra of Pr^{3+} doped in LaF3 nanocrystal in glass ceramics. Essential transitions from ground state $^3H_4$ to excited states $^3P_0$, $^3P_1$, $^3P_2$ and $^1D_2$ are displayed. The size of the crystal particle is 15 nm. The concentration of Pr^{3+} is 0.5%. The measurements were conducted at 1.5 K.

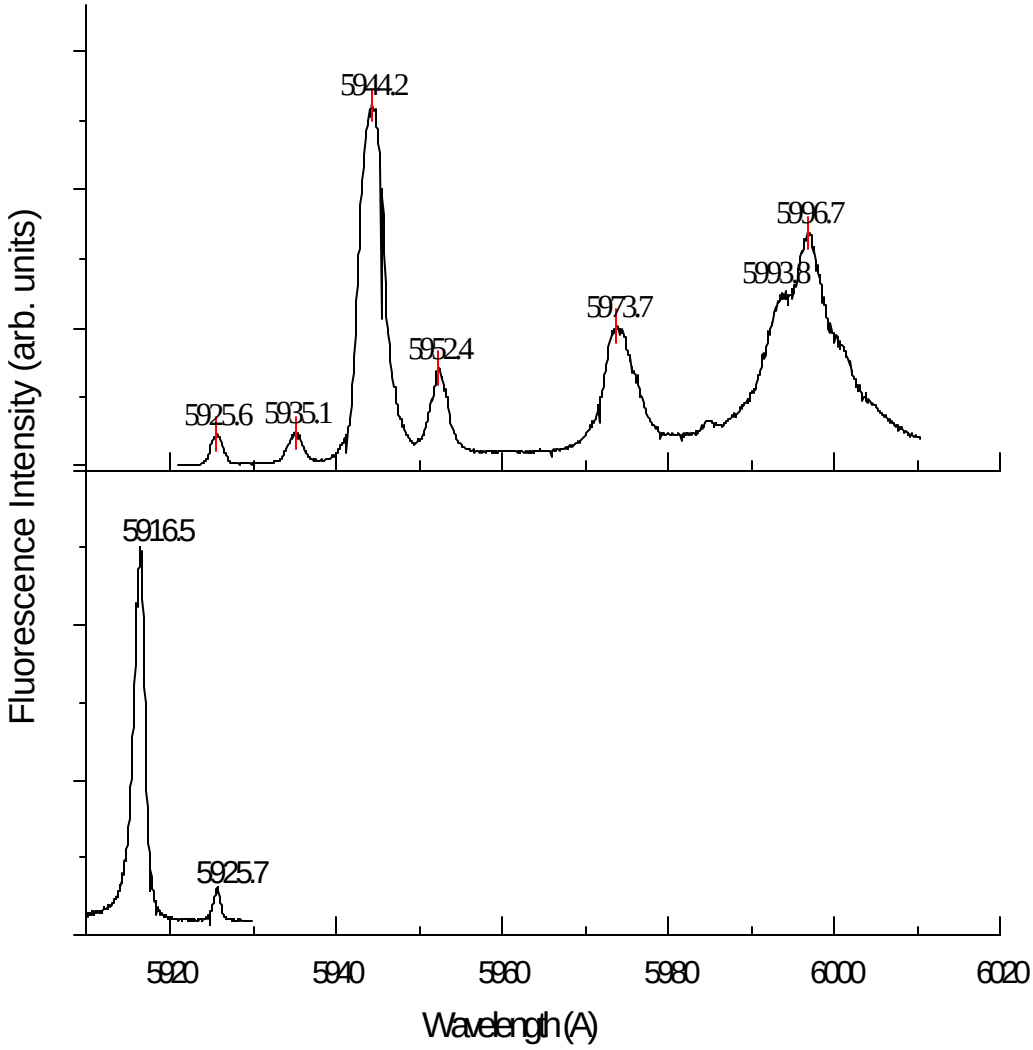

Fig4.2 The excitation (a) and fluorescence (b) spectra of Pr^{3+} $^1D_2$-$^3H_4$ transitions in the glass ceramics. The average size of the crystal particle is 15 nm. The concentration of Pr^{3+} is 0.1%. The measurements were conducted at 1.5 K.

Table 4.1 Optical transitions of Pr^{3+} in LaF_3 nanocrystals of glass ceramic and in the single bulk crystal (Corresponding transition energies observed in Fig.4.2)

Transition	Transition energy in glass ceramics (wavelength) (from Fig.4.2)	Transition energy in single crystal (wavelength) (from ref.[4.21])	Wavelength in single crystal (from ref.[4.22])
$^1D_2$ – $^3H_4$(I)	16876 cm^{-1} (592.56 nm)	16873 cm^{-1}	16873 cm^{-1}
$^1D_2$ – $^3H_4$(II)	16823 cm^{-1} (594.42 nm)	16816 cm^{-1}	16816 cm^{-1}
$^1D_2$ – $^3H_4$(III)	16780 cm^{-1} (595.24 nm)	16761 cm^{-1}	16761 cm^{-1}
$^1D_2$ – $^3H_4$(IV)	16740 cm^{-1} (597.37 nm)	16737 cm^{-1}	16736 cm^{-1}
$^1D_2$ – $^3H_4$(V)	16676 cm^{-1} (599.67 nm)	16678 cm^{-1}	16677 cm^{-1}

Additional broadening occurs for RE optical transitions in glass ceramics compared to the case in single crystals. Fig.4.3 shows the excitation and fluorescence spectra of Ho^{3+} for the $^5F_5$ – $^5I_8$ transition in oxyfluoride glass ceramics containing LaF_3:Ho^{3+} nanocrystals. It can be seen that the spectra of LaF_3:Ho^{3+} nanocrystals are almost identical to that of the bulk single-crystal, which is consistent with what was suggested by Figs.4.1 and 4.2. Yet, there is an additional broadening for the RE transition in the glass ceramic with respect to the transitions in the counterpart single crystal; the amount of the broadening is size dependent. Considering that the crystal particles in glass

ceramics are embedded in a disordered glass matrix, a further inhomogeneous broadening that increases with a decrease of the size of crystal particles suggests that this broadening is due to the increasing fraction of nanoparticles close to the crystallite surface or to the random stress experienced by the nanoparticles in the matrix. The existence of some broad fluorescence background results from the presence of some RE ions directly in the glassy component of the samples.

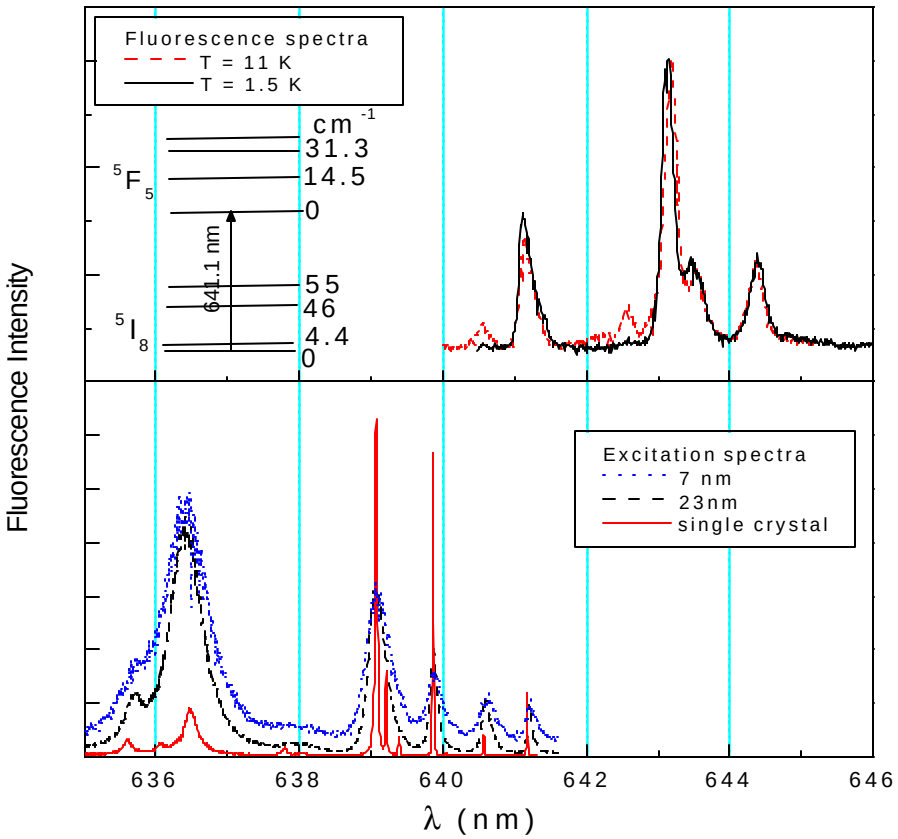

Fig4.3 (a) The excitation spectra of Ho^{3+} $^5F_5$ - $^5I_8$ fluorescence (λ=643.2 nm) in oxyfluoride glass ceramics containing LaF_3:Ho^{3+} nanocrystals of different size and of a LaF_3:Ho^{3+} single crystal. Inset: energy level scheme (simplified) of the $^5F_5$ and $^5I_8$ states of Ho^{3+} in LaF_3. (b) The fluorescence spectra of Ho^{3+} $^5F_5$ – $^5I_8$ transition in oxyfluoride glass ceramics containing LaF_3:Ho^{3+} nanocrystals (λ_{exc}=639.2 nm). The concentration of Ho^{3+} is 0.1%. T = 1.5 K. Insert: energy level scheme (simplified) of $^5F_5$ and $^5I_8$ states of Ho^{3+} in LaF_3.

4.3.2 Fluorescence lifetimes

As we have discussed above, the energy levels of RE ions, determined by their local environment, remain nearly the same except for an increased inhomogeneous broadening seen for the nanoparticles embedded in the glass ceramics. However, the dynamical processes of the RE ions can be very different for ions contained in nanocrystalline particles than for the ions in the crystallographically equivalent sites in bulk single crystals. Due to the finite size of nanocrystal particles, confinement can affect the dynamical process significantly. These confinement effects include additional dephasing due to the enhanced electron-phonon interactions[11], a slowing down of the single phonon relaxation [12], and changes in their radiative transition rates[13]. Also, if the RE ion-doped nanocrystals are embedded in glass, the surrounding glass matrix also may interact with the RE ions and therefore influence the lifetime of the transition in addition to the confinement effects.

(1) The medium dependence

In Ref.[13] it was shown that the radiative lifetimes of excited states of RE ions in nanocrystalline materials is significantly longer than that in the bulk and that the radiative rates strongly depend on the effective refractive index of the media consisting of nanoparticles and the substance filling the space between them. The radiative lifetime modification is quite sensitive to changes of the index of refraction of the media. The expression

$$t_R \sim \frac{1}{f(ED)} \frac{?_0^2}{\left[\frac{1}{3}(n_{eff}{}^2 + 2)\right]^2 n_{eff}} \qquad (4.1)$$

successfully described the dependence of the radiative lifetime of the electronic transitions of the ions to the refractive index of the medium[14,15]. Where the effective index of refraction, n_{eff}, was calculated as an average of the refractive indices of nanocrystalline material n_{nc} and the media n_{med}, as $n_{eff}(x) = x \cdot n_{nc} + (1-x) \cdot n_{med}$. The "filling factor" x describes the volume fraction occupied by the nanoparticle aggregates in the surrounding medium averaged over the wavelength of light. f(ED) is the oscillator strength for the electric dipole transition and λ_0 is the wavelength in vacuum. The dependence of τ_R on n_{eff}, arises from (i) the change in the density of states for photons in the medium of reduced light velocity and (ii) the modification of the polarizability of the surrounding medium[14].

A similar effect is described for the oxyfluoride glass ceramics containing isolated $LaF_3:Pr^{3+}$ nanocrystals [15]. In this case the index of refraction of the glass is very close to that of bulk LaF_3 (n=1.60). The measured $^1D_2$ radiative lifetime at T=1.5K is increased to τ_R=0.64 ms in LaF_3 nanocrystals embedded in the oxyfluoride ceramics (0.005%Pr) compared to τ_R=0.56 ms in LaF_3:0.01%Pr single crystals. The measurements were performed at low temperature in order to guarantee that all radiation occurs from the lowest $^1D_2$ sublevel. The measurable difference in lifetimes using Eq.4.1 yields a 4% lower index of refraction of the glass-ceramics (n_{eff}=1.54) relative to that of LaF_3, which is in a good agreement with the refractive index of the residual glass [16]. It should be noted that the measurements of radiative lifetimes provides a method of locally probing the index of refraction of the glass ceramics.

(2) The nanocrystal size dependence

The averaged nanoparticle size dependence of the lifetime of $^5F_5$ excited state was also studied with the glass-ceramics containing LaF_3:Ho^{3+} nanocrystals. Fig.4.4 shows the dependence of the excited state lifetime on the crystalline diameter. Again, the measurements were performed at 1.5K in order to avoid the contribution of the higher excited state sublevels to the radiative relaxation rate. The results show that the lifetime is shorter than that of the bulk and it increases with an increase of the nanoparticle size, reaching the bulk value for the largest nanoparticles. For the samples studied, the index of refraction of the glass, surrounding the nanoparticles was n_{eff}=1.55 [6]; thus the observed dependence cannot be explained by the modified index of refraction which would predict a larger lifetime.

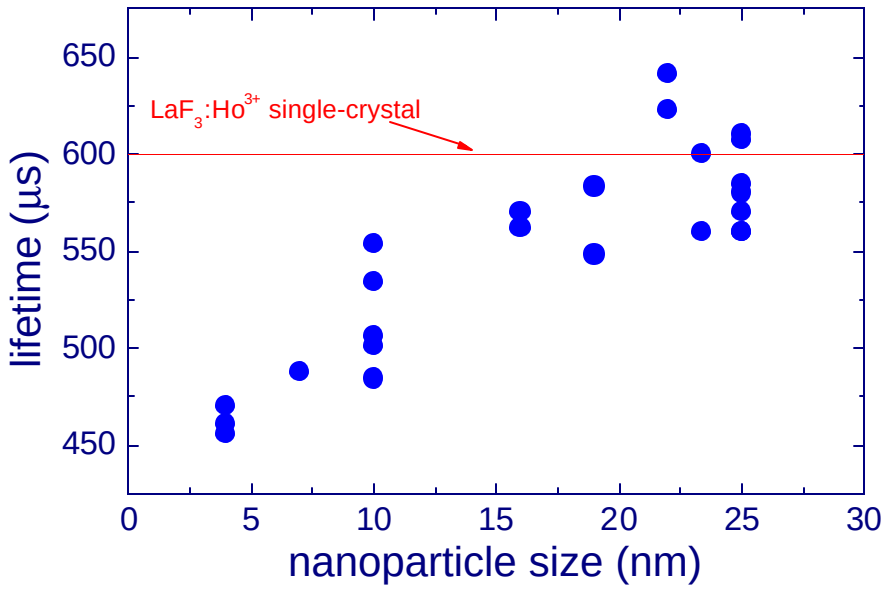

Fig. 4.4 The dependence of the $^5F_5$ fluorescence lifetime, τ_R, on the crystallite size for the Ho^{3+} in LaF_3 nanocrystals in glass ceramics. The solid line shows the lifetime for bulk single-crystals. The average size of the crystal particles is 23 nm. The concentration of Ho^{3+} is 0.1%. T = 1.5 K.

A possible explanation of the nanoparticle size dependence of the lifetime is connected with the role of increased inhomogeneous broadening of the transitions in nanocrystals. Only the "ideal" centers in the single-crystal possess exactly C_2 symmetry. The ions forming the inhomogeneous profile of $^5F_5 \rightarrow {}^5I_8$ transition are in distorted sites, which, strictly speaking, possess only C_1 symmetry. This reduction of the C_2 symmetry may change (increase in this case) the radiative transition probabilities for most of the ions in the inhomogeneously broadened transition and thus be responsible for the shorter lifetimes observed. The assumption that "non-ideal" ions have a short lifetime was confirmed by the observation of the decrease of the lifetime in the wings of the inhomogeneously broadened transition contour as shown in Fig.4.5. Such an effect was also observed for Pr^{3+} in glass-ceramics, but there the effect of the modified index of refraction played the dominant role. For the case of Ho^{3+} in LaF_3 nanoparticles in glass-ceramics it seems that the competitive effects of distortions accompanying the inhomogeneous broadening become dominant. These results are published in Ref.18.

(3) The temperature dependence

Two modes are involved in the relaxation of an excited state, radiative and non-radiative. In the usual case both radiative and non-radiative processes operate to relax an excited state. For the $^1D_2$ state of Pr^{3+} in nanoparticles the relaxation was nearly purely radiative. The relation between the total fluorescence lifetime τ_R of the state and radiative and non-radiative relaxation rate can be expressed as

$$(\tau_R)^{-1} = A_T + W_T \qquad (4.2)$$

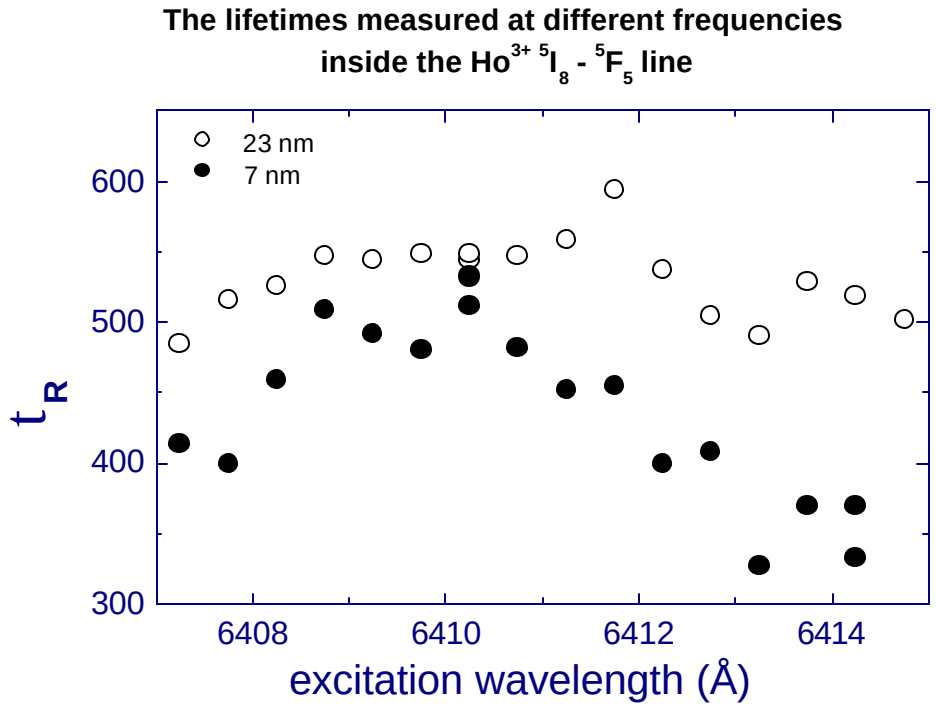

Fig.4.5 The lifetimes measured with the different excitation frequencies inside the inhomogeneously broadened $^5I_8$ – $^5F_5$ line. Full circles – 23 nm particles, Open circles – 7 nm nanoparticles.

where A_T is the radiative rate and W_T is the sum of the rates of various non-radiative processes. The non-radiative relaxation can lead to depopulation of an excited level to lower-lying levels. Both processes can have a temperature dependence which would, in general, be different from one another.

Fig.4.6 shows temperature dependence of τ_R for different sizes of Ho^{3+}:LaF_3 crystalline particles in glass ceramics and for the counterpart single crystal. The data were taken by measuring the fluorescence decay time of $^5F_3$-$^5I_8$ transition of Ho^{3+} ions in the crystal phase. In both glass ceramic and single crystal samples, the $^5F_5$ state lifetime decreases by 30% when temperature increases from 1.5K to 30K. The similar

temperature behavior of the excited state lifetimes in nanocrystals and in the bulk crystal makes it unlikely that the reduced lifetime results from additional nonradiative processes in nanocrystals, which would usually have a different temperature dependence than that of the radiative rate. However, such a temperature dependence can be ascribed to the increasing contribution of transitions from the higher sublevels of the excited state, which may have shorter radiative lifetimes. These contributions would be similar for Ho^{3+} ions in bulk and nano crystals since their energy level structure and radiative transition rates are very similar.

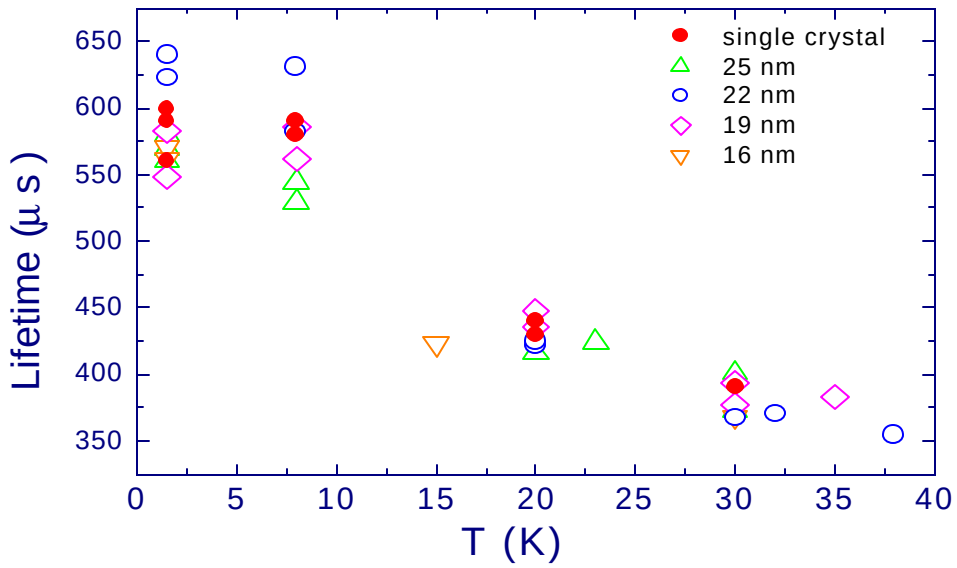

Fig 4.6 The temperature dependence of fluorescence lifetimes of the $^5F_5$ state of Ho^{3+} in LaF_3 for various crystal sizes. The solid circles shows the lifetime for bulk single-crystals. The average size of the crystal particle is 23 nm. The concentration of Ho^{3+} is 0.1%. T = 1.5K.

4.3.3 Relaxation between closely spaced electronic levels

When considering the population relaxation among electronic levels of RE ions doped in nanoparticles that are embedded in glass, two modifications relative to the single phonon direct process in bulk crystals need to be considered: (i) the modification of the vibrational spectrum of the nanoparticles due to size restriction, and (ii) the role of the interaction with the vibrational excitations of the glassy matrix. Here we will explore what processes dominate the electronic relaxation between the closely spaced (separation ~ 10 cm^{-1} or ~100 GHz) electronic levels of RE ions contained in nanoparticles when these particles are embedded in a glass matrix by studying the relaxation between the $^5F_5$ excited state sublevels of Ho^{3+} in LaF_3 nanocrystals in glass.

It has proven very difficult to probe the direct process for RE ions in glasses using optical techniques because the inhomogeneous broadening makes it very difficult to study populations of specific crystal-field levels. This inhomogeneous broadening leads to a wide energy distribution of crystal-field levels and as a result to broad spectra in which the individual crystal field levels are not resolved. However, for RE ions doped into insulating nanoparticles, sharp line optical spectra remain and these spectra are essentially identical to those of the structurally identical bulk single crystals. This occurs because the RE spectra are governed by the local environment which is the same for all RE ions in the nanocrystals as is the case for bulk crystals. However, for electronic relaxation of RE ions doped in nanoparticles surrounded by the glass, long-range interactions may make it possible for the single phonon direct process involving the phonon modes of the glass to make an important contribution to the relaxation rate.

The direct observation of the relaxation between the two lowest $^5F_5$ sublevels was performed under excitation of the upper sublevel at λ=640.5 nm. Transitions from both sublevels to one of the ground $^5I_8$ state components were observed in fluorescence at λ=642.6 nm and λ=643.2 nm which served as a measure of the sublevel populations. Initially after excitation, the population of the Ho^{3+} ions is predominantly in the second sublevel, 14.5 cm^{-1} above the metastable state (see Fig.4.3). The population then decays through the single-phonon direct process producing a 14.5 cm^{-1} phonon and an ion in the lower level. The time dependence of the luminescence decay of the upper level and the buildup of the emission from the lower level (~5-ns temporal resolution) reveal the single-phonon decay rate (see inset in Fig.4.7). The populations will relax to a quasiequilibrium value given by the effective temperature, as discussed in Ref.[17]. Because the 14.5-cm^{-1} splitting between the excited state sublevels (phonon energy) is large compared to the excited volume effective temperature, which in these experiments was estimated as 5 K, it is easily possible to follow the direct process relaxation of the phonon occupation. The relaxation times were determined from both the higher sublevel decay and lower sublevel buildup curves and the average values were used to find the experimental relaxation times T_1, i.e., the longitudinal relaxation time as we have defined in chapter 2. These relaxation times as a function of the size of the nanoparticles embedded in the oxyfluoride glass ceramics are shown in Fig.4.7. The corresponding annealing temperatures are shown on the top axis. The value of T_1 decreases with a decrease of the nanocrystal size, whereas for the largest nanoparticles it approaches the single-crystal value.

The observed dependence of the relaxation time on nanocrystal size may be explained by assuming an important role for the interaction of the electronic states of RE ions in the nanoparticles with the excitations of the glass matrix. In glass, low-lying vibrational modes of a non-acoustical nature are present[18,19]. These are responsible for an enhancement of the density of vibrational states relative to that in crystals. It is well

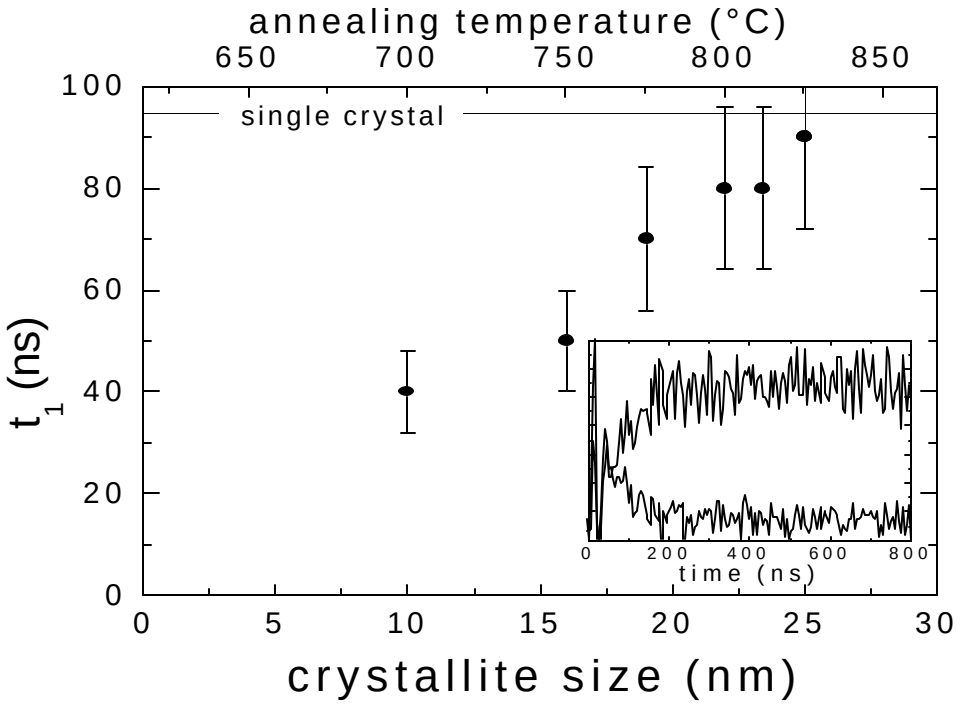

Fig.4.7 Times of relaxation between the two lowest $^5F_5$ state sublevels of Ho^{3+} in nanocrystals of different sizes embedded in oxyfluoride glass ceramics. Solid line: the relaxation time value for single crystal. Inset: typical time-resolved fluorescence decay and buildup curves.

known that the interaction with these modes makes a contribution to the homogeneous broadening of optical transitions for impurity ions in glass[18,20]. The excitation of these

modes may also be the dominant mechanism in the direct relaxation process between the closely spaced levels of RE ions in the nanocrystals embedded in glass [21] At the frequency of 14.5 cm^{-1} (0.44 THz) the density of vibrational states of the glass is significantly greater than the density of states in crystals, at this same frequency, based on a Debye model [18,19]. The vibrational modes of the glass may, together with the phonon modes of nanoparticles, form new mixed vibrational states, which may take part in the single-phonon direct relaxation process. The exact nature of these states and their vibrational wave functions are not known and their interaction with the RE ions will depend on the location of these ions with respect to the surface of the nanoparticle. An additional relaxation mechanism connected with the interaction of RE ions with TLS's can not be excluded though they are usually considered dominant in processes having smaller characteristic energies. In any case, the experimental results of Fig.4.7 clearly suggest that the interaction with the glassy matrix becomes significant for the nanocrystals smaller than 25 nm and that these new modes lead to enhanced single phonon relaxation rates.

CHAPTER 5.

THEORY OF HOMOGENEOUS BROADENING AT LOW TEMPERATURES

5.1 Phonon-induced homogeneous broadening in crystalline materials

In crystalline materials, homogeneous broadening is often determined by relaxation processes mediated by lattice phonons. The ion-lattice coupling strength and the phonon density of states determine the magnitude of the homogeneous linewidth, and its temperature dependence reflects the phonon occupation numbers and the type of process such as direct, Raman, and Orbach relaxations. One-phonon direct relaxation process happens between two adjacent energy levels (|*a*> and |*b*>) whose energy difference is in resonant with the energy of the phonons, i.e., with the phonon energy $\hbar w = |E_b\text{-}E_a|$. The relaxation rate, T_2^{-1}, is proportional to $(n+1)T_1^{-1}$ and nT_1^{-1} for the upper (|*b*>) and lower (|*a*>) levels, respectively. Where $n = (e^{\hbar w/kT} - 1)^{-1}$ is the phonon occupation number and T_1^{-1} represents the rate of the spontaneous emission of the upper energy level.

Raman and Orbach relaxation are both two-phonon relaxation processes in which one phonon is absorbed and a second is emitted. The Raman relaxation dominates most of the relaxation processes in our study. In the Debye approximation, the number density of occupied states is proportional to $w^2 / e^{\hbar w/kT} - 1$, which has a maximum at $w \approx kT/\hbar$. When the energy gap to the nearest crystal field level is such that kT<<$\hbar w = |E_a\text{-}E_b|$, the

number of phonons available for a single phonon decay is very small and the single phonon relaxation rate is negligible. In such a case the Raman process may play the major role. This process involves the absorption of a phonon at frequency $w_1 = |E_t - E_a|/\hbar$ and the emission of a phonon at frequency $w_2 = |E_t - E_b|/\hbar$ such that $w_2 - w_1 = w$. Here the state |**t**> can be a real (Orbach) or virtual (Raman). The Raman process makes use of all the phonons available at a given temperature. The initial and final levels (|**a**> and |**b**>) involved in the Raman process are usually ground or metastable states. If $\hbar w_1$ and $\hbar w_2$ are much larger than $\hbar w$, one can assume $w_1 = w_2$ and a calculation of the homogeneous linewidth based on the Debye model for phonons, in the long wavelength approximation for the matrix elements of the orbit-lattice interaction, leads to the expression [1]

$$1/T_2 = CT^7 \int_0^{\frac{T_D}{T}} x^6 \left[e^x/(e^x-1)^2\right] dx \qquad (5.1)$$

in the case for which $T << T_D = \hbar w_D / k$. Here C is a constant, T_D is the Debye temperature, and $x = \hbar\omega / kT$. Here the integral is nearly independent of T. Thus a T^7 dependence of the relaxation rate is obtained at low temperatures in the approximation of $kT << \hbar w = |E_a - E_b|$. This theory successfully explains the T^7 temperature dependence found in crystalline materials at low temperatures.

Another possible nonradiative process is the multiphonon process, which can take place between two levels whose energy difference is greater than the greatest energy of

the available phonons. However, this is a high order process, and it may be safe to assume that these processes are less probable the larger is the number of emitted phonons required for energy conservation, namely, the greater is the energy gap of the two levels involved in the transition. For metastable states with large energy gaps to the next lower level, multiphonon processes will not contribute significantly to the homogeneous linewidth, although it may be important for population relaxation.

At low temperatures, in the case of Eu^{3+} doped single crystals, the two-phonon Raman relaxation process dominates the optical dephasing (homogeneous broadening) of the $^5D_0$-$^7F_0$ transition due to the lack of sublevels in the ground ($^7F_0$) and excited ($^5D_0$) energy states. However the one-phonon direct relaxation plays the major role in the optical dephasing of the transitions of $^1D_2$-$^3H_4$ and $^3P_0$-$^3H_4$ for Pr^{3+} doped single crystals due to the presence of nearby crystal field levels in their manifolds: $^3H_4$ ground state (57 cm^{-1}) and the $^1D_2$ excited state (23 cm^{-1}).

5.2 Homogeneous broadening in glass

As an amorphous material, glass is characterized by the absence of any long-range order; i.e. no positional order exists over a macroscopic distance. From this basic definition, one may assume that no local or lattice symmetry nor any periodicity is expected in a glass. The solid state physics of disordered materials shows qualitatively different features as compared to the well-known behavior of ordered materials such as single crystals [2]. These qualitatively different physical behaviors basically result from the fact that disorder leads, in general, to broad distributions of the relevant physical parameters which, in turn, results in non-exponential relaxation patterns and non-ergodic

behavior [3]. In optical spectra, strongly inhomogeneously broadened optical absorption and emission profiles occur in glasses caused by the structural disorder. Thus, as opposed to many crystalline systems, the homogeneous linewidth is almost always obscured by the inhomogeneous linewidth that is associated with a static distribution of transition frequencies mirroring the variation in electrostatic (crystalline) fields at the sites of the optically active ions. To extract the information on optical dephasing or homogeneous broadening, one needs to overcome the extreme inhomogeneous broadening of optical transitions in impurity-doped glasses. Fluorescence line narrowing (FLN), spectral hole burning (SHB), and photon echo experiments are widely employed in the study of homogeneous broadening/dephasing in glasses [2-4]. Many experimental investigations have been carried out in inorganic and organic glasses, and a number of theories have been proposed to model the dynamic processes in glasses [5].

In inorganic, organic and ceramic glasses, there are two observed general features of dephasing that distinguish the situation from that of bulk crystalline materials. The first one is the many orders of magnitude increase of the homogeneous linewidth, Γ_{hom}, compared to crystalline systems for the temperature range well below the Debye temperature. The second is the specific form for the temperature dependence of Γ_{hom} in this regime. Reviewing investigations on optical dephasing carried out in glasses [5-6], one finds that the temperature dependence of the homogeneous linewidth for optical transitions associated with impurities is characterized by two regimes: a low temperature regime where the width varies as T^a, with $1 \leq a \leq 1.3$, and a high temperature regime, observed primarily in inorganic glasses, where the width increases with temperature as T^b, with $b \cong 2$. In doped ceramic glasses containing nanocrystals and for nanocrystals

embedded in polymers, an increased magnitude and similar quasi-linear temperature dependence of homogeneous linewidth is also observed at very low temperatures [7-8].

There is strong evidence for two distinct dephasing mechanisms/ homogeneous broadening in glasses. Most frequently observed is the Raman mechanism – a two phonon process, similar to that found in crystalline materials, where the dephasing arises from the random modulation of optical transition frequency coming from the incoherent, quasi-elastic scattering of phonons by the optically active ions. The second mechanism involves a dipole-dipole interaction, probably elastic, between the optically active ions and an array of thermally excited tunneling systems that are associated with local changes in the configuration of ions i.e. two-level systems (TLS). The former has successfully explained the dephasing in glass in the high temperature regime as well as the dephasing in crystalline materials (for both high and low temperatures). The second one (TLS) describes dephasing in glasses at low temperatures.

5.2.1 Two Level Systems (TLS)

The term two-level system is an abbreviated way of characterizing local configurationally changes in the glass. Associated with the configurationally changes are discrete energy levels. In the simplest model, only two states are considered. According to the classical picture, transitions between the states involve thermal excitation over a barrier; whereas in the quantum mechanical picture, tunneling between static configurations is allowed.

TLS were originally introduced to provide the additional density of low energy excitations required for an explanation of the anomalous magnitudes and linear

temperature dependence of the specific heat and thermal conductivity of inorganic glasses [9-10]. In the structural phase space, the model can be described by an ensemble of independent double well potentials [3,6,9]. A specific double well potential characterizes a specific local group of atoms of the disordered material under consideration. The local group is structurally metastable, it can exist in two different energy minima. Disorder is reflected in the fact that one allows for a broad distribution of the relevant parameters.

By limiting consideration to two levels, we can use a pseudospin 1/2 formalism to characterize the states and transitions of the system. The energy levels of the double well potential correspond to spin-up and spin-down states of the pseudospin ($S_z = \pm 1/2$). Transitions between the states can be interpreted as spin flips. Ultrasonic studies have established that the tunneling systems are strongly coupled to the low-lying acoustic modes; relaxation processes (spin flips) involve the emission and absorption of phonons with energies equal to the energy difference of the double well [6].

The coupling of the tunneling system to the strain field generates a long-range elastic dipole interaction in the sense that a pseudospin flip perturbs the strain field a distance r away, with the strength of the perturbation varying as r^{-3}. In addition, since the configurational changes can involve redistributions of charge, the spin flips also modulate the electric fields in the sample, with the long-range effects being determined by the electric dipole moment of the configuration [6].

5.2.2 Homogeneous broadening in glass at low temperatures

For the purpose of rationalizing and understanding the observed homogeneous linewidths of molecules and ions in glasses at low temperatures, a number of different theories have been developed [5,6,11]. The basic premise of all of these is that dephasing in glass is due to the interaction between the optical active ions and TLS [5,6,12-15]. The stochastic and linear response theories are two examples of the models proposed. These two different approaches reach the same temperature dependence at low temperatures for dipole-dipole coupling, but they give different results if other types of coupling are considered. As stated in [16], it is difficult to pinpoint the discrepancy; it appears that it arises from differences in the approaches followed in incorporating the randomness in the spatial distribution of tunneling systems.

The stochastic theory is based on the idea of spectral diffusion of the optical transition due to flipping of the TLS. The interaction responsible for homogeneous broadening is represented by a randomly fluctuating term in the optical transition frequency that is of the form

$$\Delta\omega(t) = \Sigma_j \Delta\omega_j(t) \tag{5.2}$$

where

$$\Delta\omega_j(t) = (A / r_j^s) \sigma_j(t) \tag{5.3}$$

Here A is a constant, and r_j is the distance between the jth tunneling system and optical active ion. $\sigma_j(t)$ denotes a stochastic variable associated with the jth tunneling system taking on the values ± 1. The time dependence of $\sigma_j(t)$ models the spin flip transitions between the two eigenstates of the tunneling system that are induced by phonons, the

interaction of two level systems, and the strain field. The parameter A is proportional to the difference between the diagonal matrix element of the ion-tunneling system interaction evaluated in the excited state of the optically active ion and the same matrix element evaluated in the ground state. Although the elastic dipole coupling is believed to be primarily responsible for the broadening, $\Delta\omega_j$ is written in terms of an arbitrary multipolar interaction (r_j^{-s}). With s = 3(dipole-dipole interaction), a Lorentzian shape for the homogeneous line is obtained with a dephasing rate [13]

$$1/T_2 = CN_0AT \tag{5.4}$$

where C is a constant and N_0 is the spatial density of thermally excited tunneling systems. This linear temperature dependence of the dephasing rates that follows from the model calculations is a consequence of taking the normalized density of states for the tunneling systems $\rho(E,\lambda)$ to be constant, and by only considering the contribution from thermally excited tunneling systems. If this assumption is relaxed by assuming $\int\rho(E,\lambda)\, d\lambda$ (where λ is the tunneling/overlap parameter of the TLS, i.e., $e^{-\lambda}$ represents the overlap between the wave functions for the two potential wells) to vary as E^{μ}, then [5,13]

$$1/T_2 = C\ N_0\ A\ T^{(1+\mu)\,s/3} \tag{5.5}$$

For s = 3, we get $1/T_2 \propto T^{1+\mu}$. According to this result, the variety of quasilinear temperature dependences ($1/T_2 \sim T^{\alpha}$ with α from 1 to 1.3) that are observed experimentally for the dephasing rates may reflect nothing more than small differences in the probability distribution, $\rho(E,\lambda)$, of the tunneling systems.

The linear response theory is based on assumptions as to the specific form of the microscopic Hamiltonian. The Hamiltonian in such an approach includes model terms for the interaction between the TLS and the optical center, and between the TLS and phonons. Based on this theory, homogeneous broadening results from the modulation of optical levels caused by coupling to the diagonal as well as off-diagonal elements of the two-level modes. The main contribution to the dephasing arises from diagonal modulation of abundant but weakly coupled two-level modes. For a general density distribution $\rho(E) \propto E^{\mu}$, a Green's function approach arrives at a temperature dependence of the homogeneous broadening given by [5,6,17]

$$1/T_2 \propto T^{\mu+4-9/s} \tag{5.6}$$

In the case of dipole-dipole coupling, s = 3, the temperature dependence becomes $T^{1+\mu}$. It agrees with that obtained by stochastic theory. For a dipole-quadruple coupling (s=4) a large $T^{1.75}$ behavior is obtained with $\mu = 0$.

In the approach of calculating the homogeneous broadening caused by the flipping of a TLS [11,14,16], the homogeneous linewidth for impurity ions in glass is expressed as

$$\Gamma_h = 4\pi RN_0 \int_0^{r_c} r^2 dr + 2\pi \frac{N_0 A^2}{R} \int_{r_c}^{\infty} r^{2-2n} dr \tag{5.7}$$

when the interaction between the TLS and optically active ions is in the form of A/r^n (an arbitrary multipole interaction). Here R is the relaxation rate of the tunneling systems and

r_c is a cut-off distance given by $A/r_c^n = R$, below which the TLS-ion interaction is considered distance independent. From Eq. (5.7) we obtain

$$\Gamma = 2pN_0\left[2Rr_c^3/3 + A^2 r_c^{3-2n}/(2n-3)R\right] = (2p/3)N_0 A^{3/n} R^{1-3/n}(4n-3)(2n-3)^{-1} \qquad (5.8)$$

If we assume the density of states of the tunneling systems varies as $\rho \propto E^{\mu}$, then the spatial density of thermally excited tunneling systems $N_0 \sim T^{1+\mu}$ ($N_0 = rn(T) = E^m \frac{1}{e^{kT/e} - 1} \propto (T)^m (1 - 1 + \frac{T}{e} - ...) \propto T^{1+m} + \cdots \propto T^{1+m}$). Making the usual assumptions that R is identified with the relaxation rate for tunneling systems for which E $\approx 2kT$, and that for those TLS, $R \sim T^3$, one can get that the linewidth $\Gamma \sim T^{4+\mu-9/s}$.

We have to point out that though a number of theories have been developed, including the stochastic and linear response theory, none of them is advanced enough to be a general theory to explain all of the experimental results obtained in glasses. Another question is: how do the mechanisms expected to dominate at high temperatures (i.e. two-phonon Raman processes) cross over to those active at low temperatures (e.g. two-level systems), though both mechanisms always operate (one is dominant at low T and the other dominates at high T)?

The homogeneous broadening for the ions doped in glass ceramics, which is the main interest of our study, is still under exploration. Our investigations for the homogeneous broadening of RE ions doped in nanocrystals embedded in glass with frequency and time domain techniques will be discussed in detail in chapters 6 and 7.

5.3 Spectral Diffusion

The time dependence of T_2 or Γ_{hom} due to the frequency excursions of the optical dipole is generally referred as "spectral diffusion". It results from slower dephasing processes. A well understood example is the magnetic interaction between an ion and the nearby nuclear spins, which form a frozen core that undergoes slow spin flips in a single crystal [17,18]. Another example, of special interest to this study, is the time dependence of the spectral diffusion in glass due to the large ensemble of TLS's with a broad distribution of tunnel parameters and energy separations between the two levels, which would cause a broad distribution of fluctuation rates.

One way to study spectral diffusion is to conduct optical dephasing measurements for the same system with techniques which require different time scales. For this purpose the photon echo and SHB are frequently employed due to the very different time scales required for these two optical dephasing measurements.

Investigations on the Pr^{3+}:LaF_3 single crystal suggested that optical dephasing of Pr^{3+} is due to fluctuating local fields at the Pr^{3+} ion due to ^{19}F nuclei. The spectral diffusion process induced in the time scale of the SHB measurement was interpreted by the "frozen core" picture. In this picture, most of the local field at the Pr^{3+} ions is considered as static on the time scale of the coherence memory, it behaves as an inhomogeneous broadening. Since the echo is insensitive to inhomogeneous contributions, its decay was determined by the portion of the local field which was dynamic on the time scale of the hyperfine T_2. ^{19}F nuclei nearest the Pr^{3+} ions experience a local field from a large enhanced moment of the Pr^{3+} ion. They are thus detuned from resonance with the bulk fluorine spins and are not able to undergo resonant flip-flop (spin

diffusion) processes. The local field due to these frozen spins is static, the homogeneous dephasing of the hyperfine transition being due to more weakly coupled but freely flipping fluorine spins. If the time scale of the measurement (seconds to minutes) was long enough to give the frozen core enough time to undergo spin flips as well, then spectral diffusion would occur during the measurement time of a SHB experiment.

For the nanocrystal system, because of confinement effects on the phonons, surface effects on the finite boundaries or the interactions with the environments in which the nanoparticles are embedded, spectral diffusion processes could be very different from the case when the ions are doped in single crystals or are contained directly in glass. The study of spectral diffusion in the homogeneous broadening for RE ions doped in nanocrystals embedded in glass is one of our objectives in the study of the oxyfluoride ceramics. SHB, the frequency domain technique, and the two-pulse photon echo, the time domain method, are used in this investigation.

CHAPTER 6.

HOMOGENEOUS BROADENING OF RE IONS IN NANOCRYSTALS EMBEDDED IN GLASS – FREQUENCY DOMAIN STUDY

6.1 Introduction

The dynamical processes of optical active ions have different features and behaviors for the crystalline materials and amorphous glasses. The temperature dependence of the homogeneous broadening, which is an effective way to study the dynamical process, follows different rules for the ions in crystal and glass, and is dominated by different mechanisms. In crystalline materials, relaxation such as two-phonon Raman process usually is dominant, while it is governed by the interactions of the ions with the two-level systems of the glass (TLS) in glass materials. Experimental studies show that at low temperatures the homogeneous line widths of RE ions in glass obey a power law in temperature, $\Gamma_h \sim T^{\alpha}$ with $1<\alpha<2$, while it is $\Gamma_h \sim T^7$ for the ions in crystals. Theoretical investigations suggest that this behavior can be explained by interactions with the TLS of the glass [1-5]. With the recent availability of nanocrystals containing RE ions embedded in glass, it is of great interest to determine whether the rare earth ions, separated from the glassy TLS by the crystalline nanoparticle in which they are contained, also exhibit interactions with TLS. This may provide an independent test of the TLS model and determine the length scale of the interactions.

Materials consisting of insulating nanocrystals doped with RE ions embedded into amorphous (glassy) matrices possess spectral properties very similar to those of bulk crystals including sharp line optical spectra and efficient fluorescence [6]. The sharp line spectra, which allow one to spectrally isolate ions in the nanoparticles from those in the amorphous matrix, laid the basis for applying high-resolution spectral hole burning and FLN techniques to study the dynamical properties of impurity ions doped in the nanocrystals.

Mechanisms responsible for changes in the dynamical properties of the excited states of RE ions in insulating nanocrystals embedded in amorphous matrix, compared to single crystals, can be grouped into two categories: (i) those connected with size restriction effects and (ii) those caused by the interaction of RE ions with the amorphous environment surrounding the crystallites. The effects of the first kind are due mainly to the modification of the phonon spectrum of the nanocrystals at low frequencies, which is the nature of the confinement effects. Such effects have been studied in "free-standing" nanocrystalline materials produced by a variety of techniques [7-9]. The effects of the second kind require mechanisms whose effective length scale is larger than the crystallite size. The interaction of RE ions in nanocrystals with excitations of the surrounding glass matrix is an example of the second and is the object of chapter 6 and 7. In order to determine the dominant mechanisms of the optical dephasing in these materials, low-temperature homogeneous broadening of electronic transitions of RE ions in nanocrystals embedded in amorphous matrices are studied by frequency domain techniques (SHB and FLN in chapter 6), and by time domain methods (photon echo in chapter 7). A simple calculation of the interaction of the RE ions with the TLS of glassy matrix which

excludes the nanocrystal volume containing the RE ions provide evidence that it is the interaction with the TLS that dominates the homogeneous broadening of RE ions. The long range nature of the interaction with the TLS in nanocrystals embedded in glass matrix is demonstrated by the results.

6.2 Experiments

Two types of samples are studied. Monoclinic Y_2O_3:Eu^{3+} nanocrystals dispersed in siloxane polymer, which were produced by condensation after laser evaporation [10], were selected for comparing the homogeneous broadening of nanoparticles embedded in matrix with that of free nanoparticles. In the second case, samples of Eu^{3+} and Pr^{3+} doped LaF_3 nanocrystals embedded in transparent oxyfluoride glass ceramics [6] were studied for nanoparticles sizes in the range of 10-23 nm. The concentration of RE ions was 0.05% for which the nanoparticles are contained in oxyfluoride ceramic samples, and is 0.1% for monoclinic Y_2O_3:Eu^{3+} nanocrystals. Due to segregation effect, the concentration of RE ions in the LaF_3 nanocrystals is actually a few times higher than the average and a fraction of the RE ions is always present in the matrix. Despite the drastic differences in preparation, both of these materials (Y_2O_3 and LaF_3) consist of insulating nanocrystals of similar sizes (~10-25 nm) embedded in an amorphous matrix. We interpret their general properties in terms of the same mechanism that applies to both despite their independent preparation techniques and the difference in the amorphous matrix. This is supported by the fact that the dynamics of ions and molecules in amorphous media seem to show a universal behavior for a wide range of glassy media [11-12].

The spectral HB and FLN measurements were performed with samples mounted in a liquid helium cryostat. For the HB experiments, the $^7F_0$ - $^5D_0$ transition of Eu^{3+} and the $^3H_4$ – $^1D_2$ transition of Pr^{3+} were selected. A few mW of cw light from the dye laser, Coherent CR599 (frequency jitter ~2MHz), was tuned to the corresponding frequencies and loosely (d ~ 0.5mm) focused on the samples. The transient HB spectrum (lifetime seconds (Pr) to minutes (Eu)) was obtained with a repetitive burn/scan sequence (scan time ~0.5 s) using fluorescence detection with a PMT through appropriate interference filters or a spectrometer. The data was averaged and stored on a digital oscilloscope. The hole widths obtained on single-crystals, for which the homogeneous linewidth is much less than the spectral resolution for the HB technique, were used to estimate the instrumental contribution to the line width that was subtracted from all data.

For (FLN) measurements, the same laser, resonant with the $^3H_4$ –$^1D_2$ transition of Pr^{3+}, provided ~30mW output power was employed. The resonant FLN fluorescence was selected with an interference filter and analyzed with a scanning Burleigh RC-140 Fabry-Perot interferometer. In order to block the excitation light from the detection system during the collection of fluorescence, an acoustic-optic modulator (AOM), which was electronically synchronized with the chopper wheel in fluorescence collection path, was introduced into the setup. Because the lifetime of the $^1D_2$ state, which is the time region allowing the observation of resonant FLN signal, is ~0.6 ms, the period of light on/off were set at < 0.5ms.

6.3 Results and discussion

There are three sites, A, B, and C for Eu^{3+} ions in Y_2O_3 monoclinic crystallites [13]. The coordination of two cation sites (site C and site B) can be described by six oxygens at the spaces of a trigonal prism with a seventh oxygen lying along the normal to a face. The coordination of the third site (site A) is described as a distorted octahedron with a seventh oxygen along a three-fold axis at very long distance. Fig. 6.1 shows the temperature dependence of the width of spectral holes, Γ_{HB}, burned in the $^7F_0$ - $^5D_0$ transition of Eu^{3+} ions located on the C sites (λ=582.8 nm) in 23nm Y_2O_3 monoclinic crystallites [10] dispersed in siloxane polymer. These results are compared with the analogous SHB data obtained with the free-standing, as-prepared, nanocrystals of the same size [8]. The hole burning occurs due to redistribution of the population of the ground state hyperfine levels of those ions whose hyperfine transitions are resonant with the laser [8,12]. The sample with nanocrystals embedded into the polymer matrix exhibited a drastic increase in hole width. A very different power law behavior for the temperature dependence of the hole widths relative to those of the same isolated nanoparticles is obtained too. The $\sim T^3$ temperature dependence of the hole width observed for isolated nanoparticles [8-9] becomes ~T for nanoparticles embedded in the polymer. Although the $\sim T^3$ behavior is not clearly evident for the 23 nm sample studied here, it is much more evident in the samples with smaller nanoparticles [8-9]. The nearly linear temperature behavior of Γ_{HB} in nanoparticles surrounded by the polymer matrix is very similar to that observed for Eu^{3+} doped glasses [12].

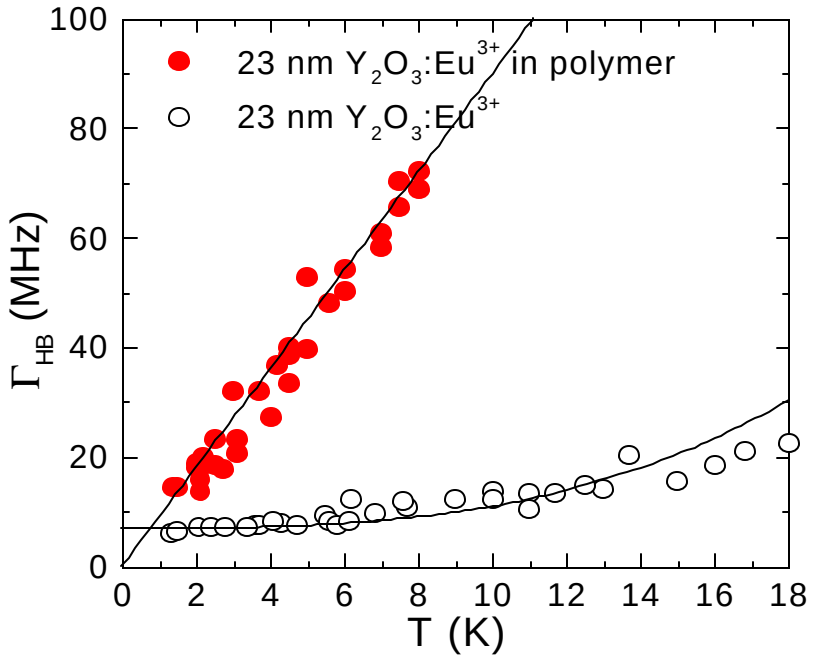

Fig.6.1. Temperature dependence of the hole width for Eu^{3+} in Y_2O_3 nanocrystals. Solid lines: Γ_{HB}~T (embedded in polymer) and Γ_{HB} ~T^3 (isolated, as prepared).

The hole-burning results, which reflect the homogeneous linewidth $\Gamma_h(T)$ of electronic transitions ($\Gamma_h=\Gamma_{HB}/2$) suggest that the dominant mechanism for the homogeneous broadening of the $^7F_0$ - $^5D_0$ transition of Eu^{3+} in Y_2O_3 nanocrystals embedded in the polymer is identical to that which is responsible for homogeneous broadening found for ions in glasses. In glasses below 10K it is typically observed that Γ_h~T^{α} ($1<\alpha<2$). As discussed above, such a temperature dependence of the homogeneous line width has been interpreted in terms of the interaction of an impurity ion with two-level systems (TLS) [1-5]. Since the TLS – rare earth ion interaction is usually assumed to be of an elastic dipole-dipole nature [1-2, 4-5] it is relatively long-range. We consider

the possibility that such a long-range interaction may be effective at distances as large as the size of these nanoparticles and hence may be responsible for the homogeneous broadening of the optical transitions of RE ions contained inside the nanocrystals.

In order to examine whether this temperature dependent broadening is in fact a general property of RE-doped nanocrystals in amorphous media, oxyfluoride glass ceramic samples containing LaF_3 nanocrystals (0.05%Eu) were also studied. In Fig.6.2 the temperature dependencies of widths of holes burned in the $^7F_0$ - $^5D_0$ transition of Eu^{3+} (λ=578.2 nm) are shown for a series of samples containing different particle sizes obtained with different annealing temperatures as discussed earlier in section 4.2. The temperature dependence of the hole width for Eu^{3+} ions contained directly in the glassy matrix is also shown (some amount of rare earth impurity ions always remains in the glass matrix). The nearly linear temperature dependence of the hole width, Γ_{HB}~T, as well as the spectral dependence of the hole width as the laser is tuned inside the broad $^7F_0$ - $^5D_0$ transition of the glassy component (not shown) is very similar to that observed for other Eu^{3+} doped glasses [12]. The character of the temperature dependencies of the hole widths for Eu^{3+} ions in nanocrystals embedded in the glass and for those ions contained directly in the glass matrix is similar (Γ_{HB} ~T), but the line width for the latter is significantly larger. It is important to note that the broadening decreases with an increase of nanocrystal size. The hole widths of the ceramic samples containing 17 and 19 nm average particle sizes were indistinguishable and for the 14 nm average particle size sample, the holes only survived to 2 K so that their temperature dependence could not be obtained.

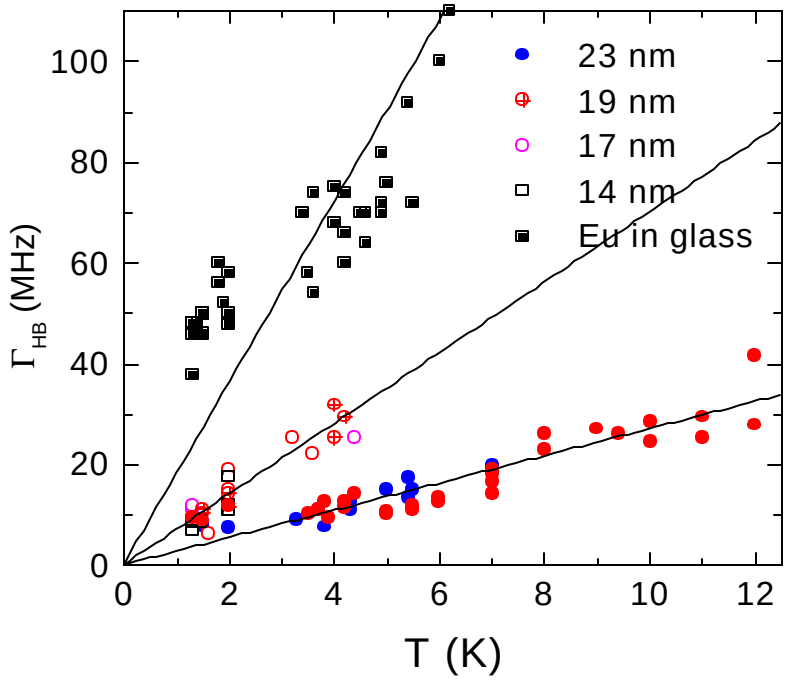

Fig.6.2. Temperature dependence of the hole width for Eu^{3+} in LaF_3 nanocrystals of different size embedded in oxyfluoride glass ceramics and for Eu^{3+} directly doped into the glass matrix. Solid lines: $\Gamma_{HB} \sim T$.

For the $^3H_4$–$^1D_2$ transition of Pr^{3+} (λ=592.5 nm) doped in LaF_3 nanocrystals embedded in oxyfluoride glass, the SHB results (shown in Fig.6.3) are little different at T < 4 K from what was observed with Eu^{3+} ions as shown in Fig.6.1 and 6.2. However, above 4K, a rapid non-linear increase in Γ_{HB} with temperature appears, as previously observed for Tm^{3+} in these oxyfluoride ceramics [14]. We have therefore fit the data with the sum of a quasi-linear plus a power law term. The best fits to the data gives us the temperature dependencies of

$$\Gamma_{HB}(^1D_2) = (42 \pm 4) + (6.4 \pm 0.5) \cdot T^{1.3} + (0.005 \pm 0.001) \cdot T^{(5\pm2)} (\text{MHz}) \quad \text{for (b)}$$

and $\Gamma_{HB}(^1D_2) = (18 \pm 6) + (1.0 \pm 0.4) \cdot T^{1.3} + (0.0036 \pm 0.0003) \cdot T^{(6\pm1)} (\text{MHz})$ for (c),

which still suggests the presence of a quasi-linear temperature dependence of the hole width at T<4K for RE ions doped in glass ceramics. This quasi-linear ($\sim T^{1.3}$) dependence, which is similar to that observed for Pr^{3+} ions in glasses (as shown in Fig. 6.3(a)), where it was found [12] that $\Gamma_{HB} \sim T^{1.3}$, further supports the idea that interactions of RE ions contained in the nanocrystals with the TLS of the glass dominate the optical dephasing. The higher power term in the hole width will be discussed in chapter 7 where the linewidth is obtained with time domain techniques such as the two-pulse photon echo.

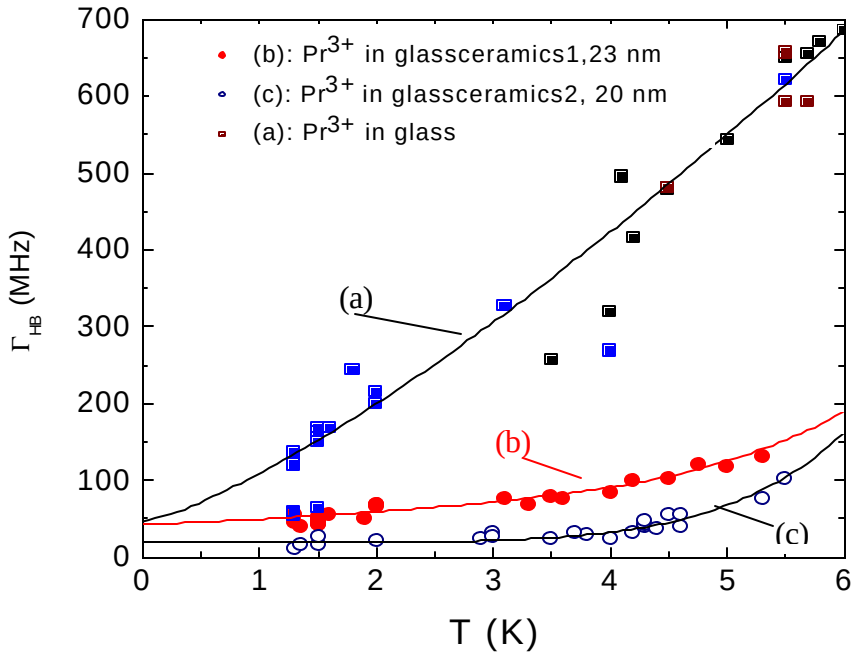

Fig.6.3. Temperature dependence of the hole width for Pr^{3+} directly doped into the glass (a); and for Pr^{3+} in LaF_3 nanocrystals embedded in oxyfluoride glass ceramics (b) and (c). Solid lines: (a): $\Gamma_{HB} \sim T^{1.3}$.

$$(b): \Gamma_{HB}(^1D_2) = (42 \pm 4) + (6.4 \pm 0.5) \cdot T^{1.3} + (0.005 \pm 0.001) \cdot T^{(5\pm2)} (\text{MHz}).$$

$$(c): \Gamma_{HB}(^1D_2) = (18 \pm 6) + (1.0 \pm 0.4) \cdot T^{1.3} + (0.0036 \pm 0.0003) \cdot T^{(6\pm1)} (\text{MHz})$$

Note: the glass ceramics 1 and 2 content different glass components.

The results of these hole burning measurements suggest that the homogeneous broadening of optical transitions of RE ions in nanocrystals embedded in amorphous materials is determined by interactions with the TLS of the amorphous matrix. The drastic effects on the magnitude and temperature dependence of the hole line width upon embedding the nanocrystals into a polymer (Y_2O_3:Eu^{3+}) and a glass (LaF_3:Eu^{3+}, LaF_3:Pr^{3+}) support this suggestion and provide direct evidence for the long-range character of the TLS-RE interaction.

In order to obtain a semi-quantitative description of the dependence of the homogeneous broadening on the size of the nanocrystals we apply Eq.5.7 to calculate the homogeneous broadening caused by the flipping of the TLS. In this approach the homogeneous broadening is calculated as a sum of contributions of each TLS. It has the advantage that it provides a simple means to calculate the dependence of the homogeneous broadening on the nanoparticle size since it makes it possible to exclude the nanocrystal volume about the RE ion that does not contain any TLS. For the case of dipole-dipole interactions (~A/r^3), Eq.5.7 gives homogeneous linewidth for an ion in glass as

$$\Gamma_h = 4p\,RN_0 \int_0^{r_c} r^2 dr + 2p\,\frac{N_0 A^2}{R} \int_{r_c}^{\infty} r^{-4} dr \qquad (6.1)$$

The first term describes the contribution of “near” TLS; the second accounts for interactions with more distant TLS whose interaction with the RE ions falls according to the dipole-dipole nature of the interaction. In order to exclude the nanocrystal volume that contains no TLS, the integration should be performed excluding $r < r_0$ (r_0 – the nanoparticle radius). For this semiquantitative description we consider all RE ions to be

located at the center of the nanocrystals. We also neglect the difference in elastic properties of the glass and crystal in calculating the elastic interaction. Then we have

$$\Gamma_h = \begin{cases} 2pN_0A - \dfrac{4p}{3}N_0Rr_0^3 & (r_0 < r_c) \\ \dfrac{2pN_0A^2}{3R}r_0^{-3} & (r_0 > r_c) \end{cases} \tag{6.2}$$

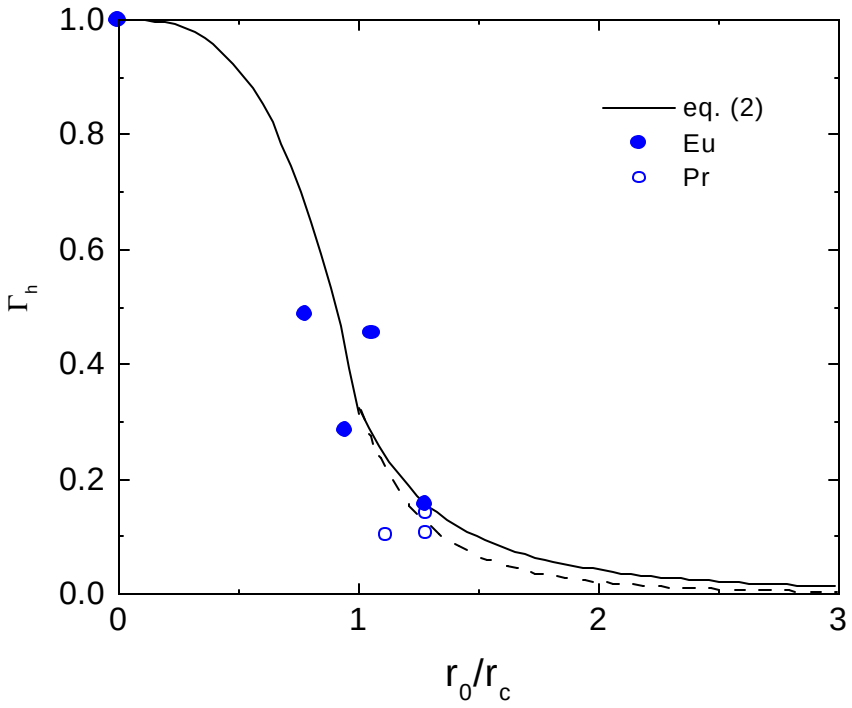

Fig.6.4. The dependence of homogeneous linewidth on nanocrystals radius (normalized to Γ_h=1 for ions in glass). Solid line – equation (1), circles – experimental data for Eu^{3+} (solid) and Pr^{3+} (open) in LaF_3 nanocrystals in oxyfluoride glass ceramics. Dashed line - the ~ r_0^{-4} behavior of $\Gamma_h(r_o)$.

In Fig.6.4, $\Gamma_h(r_o)$ of Eq. (6.2) is plotted vs. r_0/r_c normalized so that Γ_h=1 at r_o=0. On the same figure, the experimental hole widths (T=5K) obtained with oxyflouride glass

ceramic samples containing $LaF_3:Eu^{3+}$ nanocrystals of different sizes (Fig.6.2) are normalized to $\Gamma_h(r_o=0)=1$ ($\Gamma_h=1$ for ions in glass) and fitted to the curve (Eq.6.2) using r_c as an adjustable parameter. The hole widths were estimated from the experimental data (Fig.6.2) by fitting the linear $\Gamma_h(T)$ dependence to the experimental hole widths in the vicinity of T=5K. The temperatureT=5K was chosen because around this temperature we have the most complete set of data for all nanoparticles sizes. At the same time the data do not suggest a significant temperature dependence of r_c. A reasonable fit of the experimental data to Eq. (6.2) occurs at r_c=9nm which may be considered as an independent estimate of r_c for Eu doped oxyfluoride glass. The more limited set of data (obtained with the samples with different chemical compositions) for Pr^{3+} doped samples, also shown on Fig.6.4, is also consistent with Eq.6.2 assuming the same value of r_c=9nm. The dashed curve in Fig.6.3 presents the $\sim r_0^{-4}$ behavior of $\Gamma_h(r_o)$ appropriate for the case $r_o>r_c$ (normalized) which would correspond to the situation in which the dominant role in homogeneous broadening belongs to the TLS located at the nanocrystal-glass interface if their concentration was much greater than that in the bulk. Data for larger nanocrystals are necessary to exclude (or confirm) such a possibility.

While the calculation using Eq.6.2 is not very rigorous, it does provide an estimate of the dependence of the homogeneous broadening of the optical transitions of RE ions on the size of nanocrystals. The result of the calculation supports the hypothesis that the homogeneous line width is dominated by interactions of RE ions with the TLS of the glass matrix [15]. A more careful theoretical treatment as well as experimental studies with nanocrystals of larger size are necessary to further test this hypothesis.

FLN experiments were performed with oxyfluoride glass ceramics containing Pr^{3+} doped LaF_3 nanocrystals. The transition from the upper sublevel of the two lowest $^1D_2$ excited states to the ground state is π-polarized and lies at 591.7 nm, whereas the 592.5 nm transition from the lower sublevel is σ-polarized (inset in Fig.6.4). Previous studied of Pr^{3+} in LaF_3 crystals show that the one-phonon relaxation process is responsible for the homogeneous broadening of the fluorescent transitions between the sublevels of excited and ground states [10]. In nanocrystals the low-frequency phonon spectrum is modified and the one-phonon relaxation rate between the excited state sublevels may be changed compared to that of single-crystals. The change of the relaxation rate could be reflected by the homogeneous broadening of the upper sublevel.

Fig.6.5 shows the temperature dependence of the homogeneous linewidth of the $^1D_2$–$^3H_4$ π–transition for LaF_3:Pr^{3+} 23 nm nanocrystals in oxyfluoride glass ceramics doped with 0.05% Pr, and that of the same transition in a LaF_3:0.1%Pr^{3+} single-crystal. No difference in the homogeneous linewidth was observed between the embedded nanocrystals and the single-crystal, which suggests that the phonon spectrum in nanocrystals is not significantly modified at 23 cm^{-1}. This may be because the size of nanocrystals is not small enough to cause significant changes their phonon spectra at low frequencies. Comparing these FLN results with the HB results obtained in the previous section, the interaction between Pr^{3+} ions and the TLS system, which significantly modified the homogeneous linewidth of the σ transition at $T<5\ ^oK$, seems to play no role in relaxation between the excited state sublevels at $T>10\ ^oK$.

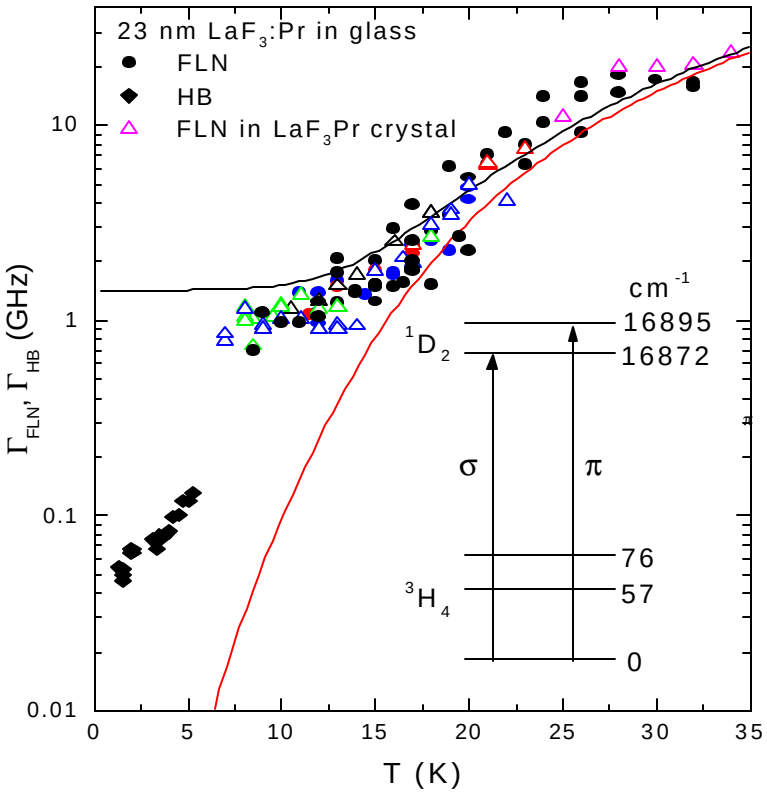

Fig.6.5. Temperature dependence of the fluorescence line narrowed width for Pr^{3+} in LaF_3 nanocrystals embedded in oxyfluoride glass ceramics and for Pr^{3+} in LaF_3 single-crystals. The hole burning data for the glass ceramics are also shown. Thin solid lines – theoretical curves from Ref.[2].

The width of the holes burned in $^1D_2$–$^3H_4$ σ transition as well as the theoretical homogeneous linewidth of σ and π transitions [10] are also plotted in Fig.6.5. A good agreement of the experimental data with theoretical predication is clearly displayed. At higher temperatures T>20 ^oK the homogeneous widths of σ and π transitions are getting similar, therefore the FLN data obtained for π transition may be used for the σ transition. Thus, the HB data on the σ transition together with the FLN data on the π transition (with

some interpolation) give an estimate of the homogeneous broadening of $^1D_2$–$^3H_4$ σ transition in Pr^{3+} ions in nanocrystals embedded in glass.

It may be concluded that at low temperatures the homogeneous broadening is determined by the interaction of RE ions in nanocrystals embedded in the glassy matrix with TLS of the glass, whereas at higher temperatures the one-phonon processes dominates the homogeneous broadening [16]. In addition, for nanoparticles ~ 20 nm in size, the phonon density of states for 23 cm^{-1} phonons and their coupling to the electronic states of the RE ions in nanoparticles are nearly identical to those in bulk single crystals.

At the end of this chapter, we need to point out that there could be some spectral diffusion effects that contribute to the homogeneous linewidth in the frequency domain methods such as SHB and FLN, for which a long time scale is required for the measurement. A discussion on the contribution of spectral diffusion to the linewidth will be presented in chapter 7 following the time domain measurement of the homogeneous broadening.

CHAPTER 7

HOMOGENEOUS BROADENING OF RE IONS DOPED IN NANOCRYSTALS EMBEDDED IN GLASS – TIME DOMAIN STUDY

7.1 Introduction

The photon echo method has been an excellent technique for studying coherent optical phenomena such as homogeneous broadening in many materials [1]. A comparison of the results of this technique with that of spectral hole burning (SHB), enables one to minimize the effects of spectral diffusion, which occur on the time scale of SHB measurements. The photon echo method is also employed to gain information on the physical properties of the system hosting the echo generating species, though initially it was designed to investigate the nature of coherence itself [1,2]. Since optical coherence is very sensitive to fluctuations in the environment, photon echoes can be used for investigating the dynamical processes that result from the ubiquitous "two-level systems" (TLS) [3-6]. The high optical frequency selectivity of rare earth (RE) doped inorganic crystals, whose homogeneous linewidths can be of the order of kHz, combined with the high frequency resolution of the photon echo technique has rendered possible the study of phenomena not amenable by other techniques.

For RE ions doped nanocrystals embedded in glass, our study of SHB, as presented in the previous chapter, suggests that at low temperatures, the interaction of RE ions with TLS of the glass dominates the optical dephasing [7]. The homogeneous line

widths are sensitive to the size of the nanocrystals, and they exhibit a quasi-linear temperature dependence. Since a rather longer time scale (ms) is necessary in the dephasing measurement of SHB, the effects of spectral diffusion can contribute to the obtained homogeneous linewidth. This possible spectral diffusion effect can be minimized with the photon echo technique, and the spectral diffusion can be investigated by combining the study of photon echo and SHB. In this chapter, the optical dephasing process of RE ions doped in LaF_3 nanocrystals embedded in oxyfluoride glass is studied by the two-pulse photon echo technique. The optical dephasing time T_2 of Pr^{3+} ions contained in different size LaF_3 nanocrystals embedded in the glass ceramics is presented. An exponential temperature dependence of the echo intensity is observed and a quasi-linear temperature dependence of the dephasing time is obtained. We also discuss the possible spectral diffusion effects involved in the optical dephasing during the time scale of SHB measurement.

7.2 Experiments

Samples used for the photon echo studies are 0.5 mol % Pr^{3+} doped LaF_3 nanocrystals embedded on oxyfluoride glass annealed at different temperatures. The specific fabrication procedure of the Pr^{3+} doped glass sample is the same as discussed in section 4.2. The glass samples were annealed at 750 ^oC and 725 ^oC for 4 hours in air, respectively, to obtain the different size nanocrystals. The characterization of the samples annealed at different temperatures was made by XRD (X-Ray Diffraction). We will denote the sample annealed at 750 ^oC for 4 hours, which looks cloudy after the annealling, as 750-4 (cloudy). The one annealed at 750 ^oC for 4 hours, but looks clearer,

is named as 750-4 (clear). 725-4 refers to the sample annealed at 725 ^{o}C for 4 hours. The samples were mounted in a liquid helium cryostat, and all of the measurements were conducted at 1.3 K. The measurement on the temperature dependence of echo intensity were carried out under temperatures from 1.3 K to 8 K.

The experimental apparatus consists of a pair of Nd:YAG-pumped dye lasers and three electro-optical modulators (EOMs) with a response time of less than 10 ns. The specific setup and detailed synchronization is the same as discussed in section 3.2.(3). The timing of two dye lasers were set in such a way that the delay of the second beam (π pulse) with respect to the first one ($\pi/2$ pulse) is continuously adjustable from zero to hundreds of ns. The two pulses are completely overlapped in frequency and spatial configuration. The two collimated and superimposed pulses were focused at the sample with a 30 cm focal lens. The size of the focal point at the sample is about 0.2 mm^2, and the energy of the lasers at the sample are about 100 μJ for both pulses. Three EOMs, acting as fast shutters, are synchronized with the laser pulses so that the scattered light from the sample can be effectively gated from the echo signal by properly choosing the trigger position of the EOMs. The echo signals were detected with a PMT and a digital oscilloscope was used to display and collect the data of the echo signal. During the photon echo measurements, the two laser pulses, which have a 3 GHz bandwidth for both, are tuned so as to be resonant with the lowest $^3H_4$ to $^3P_0$ optical transition of Pr^{3+} ions in the LaF_3 nanocrystals (λ=477.8 nm).

7.3 Results and discussion

7.3.1 Optical dephasing of Pr^{3+} ions in LaF_3 nanocrystals embedded in oxyfluoride glass

As a group, the RE ions with an even number of 4f electrons, when doped into crystalline sites of less than axial symmetry, show long optical coherence times at low temperatures. This is because their f-f transitions are between nonmagnetic electronic levels and optical dephasing at low temperatures is magnetic in origin, arising from nuclear- or electronic-spin fluctuations of host lattice nuclei or paramagnetic ions. The system of Pr^{3+} doped LaF_3 crystal is a good example of the case. For Pr^{3+}:LaF_3 single crystals, the previous study of SHB and the photon echo has shown that the dephasing time, T_2, is 6 μs (Γ_{hom} = 53 kHz) for the $^3H_4 - {}^1D_2$ transition and 2.4 μs (Γ_{hom} = 133 kHz) for the $^3H_4 - {}^3P_0$ transition [1]. The similarity of T_2 for these two transitions is to be expected since the dominant contribution comes from magnetic interactions within the ground state (magnetic interactions between the Pr^{3+} ions and surrounding ^{19}F nuclei, or at higher temperatures, by phonon induced dephasing). The study of modulations of the photon echo decay of the $^3P_0$ transition revealed the splitting of the ground and excited states [8].

For Pr^{3+} ions doped in LaF_3 nanocrystals embedded in oxyfluoride glasses, SHB and FLN (fluorescence line narrowing) studies on the $^1D_2$ transition exhibit much broader homogeneous linewidths (10 to 100 MHz) than that of the transition in a single crystal [7]. This corresponds to a ~10^1 nanosecond dephasing time, $T_2=1/\pi\Gamma_{hom}$. For the $^3P_0$ transition, our two-pulse photon echo study also suggests a similar optical dephasing time of Pr^{3+} ions in nanocrystals embedded in the glass ceramics. Fig.7.1 shows the photon

echo signal obtained at various delay times. Since the photon echo is always just following the second pulse, we need to exclude the possible overlap of the second pulse on the echo signal when we measure the intensity of the echo signal. In Fig. 7.1, the solid lines are the echo signal with two laser pulses, and the dash lines are isolated second laser pulses that were obtained with the first laser pulses blocked. The intensity of the photon echo is obtained as the peak height of the echo signal (solid line) after subtracting the corresponding peak height of the isolated pulse 2 (dashed line). No echo signal was detected when the delay time was increased above 55 ns for the sample with the biggest available nanocrystals (sample 750-4 (cloudy)). We did not observe any echo signal for the samples annealed at 700 ^{o}C or lower even with the shortest practical delay time (15 to 20 nanoseconds). Fig.7.2 shows the photon echo decay of the $^{3}H_{4}$-$^{3}P_{0}$ transition at 1.3 K in 0.5%Pr^{3+}:LaF_{3} nanocrystals embedded in oxyfluoride glass annealed at different temperatures. The solid lines are exponential fits to the experimental data (shown by circles in the figure). The results of the data fit to the decay of echo intensity gives dephasing times of T_2 = 48 $\pm$ 3 ns, 36 $\pm$ 3 ns, and 32 $\pm$ 2 ns for samples of 750-4 (cloudy), 725-4, and 750-4 (clear), respectively.

The previous SHB study showed that the homogeneous line width increased as the size of the nanoparticles decreased, i.e., the dephasing time, T_2, increases with nanoparticle size. In principle, bigger nanocrystals should be nucleated from higher annealing temperatures. The T_2 values in Fig.7.2 are not consistent with this statement since the 750-4 clear sample has a shorter T_2 value than that of the 725-4 sample. Therefore, we attempted to measure the size of the nanoparticles by X-Ray Diffraction

(XRD). The results of the characterization done at Corning on the samples used in the photon echo study are shown in table 7.1.

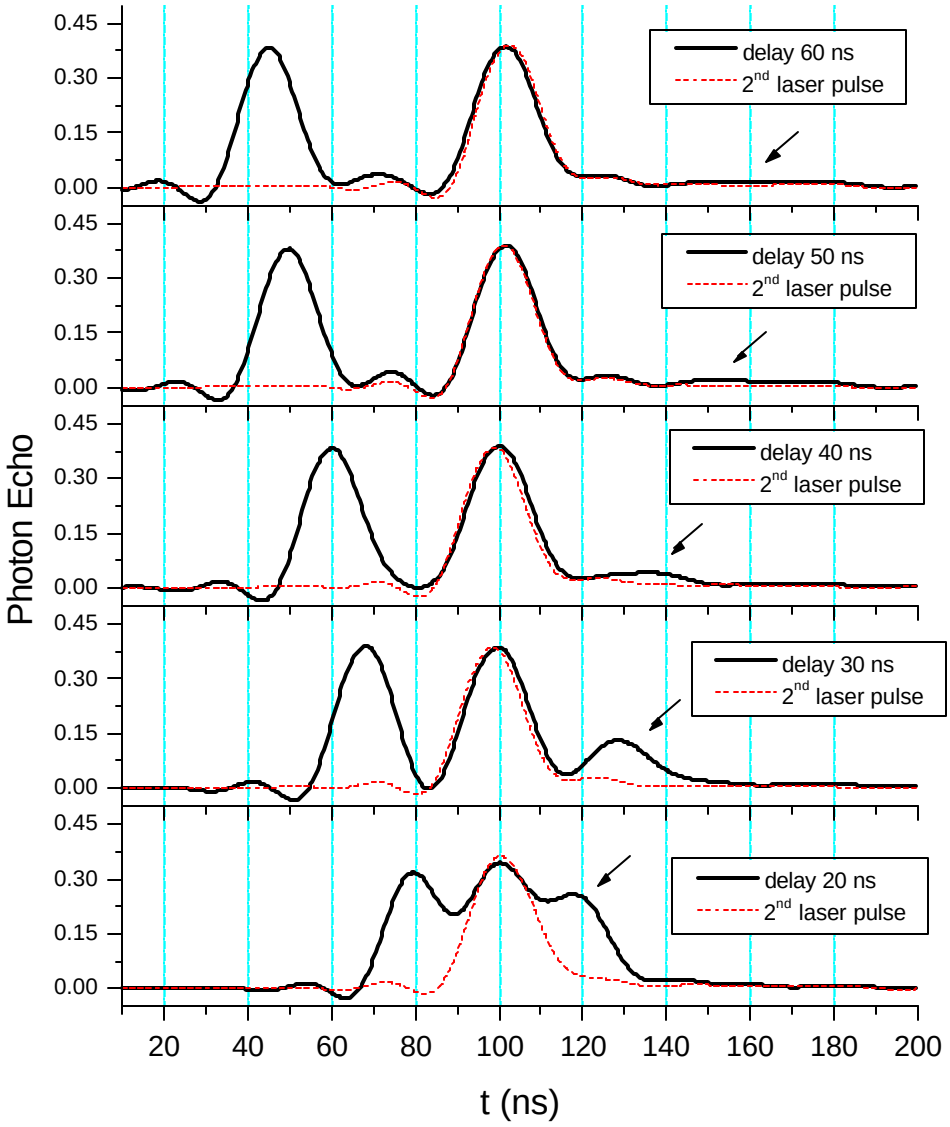

Fig.7.1: Two-pulse photon echo for $^3H_4$-$^3P_0$ transition of Pr^{3+} ions with different delay times. The sample is 0.5%Pr^{3+}:LaF_3 nanocrystals embedded in oxyfluoride glass ceramics annealed at 750^{o}C for 4 hours (750-4 (cloudy)). T = 1.3 K.

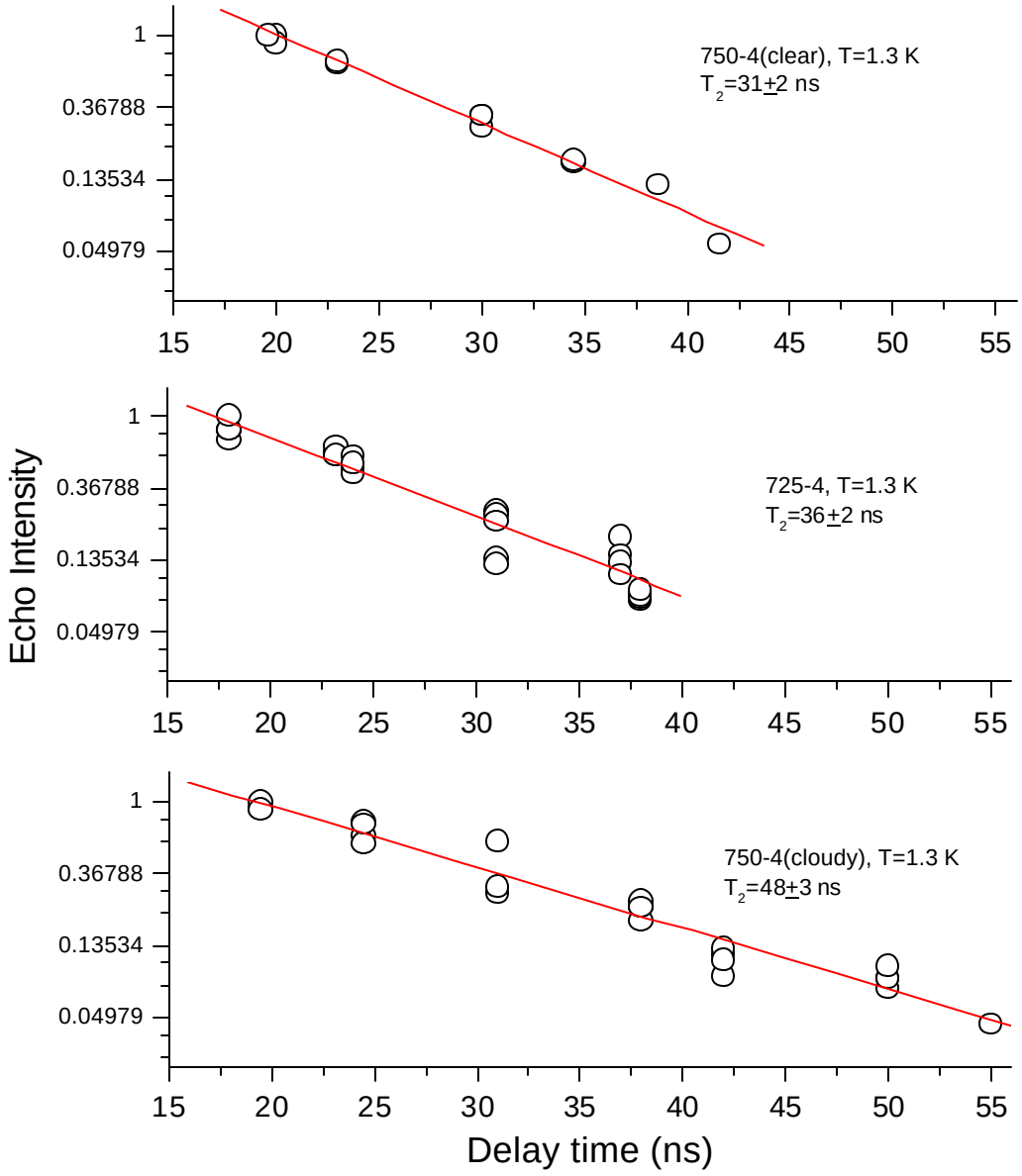

Fig.7.2: The echo intensity versus delay time for $^3H_4$-$^3P_0$ transition of Pr^{3+} ions. The samples are 0.5%Pr^{3+}:LaF_3 nanocrystals embedded in oxyfluoride glass ceramics annealed at 750 ^oC for 4 hours (750-4 (cloudy)) (a); 725 ^oC for 4 hours (b); and 750 ^oC for 4 hours (clear) (c), respectively. T = 1.3 K. Solid lines data fit results. The T_2 obtained form the data fit are 48±3 ns for (a), 36±2 ns for (b), and 31±2 ns for (c).

Table 7.1 Characterization of the samples with XRD

Sample	Particle size (nm) (Low angle line)	Particle size (nm) (High angle line)	Particle size (nm) (Average)
750-4 (clear)	34.1	39.7	36.9
725-4	37.1	36.2	36.6
750-4 (cloudy)	36.4	34.5	35.4

The XRD results show that the three samples have average sizes that are essentially indistinguishable. Obviously, the XRD results do not give us the distribution of nanoparticle sizes as we expected from the values of T_2 in Fig.7.2. This might be explained by considering the following factors: Firstly, there is a broad size distribution for nanoparticles in glass obtained by the heat treatment of the glass sample. Usually, about 90 % of the particles are within 7.5 nm of the average. Next, the nanoparticles obtained through heat treatment of the glass sample are inhomogeneously distributed in the glass matrix. There could be a significant difference in the region where the echo was produced from where the characterization of the sample was done by the XRD. In addition to these uncertainties, the photon echo experiment only was able to be carried out with the samples annealed over a very limited range of the annealing temperature, namely, around 725 ^{o}C to 750 ^{o}C in our study. If the annealing temperature goes too high, the sample becomes so opaque that it will not be possible to transmit enough light to detect the echo and scattering increases. Samples with lower annealing temperatures do not have enough absorption to create the echo signal due to the smaller volume fraction of nanocrystals nucleated in the glass matrix. Furthermore, the smaller nanoparticles will

reduce T_2 even further, making the observation of the photon echo signal more difficult. As shown in Fig.7.2, our photon echo study was only done with the samples annealed from 725 ^oC to 750 ^oC. Considering fluctuations of the actual temperature during the heat treatment process, we can see that within this narrow range of temperatures it is hard to characterize the particle size based on the annealing temperature.

7.3.2 Temperature dependence of T_2 and corresponding homogeneous broadening

The observed T^7 temperature dependence of the homogeneous broadening at low temperatures for Eu^{3+} ions doped in single crystals has been well described by the two-phonon Raman process [9]. For Pr^{3+} ions, the direct single-phonon process coupling the nearby electronic levels, determines dephasing in bulk LaF_3. However for the nanocrystals at low temperature, coupling with the TLS dominates the direct process which therefore does not play a significant role as explained in detail later. As the size of the crystal is reduced to the nanoscale, the dynamical properties of the homogeneous broadening exhibit very distinct behaviors. For isolated free nanocrystals doped with RE ions, the homogeneous broadening follows a T^α (where α is 3 ~ 4) temperature dependence at low temperatures due to the discrete acoustic-phonon modes energies with a low-frequency gap, which is a result of the confinement effect of the nanoscale size [10]. When the nanocrystals are embedded in glass, a T^β (β is 1 ~ 2) temperature dependence of the homogeneous broadening is observed [7] for RE ions doped in the nanocrystals, which is similar to what happens when the ions are directly in the glasses [11]. The interaction of the RE ions doped in nanocrystals with the TLS of the glass in which the nanocrystals are embedded can explain the observed quasi-linear temperature dependence [3-7]. Since spectral diffusion might contribute to the broad Γ_{hom} over the

time scale of a frequency domain method such as SHB, it is also necessary to investigate the dynamical process of the homogeneous broadening with a time domain method, for which a long time scale measurement is not required.

To explore the mechanisms governing the dynamical properties of T_2 using the photon echo measurement, we measured the temperature dependence of the photon echo intensity at a fixed optical delay. Fig.7.3 shows the photon echo intensity versus temperature with a fixed 18.5 ns delay for the sample 750-4 (clear). No photon echo signal was observed when the temperature T is over 8 K. Since the echo intensity is proportional to $\exp(-4\tau/T_2)$, where τ is the delay time of the second laser pulse, the best data fit to the experimental data presented in Fig. 7.3 with the function of the echo intensity $I = Ae^{-4t/T_2}$ (solid line in Fig.7.4) gives us a temperature dependence of T_2 as $1/T_2 \propto T^{1.1}$.

If the homogeneous linewidth Γ_{hom} has a temperature dependence $\Gamma_{hom} = A + B*T^{\alpha}$, as found from the SHB results, then the parameters A, B, and α can be determined by fitting the experimental data. Considering that T_2 is related to Γ_{hom} by $T_2=1/\pi\Gamma_{hom}$, and the echo intensity $I = Ae^{-4t/T_2}$, the best fit to the experimental data plotted in Fig.7.3 and Fig.7.2(c) gives the temperature dependence of the homogeneous broadening as

$$\Gamma_{\mathrm{hom}}^{echo}({}^3P_0) = (7.3 \pm 0.6) + (1.4 \pm 0.1)T^{(1.1\pm0.3)}(\mathrm{MHz}) \qquad (7.1)$$

for the $^3H_4$ - $^3P_0$ transition. A quasi-linear temperature dependence of the homogeneous broadening is obtained with the two-pulse photon echo technique for Pr^{3+} ions in nanocrystals embedded in glass.

As discussed previously for SHB, this quasi-linear temperature dependence can be explained by assuming that the RE ions doped in nanocrystals are dipolar coupled to a bath of two-level system (TLS) of the glass [5, 12-14], i.e., by the interactions of RE ions with TLS of the glass.

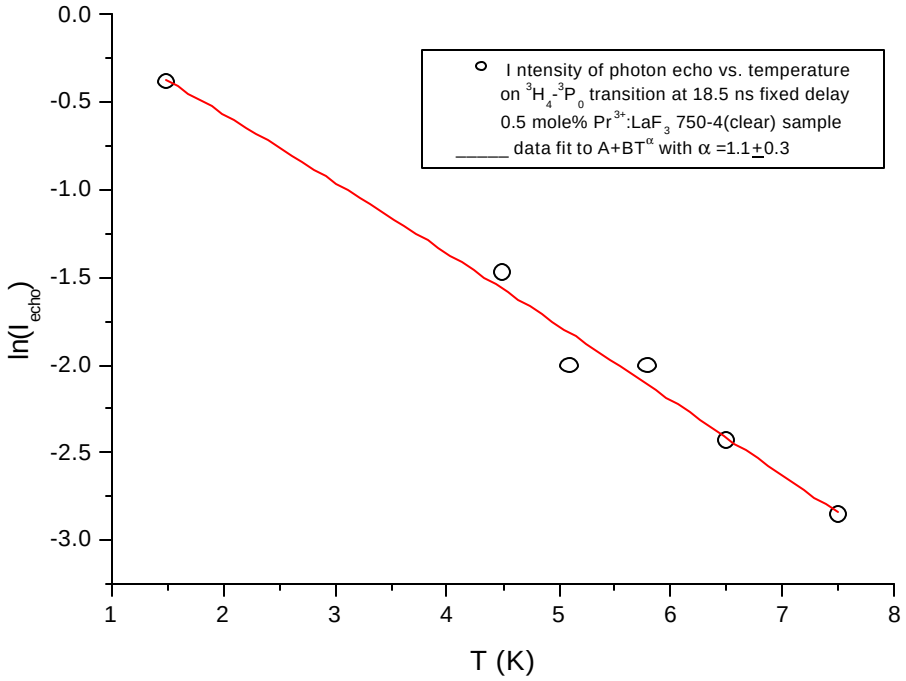

Fig.7.3: Temperature dependence of the echo intensity of $^3H_4$-$^3P_0$ transition of Pr^{3+} ions with fixed 18.5 ns delay. The sample is 0.5%Pr^{3+}:LaF_3 nanocrystals embedded in oxygluoride glass ceramics annealed at 750 ^oC for 4 hours (750-4 (clear). Open circles: the experimental data; Solid line: best data fit to the experimental results with I_{echo} = $A*exp(-4*B*\tau*T^{\alpha})$, where α = 1.1 from the data fit. A and B are constants.

We have to point out that the one-phonon direct process contributes to the temperature dependence of the homogeneous broadening too, but this contribution is small and can be neglected in the study. For the $^3P_0$ – $^3H_4$ transition, since the $^3P_0$ level is

well isolated from adjacent levels, the one-phonon direct processes which may contribute to the homogeneous broadening occurs mainly from the two higher sublevels of the $^3H_4$ ground state manifold (57 cm^{-1} = 82 K) and $^3H_4$ (76 cm^{-1} = 109 K). Considering that the spontaneous emission rate for $^3H_4$ (57 cm^{-1}) and $^3H_4$ (76 cm^{-1}) levels are A_{57} = (20 ps)$^{-1}$ and A_{76} = (8 ps)$^{-1}$, respectively [15,16] we get the total homogeneous broadening resulting from one-phonon direct process of these levels at temperature T as

$$\Gamma_{\text{hom}}^{direct} = A_{57}\,\overline{p}(82) + A_{76}\,\overline{p}(109) \cong 50 \cdot e^{-82/T} + 125 \cdot e^{-109/T}\,(\text{GHz}) \qquad (7.2)$$

where $\overline{p} = 1/\left(e^{\Delta/kT} - 1\right) \approx e^{-\Delta/kT}$. From Eq.6.3, $\Gamma_{\text{hom}}^{direct}$ is only 9.1x10^{-20} +3.4x10^{-27} MHz at T=1.5 K and 1.77+0.15=1.92 MHz at T=8 K. This justifies the assumption that the homogeneous broadening induced by the direct phonon process is weak enough in the ceramics to be ignored in the investigation of $^3P_0$ – $^3H_4$ transition at low temperatures.

7.3.3 Possible spectral diffusion effects involved in the time scale of SHB measurement

To investigate the contribution of the spectral diffusion effects to the homogeneous broadening, it is better to study the linewidth of the same transition with techniques such as SHB and the photon echo due to their different time scales required for the measurement. However, because a single frequency source was not available at ~478 nm, we were not able to conduct the SHB experiments for the $^3P_0$ transition. While we have observed nice photon echo signals for the $^3H_4$ - $^1D_2$ transition with 0.5 % Pr^{3+} doped the LaF_3 single crystals, the photon echo from the $^1D_2$ transition for Pr^{3+} ions doped in nanocrystals embedded in glass was not observable due to the very weak absorption of

the lowest $^1D_2$ sublevel (~5 % absorption even for 6 mm long sample as seen in Fig. 4.1). But the comparison of the homogeneous broadening of the $^3H_4$ - $^1D_2$ transition by SHB and that of the $^3H_4$ - $^3P_0$ transition with the two-pulse photon echo still may provide us important information on the spectral diffusion that occurs with the ions doped in nanocrystals embedded in the glass.

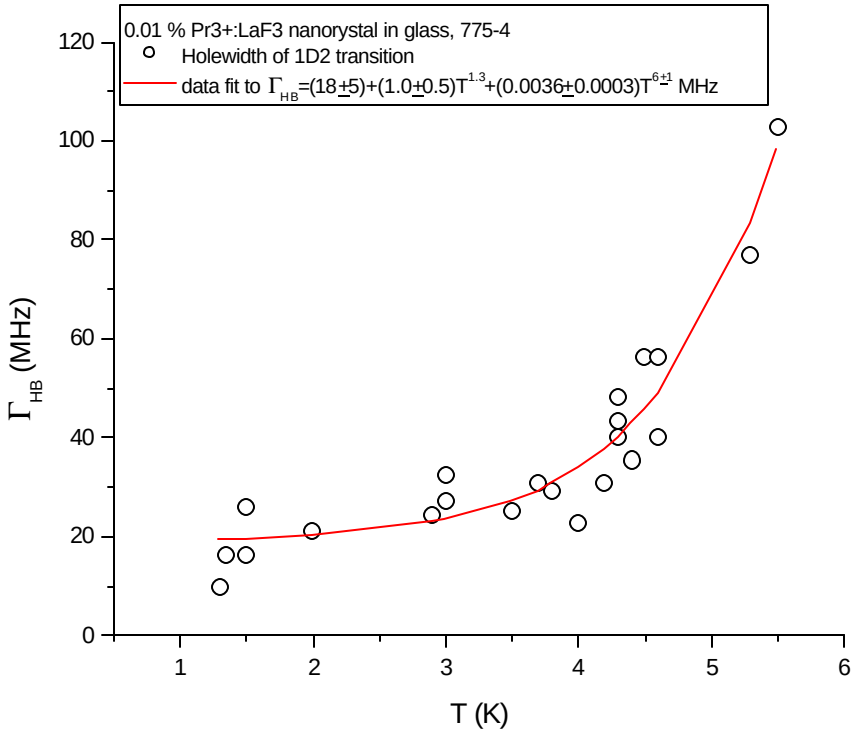

Fig.7.4: Temperature dependence of the homogeneous linewidth from SHB measurement for $^1D_2$-$^3H_4$ transition of 0.01 % Pr^{3+} ions doped in LaF_3 nanocrytsals embedded in oxyfluoride glass ceramics annealed at 775 ^oC for 4 hours. Solid line is the data fit results with the formula of $\Gamma_{HB} = P1+P2*T^{P3}+P4*T^{P5}$, where P1 to P5 are parameters determined from the data fit process.

As shown in Fig.7.4, the temperature dependence of the hole width, $\Gamma_{HB,}$ obtained from the SHB measurement is different from that which is obtained from the two-pulse

photon echo measurement (see Fig.7.3). The best data fit to the experimental results of hole width presented in Fig.7.4 is

$$\Gamma_{\text{hom}}^{SHB}(^1D_2) = \frac{1}{2}\Gamma_{HB}(^1D_2) = (9 \pm 3) + (0.5 \pm 0.2) \cdot T^{1.3} + (0.0018 \pm 0.0002) \cdot T^{(6\pm1)} (\text{MHz}) \tag{7.3}$$

for the 0.01 % Pr^{3+}:LaF_3 nanocrystals embedded in oxyfluoride glass annealed at 775 ^oC for 4 hours (Fig.7.4).

In Fig. 7.5 we compare the best fits for the homogeneous linewidth for ions doped in nanocrystals embedded in glass obtained with SHB on the $^1D_2$ transition (curve c) and the photon echo results on the $^3P_0$ transition (curve b) with that of the previous measurements [16] on the $^1D_2$ transition in bulk single crystals (curve a). An obvious increase in the homogeneous linewidth relative to bulk single crystal is seen for the nanocrystals based on both the photon echo and SHB results. It is seen that besides the quasi-linear term, an additional broadening occurs during the SHB study when the temperature is above 4 K. A much higher power temperature dependence dominates the homogeneous broadening for T > 4K. But for T < 4K, this high power terms becomes insignificant. The quasi-linear part, which dominates the line width of the SHB measurement at T < 4 K, is similar to what we have observed with the photon echo method for the $^3H_4$ - $^3P_0$ transition. However $\Gamma_{\text{hom}}^{SHB}(^1D_2)$ is always greater than that of $\Gamma_{\text{hom}}^{echo}(^3P_0)$. In the temperature range above 4 K, the higher power term ($T^{(6\pm1)}$) begins to make the major contribution to the broadening in the SHB study, while the broadening remains quasi-linear in the photon echo study.

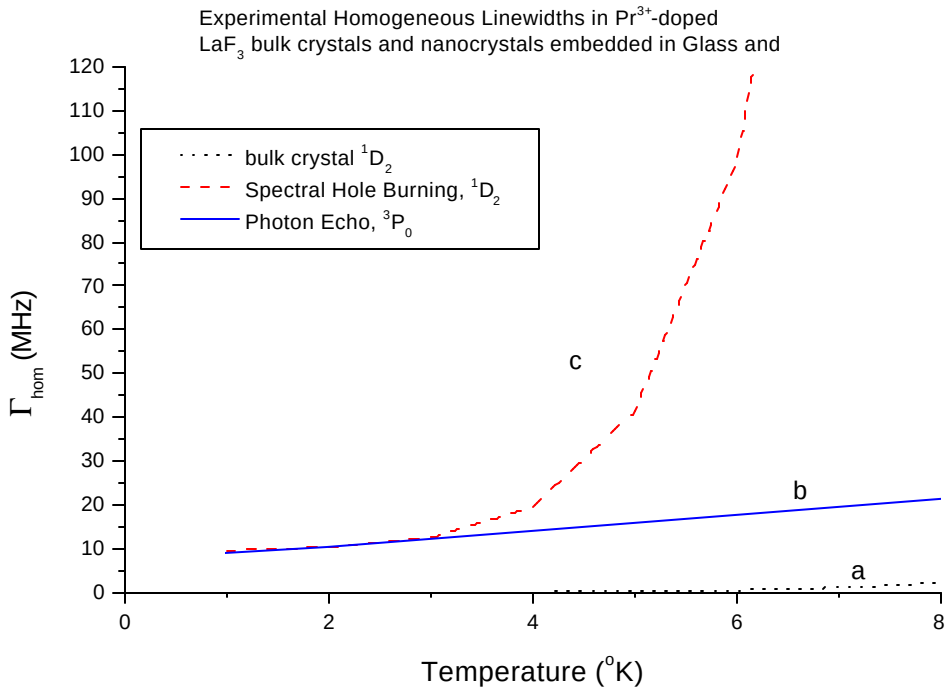

Fig.7.5: (a): the temperature dependence of the homogeneous linewidth for Pr^{3+} ions doped in LaF_3 single crystal from ref [22]; (b) the data fit results of the temperature dependence of the homogeneous linewidth with the photon echo method for $^3P_0$-$^3H_4$ transition of Pr^{3+} ions doped LaF_3 nanocrytsals embedded in oxyfluoride glass ceramics (Eq.7.1); (c) the data fit results of the temperature dependence of the homogeneous linewidth with the SHB measurement for $^1D_2$-$^3H_4$ transition of Pr^{3+} ions doped LaF_3 nanocrytsals embedded in oxyfluoride glass ceramics (Eq.7.5).

Let's first consider the possible contribution of spectral diffusion in the temperatures below 4 K. In Fig. 7.5, comparing curve (c) for the $^3H_4$ - $^1D_2$ transition with the curve (b) for the $^3H_4$ - $^3P_0$ transition, we find that $\Gamma_{\text{hom}}^{SHB}(^1D_2)$ and $\Gamma_{\text{hom}}^{echo}(^3P_0)$ are similar. Since the oscillator strength, which is proportional to the square of the transition dipole moment, of the $^3H_4$ - $^1D_2$ transition ($3\text{x}10^{-8}$) is smaller than that of the $^3H_4$ - $^3P_0$ transition ($1\text{x}10^{-7}$), one would expect a weaker coupling of the TLS to the $^1D_2$ transition;

thus a slower dephasing rate and a smaller homogeneous linewidth is expected for the $^1D_2$ transition. The fact that the $\Gamma_{\text{hom}}^{SHB}(^1D_2)$ is as large as $\Gamma_{\text{hom}}^{echo}(^3P_0)$ suggests that a spectral diffusion process may be occurring on the time scale of the SHB measurement. This can be understood from the point of the TLS model. In the TLS model, the glass should be thought to consist of a large ensemble of TLS's with a broad distribution of tunnel parameters and energy separations between the two levels, which would cause a broad distribution of fluctuation rates. Apart from being able to explain the quasi-linear temperature dependence of the thermodynamic properties of glasses, this model also predicts that these quantities will be time dependent. This dispersive time behavior traces back to a very broad distribution of tunneling rates of the TLS. The underlying physical phenomenon is that glass dynamics not only comprises very fast fluctuations around an equilibrium structure, but also includes an evolution of the glass structure as a whole on a much slower time scale. Thus, the optical dephasing time T_2 and the homogeneous broadening Γ_{hom} can be time dependent, and the experimental studies of the homogeneous linewidth will depend on the time scale of the observation.

Unfortunately, the indication for the role of spectral diffusion cannot be argued with great confidence here as a result of a number of differences between the two samples used in the two different techniques. It was not possible to perform the echo experiments on the samples used for SHB since the Pr^{3+} concentration was too low. The higher concentration samples that were available for the photon echo studies were prepared from a different glass composition so that the density of TLS and their coupling to the RE ions might be slightly different than in the samples used for SHB. Finally, in order to obtain sufficiently strong echo signals, it was necessary to work with larger

particle sizes (~35 nm) than those used in the SHB experiments (~23 nm). The larger average particle size will lead to smaller homogeneous linewidth, working in an opposite manner to the effect of the larger dipole transition moment of the $^3H_4$-$^3P_0$ transition. It is not clear which of these effects will dominate. Clearly, future work will require that these two methods be used on identical samples in order to define the role of spectral diffusion.

The higher power component that contributes most to the linewidth observed in our SHB study was also reported by Macfarlane and Dejneka for Tm^{3+} ions in these oxyfluoride ceramics [17]. For the ions doped in the nanocrystals embedded in glass matrix, in principle, both the TLS of the glass matrix and the two-phonon Raman process modified by the confinement effects on the phonon density of states contribute to the homogeneous broadening at the temperatures of our study. The point is which one will play the key role in the broadening as a result of the competition between these two mechanisms.

Macfarlane and Dejneka [17] proposed that the modified two-phonon Raman process, like that observed in isolated nanoparticles, is the major contribution to the broadening for T > 4 K. The previous investigation of the frequency spectrum of the spheroidal and torsional modes of the nanocrystals and the homogeneous line broadening due to two-phonon Raman scattering for free–standing crystallites gave $\Gamma_{hom} \sim T^3$ [18]. The calculation of the phonon density of states for different nanoparticle sizes in [10] suggests that the lowest confined mode frequencies for our samples are about a few wave numbers. In ref. [17], the authors attributed the presence of the higher exponent temperature dependence of the linewidth above 5 ^oK to the excitation of the confined modes of the approximately spherical nanocrystal. They argued that the suppression of

the amplitude of the lowest-frequency surface modes due to the glass matrix [19] increases the onset temperature for contributions of those confined modes so that they only began to appear above 4 K.

However, there are some concerns if we use the arguments proposed in ref. [17] to explain our results observed in SHB study at the temperatures above 4 ^{o}K. The thermal excitation of the confined modes proposed in ref. [17] is a modification of the two-phonon Raman process, which is a fast process and should show up in the photon echo technique as well. But it doesn't based on the observation of the quasi-linear temperature dependence in our photon echo study at temperatures up to 8 ^{o}K. In addition, the higher power term observed in our study is ~T^6, whereas it is T^3 for free-standing nanoparticles. Considering the confinement effects and surface defects at the boundary of the nanoparticles embedded in glass, we alternatively attribute the high power temperature dependence of the linewidth to the interaction of local defect modes at the surface of the nanocrystals with the RE ions located in the nanoparticles embedded in the glass. For glasses, the multi-average (over both the phonon energy and the distance between the TLS and the RE ions) of the interaction with many TLS in the surrounding glass gives the quasi-linear temperature dependence. However, here the interaction with individual strongly coupled modes near the surface could contribute a much higher power dependence [14]. These are effectively additional local modes at the boundary between the nanocrystals and glass with certain resonant frequencies that are thermally activated with an exponential temperature dependence. Further investigation is needed for evaluating this suggestion.

A zero temperature 9 MHz homogeneous linewidth, extrapolated from the behavior of linewidth to zero temperature is observed in our SHB measurements. Macfarlane and Dejneka [17] suggest that one can attribute this width to spectral diffusion resulting from slowly varying strain fields. While there could be some spectral diffusion effects at zero temperature as suggested in [17], this can not be the only contribution since a similar zero temperature homogeneous line width (7 MHz) is also observed in the photon echo experiment. Therefore there must be another important contribution to the linewidth which does not depend on the time scale of the measurement.

CHAPTER 8

CONCLUSIONS

The optical dynamical processes of rare earth ions doped in nanocrystals embedded in amorphous matrix have been studied with coherent spectroscopic techniques and conventional spectroscopic methods. In this work, we mainly focused on the properties of the optical dephasing and /or homogeneous broadening for ions doped in nanocrystals embedded in glass. The work reported herein can be summarized as follows:

The first approach to the investigation of the homogeneous broadening at low temperatures was done with the spectral hole burning (SHB). The homogeneous linewidth; its temperature dependence and nanocrystal size dependence have been obtained by measuring the corresponding hole width of the Eu^{3+} ions and Pr^{3+} ions doped in nanocrystals embedded in glass matrices. It was found that the homogeneous linewidths are about 10 to 40 MHz for the $^7F_0$-$^5D_0$ transition of Eu^{3+} ions and are 10 to 100 MHz for the $^1D_2$-$^3H_4$ transition of Pr^{3+} ions in nanocrystals embedded in glass in the temperature range of 0 ^oK to 10 ^oK. The linewidths increase with a decrease of the nanocrystal size, and at low temperatures they follow a quasi-linear temperature dependence. We explained the observed phenomena by the interaction of the ions with the two-level system (TLS) of the glass matrix and suggested that the interaction of the TLS dominates the optical dephasing of the ions doped in nanocrystals embedded in glass. From the faster increase of the homogeneous linewidth for $T > 4$ ^oK for Pr^{3+} ions

doped in LaF_3 nanocrystals embedded in glass, we found that in the time scale of the SHB measurement, another process, in addition to the interaction with the TLS of the glass, begins to dominate the homogeneous broadening as the temperature goes above 4 ^oK. We have attempted to explore the mechanism that results in the high power term (T^6) in the temperature dependence of the homogeneous linewidth, and we suggested a role of local modes at the nanocrystal-glass interface. Further investigation is needed for understanding and modeling the process.

In addition to the SHB, two-pulse photon echo technique, which measures the optical dephasing directly in time domain, was also employed in the study of the homogeneous broadening. With the collinear two-pulse photon echo experiment, we measured the decay time of the photon echo intensity on the $^3P_0$ - $^3H_4$ transition of Pr^{3+} ions doped in LaF_3 nanocrystals embedded in oxyfluoride glass. The dephasing time, T_2, was obtained as 32 ns to 47 ns for the $^3P_0$ - $^3H_4$ transition of Pr^{3+} doped nanoparticles of size about 35 nm LaF_3 nanocrytsals embedded in glass, which is about 50 to 100 times shorter than that of the T_2 (2.4 μs) obtained from the Pr^{3+}:LaF_3 single crystal. A quasi-linear temperature dependence of the homogeneous linewidth was obtained from the temperature dependence of the dephasing time, which further supports the conclusion from the SHB study that it is the interaction of the TLS dominate the dephasing of the Pr^{3+} ions doped in nanocrystals embedded in glass at low temperatures.

Since a longer time period is required for the SHB measurement, spectral diffusion resulting from slower processes may contribute to the homogeneous linewidth. An effective way to investigate the spectral diffusion process is to use both the photon echo and SHB methods in the same study. Ideally, one wants to work with the same

transition of the same sample in the study of the dephasing with SHB and photon echo. Unfortunately, we were not able to do it exactly that way due to practical difficulties of the laser sources and the available samples. But the results obtained from our SHB and photon echo study for the Pr^{3+}:LaF_3 nanocrystals embedded in glass, especially the higher power term detected in the temperature dependence of the homogeneous linewidth from the SHB, still provides us important information on the spectral diffusion that occurs in the time scale of the SHB measurement. Further confidence in this conclusion would be obtained if the SHB and photon echo study could be done with the identical transition and identical sample.

Besides the intensive study on the homogeneous broadening with both SHB and photon echo techniques, other dynamical properties of the trivalent RE ions doped in nanocrystals embedded in amorphous matrices were also studied. It was found that the fluorescence lifetime of the RE ions doped in nanocrystals depends on the medium that surrounds the ions and nanocrystals, the size of the nanocrystals, and the temperature. The individual spectral lines are inhomogeneously broadened compared with the lines from the single crystals and the width of the line increases with the decrease of the nanocrystal size. The relaxation between two closely spaced electronic levels has also been studied, and a size dependence of the relaxation rate was reported, suggesting the role of vibrational modes of the glass in relaxation processes among electronic levels of ions in the nanoparticle. This implies that a similar role for these vibrational modes must occur for RE ion contained directly in glasses.

Further studies will require photon echo and SHB measurements on the same sample and transition. A likely prospect is the $^3H_6(1)$-$^3F_3(1)$ transition of Tm^{3+} in LaF_3

nanocrystals embedded in glass. This transition has already been studied in SHB and should have sufficient absorption for photon echo studies.

REFERENCES

Chapter 1

1. R.M.Macfarlane and R.M.Shelby in Spectroscopy of Solids Containind Rare Earth Ions, editted by A.A.Kaplyaskii and R.M.Macfarlane, 51(1987).
2. Optical Linwsidths In Glass, Journal of Luminescence, 1987.
3. R.S.Meltzer and K.S.Hong, Physical Review B, 61(5), 3396(2000).
4. R.M.Macfarlane and M.J.Dejneka, Optics Letters, 26(7), 429(2001)

Chapter 2

1. Marc D. Levenson, and Satoru S. Kano, *Introduction to Nonlinear Laser Spectroscopy*, editted by Paul F. Liao, Academic Press , Inc. 1988, pp 29.
2. L. Allen, and J.H.Eberly, *Optical Resonance and two-level atoms*, John Wiley and Sons New York, 1975, pages 52.
3. B. Henderson and G. F. Imbusch, *Optical Spectroscopy of Inorganic Solids*, Clarendon press, Oxford, 1989, pp146.
4. C. Kittel, *Introduction to Solid State Physics*, 7^{th} edition, John Wily & Sons, Inc., New York, 1996, pp117.
5. B. Di Bartolo, *Optical Interactions in Solids*, John Wily & Sons, Inc., 1968, pp404.
6. Ref.3, pp258.

Chapter 3

7. R.M.Macfarlane and R.M.Shelby, *Coherent Transient and Hole burning spectroscopy*
   of rare Earth ions in Solids, Elsevier Science publishers B.V., 1987.
8. A. Szabo, **B 11** 4512 (1975).

9. L.E.Erickson, *Phys. Rev*. **B 16** 4731 (1977).
10. B. Henderson and G. F. Imbusch, *Optical Spectroscopy of Inorganic Solids*, Clarendon press, Oxford, 1989, pp258.
11. W. E. Moerner, *Persistent Spectral Hole-Burning: Science and Applications*, Springer-Verlag, Berlin, 1988
12. Marc D. Levenson, and Satoru S. Kano, *Introduction to Nonlinear Laser Spectroscopy*, edited by Paul F. Liao, Academic Press , Inc. 1988, p 47 and P216.
13. E.L.Hahn, *Phys.Rev*. **80**, 580(1950)
14. I.D.Abella, N.A.Kurnit and S.R.Hartmann, *Phys. Rev*. **141**, 391(1966)
15. L. Allen, and J.H.Eberly, *Optical Resonance and two-level atoms*, John Wiley and Sons New York, pages 1975. P.195

Chapter 4

1. G.H.Dieke, *Spectra and energy levels of rare Earth ions in crystals*, 1968; *American Institute of Physics Handbook*, 3rd edition, McGraw-Hill, 7-25(1972)
2. D.C.Tran, G.H.Sigel, Jr. B.Bendow, *J. Lightwave Technol*. **LT-2**, 566(1984).
3. T.J.Whitely, *J. Non-Cryst. Solid*. **184**, 352(1995).
4. E.Downing, L.Hesselink, J. Ralson, R. Macfarlane, *Science* **273**, 1185(1996).
5. Y.Wang, J.Ohwaki, *Appl. Phys. Lett*. **63(24)**, 3268(1993).
6. Matthew J. Dejneka, *J. Non-Cryst. Solid*. **239**, 149(1998).
7. Matthew J. Dejneka, *MRS Bulletin*, **November**, 57(1998).
8. R.S.Meltzer, W.Yen, Hairong Zheng, S.P. Feofilov, M.J. Dejneka, B.M. Tissue, and H.B. Yuan, Phys. Rev.B, **64** 100201 (R) (2001).
9. A.K.Cheethan, B.E.F.Fender, H.Fuess, and A.F.Wright, *Acta Crystallogr.* **B 32**, 34(1976).
10. W. Yen, *Optical Spectroscopy of Glasses*, edited by I. Zschokke, D.Reidel Publishing Company, 1986, pp 23-64.
11. K.S.Hong, R.S. Meltzer, S.P.Feofilov, R.I.Zakharchenya, W.Jia, H.Liu, B. Tissue, and H. B.Yuan, *J.Lumin*. **83-84**, 393 (1999).
12. H.-S. Yang, S.P. Feofilov, D.K. Williams, J.C. Milora, B.M. Tissue, R.S. Meltzer, W.M. Dennis. *Physica B*, **263**: 476(1999).

13. R. S. Meltzer, S.P.Feofilov, B. Tissue, H. B.Yuan, *Phys. Rev. B* **60**, R14012 (1999).
14. B. Bihari, H. Eilers, and B.M.Tissue, *J. Lumin*. **75**, 1 (1997).
15. R.S.Meltzer, W.M.Yen , Hairong Zheng, S.P.Feofilov, M.J.Dejneka, B.Tissue, H.B.Yuan, *J. Lumin*. **94-95**, 217(2001)
16. M.J. Dejneka, *J. Non-Cryst. Sol*. **239**, 149 (1998)
17. R.S.Meltzer, W.Yen, Hairong Zheng, S.P. Feofilov, M.J. Dejneka, Phys. Rev.B, **66** 224202 (2002).
18. D.L. Huber, J. Lumin. **36**, 327 (1987), Materials Science Forum. **50**, 77 (1989).
19. U. Buchenau, M. Prager, N. Nücker, A.J. Dianoux, N. Achmad, and W.A. Philips, Phys. Rev. B **34**, 5665 (1986).
20. J. Limin. 36, N4&5, Special issue (1987).
21. S.B.Stevens and H.J.Stapleton, Phys. Rev. B42, 9794(1990).

Chapter 5

1. B. Henderson and G. F. Imbusch, *Optical Spectroscopy of Inorganic Solids*, Clerandon press, Oxford, 1989.
2. Optical linewidth in glasses, edited by Marvin J. Weber, *Journal of luminescence*, **vol.36(4&5)**, (1987)
3. R. Richert, and A. Blumen, *Disorder effects on relaxational processes: glasses, polymers, proteins*, Springer-VerlagR. M, 1993,
4. W. Yen, *Optical Spectroscopy of glasses*, edited by D. Reidel Publishing Company, 23(1986).
5. R. M. Macfarlane and R. M. Shelby, *Journal of luminescence*, **vol.36(4&5)**, 179(1987).
6. D. L. Huber, *Materials Science Forum*, **vol.50**, 77(1989).
7. F. J. Bergin, J. F. Donegan, T. J. Glynn and G. F. Imbusch, *Journal of luminescence*, **vol.36**, 231(1987).
8. R. S. Meltzer, W. M. Yen, Hairong Zheng, S. P. Feofilov, M. J. Dejneka, B. M. Tissue, and H. B. Yuan, *Phys. Rev. B*, **vol.64**, 100201(R)(2001).
9. P. W. Anderson, B. I. Halperin and C. M.Varma, *Philosophical Maganize*, **vol. 25**, 1(1971).

10. W. A. Phillips, *J. Low Temperature Physics*, **vol.7(3/4)**, 351(1971)
11. R. Silbey and K. Kassner, *Journal of luminescence*, **Vol.36**, 283(1987).
12. D. L. Huber, *Journal of luminescence*, **Vol.36**, 327(1987).
13. D. L. Huber, M. M. Broer, and B. Golding, *Phys. Rev. Lett*. , **vol.52(25**), 2281(1984).
14. S. K. Lyo, *Phys. Rev. Lett*. **Vol. 48(10),** 688(1982).
15. S. K. Lyo and R. Orbach, *Phys. Rev. B,* **Vol. 22(9**), 4223(1980).
16. D.L.Huber, *Journal of luminescence,* **Vol. 36(4,5),** 307(1987).
17. R.M.Macfarlane and R.M.Shelby, *Spectroscopy of Solids Containing rare Earth Ions*, edited by A.A.Kaplyanskii and R.M.Macfarlane, Elsevier Science Publishers B.V.1987, P51.
18. R.M.Shelby and R.M.Macfarlane, Opt. Commun. **27**, 399(1978).

Chapter 6

1 R. Silbey and K. Kassner, *Journal of luminescence*, **Vol.36**, 283(1987).
2 D. L. Huber, M. M. Broer, and B. Golding, *Phys. Rev. Lett*. , **vol.52(25**), 2281(1984).
3 S. K. Lyo, *Phys. Rev. Lett*. **Vol. 48(10),** 688(1982).
4 D.L.Huber, *Journal of luminescence,* **Vol. 36(4,5),** 307(1987).
5 L.W. Molenkamp and D.A. Wiersma, *J. Chem. Phys*. **83**, 1 (1985).
6 M.J. Dejneka, *MRS Bulletin*, **23**, 57 (1998); *J. Non-Cryst. Sol*. **239**, 147 (1998).
7 S.P. Feofilov, A.A. Kaplyanskii, R.I. Zakcharchenya, Y. Sun, K.W. Jang, and R.S. Meltzer, *Phys. Rev*. **B 54**, 3690 (1996).
8 K.S. Hong, R.S. Meltzer, B. Bihari, D.K. Williams, and B.M. Tissue, *J.Lumin*. **76-77**, 234 (1998).
9 K.S.Hong, R.S. Meltzer, S.P.Feofilov, R.I.Zakharchenya, W.Jia, H.Liu, B. Tissue, and H. B.Yuan, *J.Lumin*. **83-84**, 393 (1999).
10 B. Bihari, H. Eilers, and B.M. Tissue, *J. Lumin.* **75**, 1 (1997).
11 R. M. Macfarlane and R. M. Shelby, *Journal of luminescence*, **vol.36(4&5)**, 179(1987).
12 Th. Schmidt, R.M. Macfarlane, and S. Völker, Phys. Rev. **B 50**, 15707 (1994).
13 J. Dexpert-Ghys, M. Faucher, and P. Caro, Phys. Rev. **B 23**, 607(1981).
14 R.M.Macfarlane, Optics Letters, 18(22), 1958(1993).

15 R. S. Meltzer, W. M. Yen , Hairong Zheng, S. P. Feofilov M. J. Dejneka, and B. M. Tissue, H. B. Yuan, Phys.Rev. **B 64**, 100201(R)(2001).

16 R. S. Meltzer, W. M. Yen , Hairong Zheng, S. P. Feofilov M. J. Dejneka, and B. M. Tissue, H. B. Yuan, J. Lumin. **94-95**, 221(2001).

Chapter 7

1. R.M. Macfarlane and R.M.Shelby, in Spectroscopy of Solids Containing Rare Earth Ions, A.A. Kaplyanskii and R.M.Macfarlane, eds. (North-Holland, Amsterdam, 1987, p.51
2. E.L.Hahn, *Phys.Rev*. **80**, 580(1950)
3. R.M.Shelby, Opt. Lett. 8, 88(1983)
4. J. Hegarty, *Optical Dephasing in Doped Glasses*, Journal of Luminescence 36, 273(1987).
5. D.L.Huber, *Analysis of a Stochastic Model for the Optical Linewidths and Photon-Echo Decays of Impurities in Glass*, Journal of Luminescence 36, 307(1987).
6. Hans C. Meijers and Douwe A. Wiersma, *Low Temperature Dynamics in amorphous solids: A photon echo study*, Journal of Chemical Physics, 101(8), 6927(1994).
7. R. S. Meltzer, W. M. Yen , Hairong Zheng, S. P. Feofilov, M. J. Dejneka, B. M. Tissue, and H. B. Yuan, Phys. Rev. B 64, 100201-1(R), 2001.
8. Y.C. Chen, K. Chiang, and S.R. Hartman, Photon echo relaxation in LaF3:Pr3+, Optics Communications, **29(2),** 181(1979).
9. R. Orbach, Proc. R. Soc. London, Ser. **A264**, 458(1961).
10. R.S.Meltzer and K.S.Hong, Phys. Rev. **B61(5)**, 3396(2001).
11. *Optical linewidth in glasses*, J. Lumin. 36(4 &5), (1987).
12. S.K. Lyo, Phys. Rev. Lett. **48**, 688 (1982).
13. D.L.Huber, M.M. Broer, and B. Golding, Phys. Rev. Lett. **52**, 2281 (1984); Phys. Rev. B **33**, 7297 (1986).
14. R. Silbey and K. Kassner, AJ. Lumin. **36**, 283 (1987).
15. W.M. Yen, W.C.Scott, and A.L.Schawlow, Phys. Rev. **136(1A)**, A271(1964).
16. L.E. Erickson, Optics Communications, **15(2)**, 246(1975).
17. R.M. Macfarlane and M.J.Dejneka, Optics Letters, **26(7)**, 429(2001).

18. A. Tamura, Phys. Rev. B52, 2668(1998).

19. A. Tamura, K. Higeta, and T. Ichinokawa, J. Phys. C, 15, 4975(1982).

APPENDIX

SYNCHRONIZING OF THE PULSED LASERS AND THE ALIGNMENT OF THE EOMS IN THE TWO-PULSE PHOTON ECHO EXPERIMENT

1. Synchronizing of the two pulsed lasers

As it is shown in Fig.3.5, the delay of the two pulses was accomplished by synchronizing two Nd:YAG pulsed lasers. Initially, one wants to trigger the DCR-1 pulsed laser externally by the GCR-100 since the delay between the lamp and the Q-switch in the DCR-1(280 μs) is longer than that of the GCR-100 (180 μs). But due to the output problem of the Q-switch of the laser GCR-100, we had to do it in another way. As shown in Fig. A1 and A2, we use the DCR-1 as the master laser in the triggering sequences. The lamp out put of GCR-100 externally trigger the blank lamp of the DCR-1 in the next period of the pulses after it is delayed by a time of $\underline{T+T(GL)-[T(DB)+T(DL)}]$, which is about 96.90 ms in our experiment. Here T = 100 ms is the reputation period of the two pulsed lasers. T(GL) = 180 μs and T(DL) = 280 μs are the delays between the lamp and Q-switch of the GCR-100 and the DCR-1, respectively. T(DB) = 3 ms is the delay between the blank and the lamp of the DCR-1. For the trigging of the Q-switches, we use the variable output of the DCR-1 to externally trigger the Q-switch of the GCR-100. Adjusting the variable output of the Q-switch of the DCR-1 varies the delay between the two pulses.

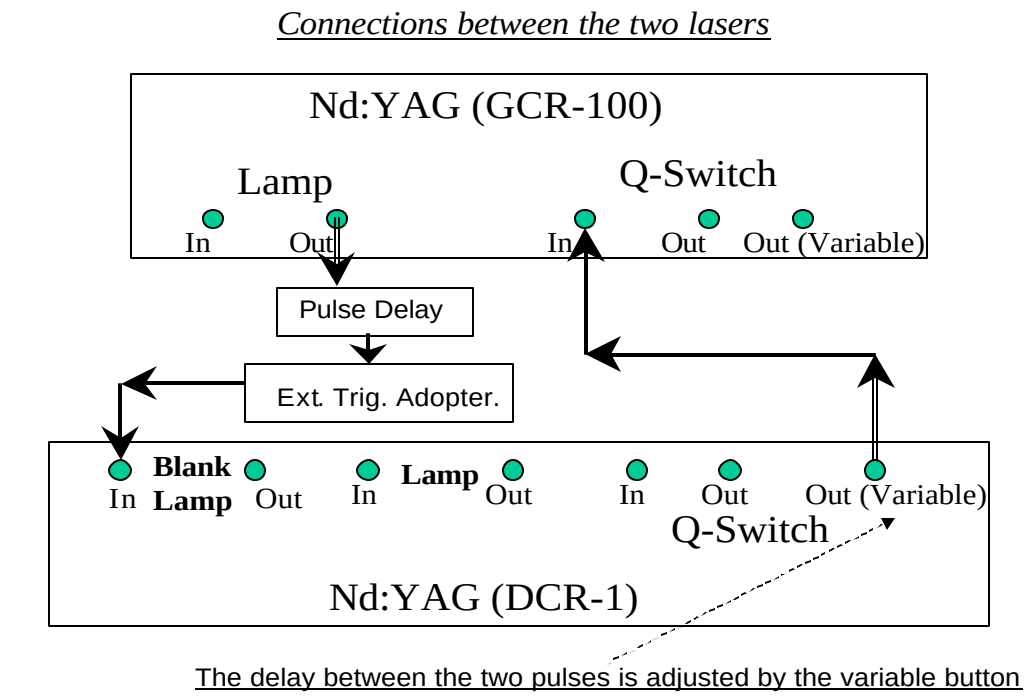

Fig. A1. The connections between the two pulsed lasers

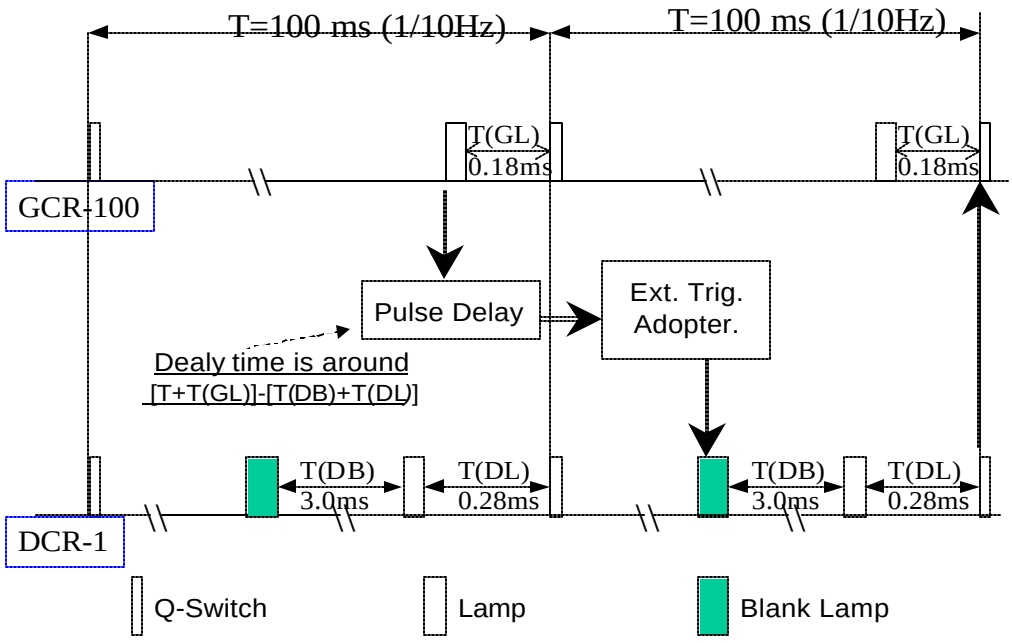

Fig.2A. The sequence of the pulses in the trigging process.

2. The alignment of the EOMs

Three EOMs (EOM1 to EOM 3), with four linear polarizers that perpendicular its next (LP1 to LP4), have been used in our two-pulse photon echo experiment (see Fig.3.5). The following outlines the basic procedures for the alignment of the EOMs.

(1). Adjust the spatial position of the pulse1 and pulse2 so that they are completely overlapped all the way after the Beamsplitter (BS) next to the cryostat. Meanwhile, the beam should be horizontally reach the entrance of the PMT, which is necessary for the alignment of the EOMs.

(2). Insert the LP1, EOM3. The direction of the polarization of the LP1 is along the polarization of the lasers. Connect all of the cables for operating the EOM3, but leave the power and trigger switches off. Adjust the spatial position and rotation of the EOM3 until the complete light spot hitting on the entrance of the EOM3 is observed without any distortions.

(3). Place the LP4 in a way that its polarization is perpendicular to that of the LP1. This can be optimized by minimizing the light intensity after the LP4. If the EMO3 and the LP4 are well aligned, a very weak light spot with a dark line crossing it should be observed behind the LP4.

(4). Turn on the power and the trigger of the EOM3, Adjust the bias and you should see the changes of the intensity of the light spot after the LP4 and the movement of the dark line crossing the spot. If this does not appear, further adjustment of the spatial position of the EOM3 and the polarization of the LP4 is necessary.

(5). Turn on the trigger of the EOM3 and adjust the trigger voltage to a proper level. Varying the delay time of the trigger, one should see the “on” and “off” of the light after the LP4.

(6). Insert the EOM2. Adjust it spatial position so that the light spot can go through it without any obstacles (it is better to let the light go through the center of the entrance window and exit window of the EOM). Insert LP3 and make its polarization perpendicular to that of the LP1. Further adjust the position of the EOM2 and the polarization of the LP2 until a pattern of dark cross over the weak spot is seen after the LP3.

(7). Turn on the power supply and the trigger of the EOM2. Adjust the delay time of the trigger until the light “on” and “off” is seen after the LP3 during the variation of the trigger delay time. Leave the delay time in a position where the light after the LP3 is “on”.

(8). Insert the EOM1 and LP2. Repeat the steps (6) to (7). Here the polarization of the LP2 should be aligned in a way that its polarization perpendicular to that of the LP1.

(9). Until now the individual alignment for each EOM is basically done. To get them work together, the polarization of the LP3 should be adjusted so that its polarization is perpendicular to its neighbors Lp1 and Lp3. Turn on the PMT and open its shutter (make sure the light is switched off by EOMs before turn the PMT). Adjusting the delay time of three EOMs one should see the light on and off on the oscilloscope through the PMT. Further spatial and timing alignment can be done by monitoring the signal on the oscilloscope.

In the above process, the master trigger for the triggering pulses of the EOMs is from the variable Q-switch output of DCR-1 laser.